UNIVERSITÉ DU QUÉBEC À MONTRÉAL

ÉTUDES DE LA DISPERSION ET DE L'ENCAPSULATION DES NANOTUBES DE CARBONE EN MILIEU AQUEUX

MÉMOIRE

PRÉSENTÉ

COMME EXIGENCE PARTIELLE

DE LA MAÎTRISE EN CHIMIE

PAR

WEI HENG ZHONG

JANVIER 2013

REMERCIEMENTS

Je tiens en premier lieu à remercier mon directeur de recherche, Pr. Jérôme Claverie, de m'avoir confié ce travail de recherche ainsi que ses conseils précieux aux cours de ces années. Mes débuts en tant que polymériste colloïdal, je les dois à Pr. Claverie, qui m'a laissée découvrir le coté fascinant des polymères.

J'ai pu travailler dans un cadre en même temps agréable et professionnel, grâce à toute l'équipe de recherche. Merci tout d'abord à Kirill Skupov qui m'a initié la recherche dans ce laboratoire, Laurence Piché et Jean-Christophe Daigle qui m'ont toujours enseigné la bonne pratique du laboratoire. Paramita Das, Souryvanh Nirasay, Mitra Vasei et Basile Commarieu pour leur collaboration et leur agréable compagnie. Je remercie également Jules Nguendia Zeuna pour ses nombreuses mesures d'isotherme. Pour Oumar Bachir et Alex Michel, bon courage pour la suite.

Je remercie aussi tous les personnes qui m'ont aider sur diverses analyses et caractérisations: Volodymyr Kriuchkov pour les analyses de GPC et de DSC, Alexandre Arnold les analyses en HPLC et en RMN, André Leblanc et Lekha Sleno pour les analyses en LC-MS. Je remercie également Jean-Philippe Masse du (CM)2 pour les analyses en MET et Nicolas Cottenye du LCM pour les analyses en spectroscopie de Raman. Je remercie Gwenaël Chamoulaud pour son soutien technique avec les appareils de NanoQAM.

Je tiens à remercier mes parents, Wu Xiaosui et Zhong Zhenqiu. Leurs soutiens m'ont permis de poursuivre mes études jusqu'à aujourd'hui. Merci à mes amis de longue date, spécialement Antonio, Giovanni et Sophie de m'avoir aider à m'installer dès mon arrivée à Montréal. Merci à Fabrice et Stephen de m'avoir changé les idées quand j'en avais besoin.

Enfin, je remercie le département de chimie de l'UQAM, le nanoQAM, le Fonds à l'accessibilité et à la réussite des études (FARE) et NanoQuébec pour leurs soutiens techniques et financiers.

TABLE DES MATIÈRES

LISTE DES FIGURES iv
LISTE DES TABLEAUX vii
LISTE DES ABRÉVIATIONS, SIGLES ET ACRONYMES viii
RESUMÉ ix
CHAPITRE I
INTRODUCTION 1
1.1 INTRODUCTION DES NANOTUBES DE CARBONE (CNT) 2
1.2 LA STRUCTURE DES CNT 3
1.3 LA SYNTHÈSE DES CNT 7
1.3.1 DÉCHARGE D'ARC 7
1.3.2 ABLATION LASER 8
1.3.3 DÉPÔT CHIMIQUE EN PHASE VAPEUR (CVD) 8
1.3.4 AUTRES MÉTHODES ET PURIFICATION DES CNT 9
1.4 PROPRIÉTÉS ET APPLICATIONS DES CNT 10
1.5 DISPERSION DES CNT 11
1.5.1 STABILISATION DES CNT 12
1.5.2 ADSORPTION DES TENSIOACTIFS 16
1.6 POLYMÉRISATION PAR RAFT 18
1.7. BIBLIOGRAPHIE 22
CHAPITRE II
REVUE DE LA LITTÉRATURE: PROBING THE CARBON NANOTUBE-SURFACTANT INTERACTION FOR THE PREPARATION OF COMPOSITES 25
ABSTRACT 27
2.1 INRODUCTION 27
2.2 EXPERIMENTAL 29
2.2.1 MATERIALS 29
2.2.2 CNT PURIFICATION 29
3.2.3 CNT DISPERSION 30
2.2.4 DETERMINATION OF CNT POROSITY BY BET 30

2.2.5 TRANMISSION ELECTRON MICROGRAPHY (TEM) 30
2.2.6 CONDUCTMETRY 31
2.2.7 DETERMINATION OF ADSORPTION ISOTHERM BY DIALYSIS AND HPLC QUANTIFICATION 31
2.2.8 CNT FILM PREPARATION 33
2.2.9 RAMAN CARACTERIZATION OF THE SWCNT DISPERSION..... 34
2.3 RESULTS AND DISCUSSION 34
2.3.1 NANOTUBE DISPERSION 36
2.3.2 BUILDING ADSORPTION ISOTHERMS 37
2.4 CONCLUSION 51
ACKNOWLEDGMENTS 52
REFERENCES 52
CHAPITRE III
REVUE DE LA LITTÉRATURE: A VERSATILE METHODE OF NON-COVALENTLY MODIFIED CARBON NANOTUBE BY RAFT POLYMERIZATION 56
ACKNOWLEDGMENTS 66
REFERENCES 67
CHAPITRE IV
CONCLUSION 68
4.1 SOMMAIRE 68
4.2 TRAVAUX FUTURS 69
ANNEXE A
TEXTE DE L'ENTRETIEN: PROBING THE CARBON NANOTUBE-SURFACTANT INTERACTION FOR THE PREPARATION OF COMPOSITE 71
ANNEXE B
TEXTE DE L'ENTRETIEN: A VERSATILE METHODE OF NON-COVALENTLY MODIFIED CARBONE NANOTUBE BY RAFT POLYMERIZATION 92

LISTE DES FIGURES

Figures		Pages
1.1	Enroulement du feuillet de graphène pour former un SWNT	3
1.2	Les différentes formes des SWNT construites à partir du feuillet de graphène selon le vecteur $\vec{C}$	4
1.3	DWNT comme modèle simple de MWNT, observation par TEM des MWNT	5
1.4	Arbre généalogique des nanotubes primaires montrant les relations topologiques entre eux	6
1.5	Représentation schématique de la méthode de décharge d'arc	7
1.6	Représentation schématique de la méthode d'ablation laser	8
1.7	Séparation des MWNT/DWNT par ultracentrifugation à gradient de densité	10
1.8	Diagramme du potentiel total d'interaction entre 2 surfaces en fonction de la distance D	14
1.9	Diagramme du potentiel total de répulsion stérique entre 2 surface en fonction de la distance D	16
1.10	Adsorption des SDS sur les nanotubes (a) SWNT de diamètre 1,2nm. (b) SWNT de diamètre 15 nm	17
1.11	Mécanisme réactionnel de la polymérisation RAFT	20
1.12	L'activité relative du CTA en fonction du groupement activateur (Z)	21
2.1	Determination of the concentration of free surfactant	32
2.2	TEM of the MWCNTs and SWCNTs before and after washing	35
2.3	Dispersion of SWCNTs in water and in saline solution with various concentration of SDS	37
2.4	Surfactant adsorption isotherms on CNTs	40
2.5	Composition of SDBS surfactant by HPLC-MS	44
2.6	Conductivity vs SDS concentration with MWCNTs. Displacement of deposited $M(SDS)_x$ by SDS	46
2.7	Scheme of the film formation process using aqueous dispersions of MWCNTs and polymer nanoparticles. Picture of the resulting film.	

Conductivity vs amount of MWCNTs in the CNT/polymer composite (wt%) 49

2.8 Proportion of SDS adsorbed and relative surface coverage vs the total SDS concentration 50

3.1 Structure of the RAFT dispersants and CNT encapsulation in aqueous medium by RAFT polymerization 60

3.2 Adsorption isotherms and pictures of the CNT dispersed in water with the RAFT dispersants 61

3.3 TEM of CNT and CNT-polymer nanocomposites 64

A.1 Raman spectrum of SWCNT 83

A.2 Raman spectrum of SWCNT 84

A.3 Raman spectrum of SWCNT 85

A.4 Raman spectrum of SWCNT 86

A.5 Raman spectrum of SWCNT 87

A.6 Tg of the polymer dispersion measured by DSC 88

A.7 Absorption Spectrum of a MWCNT Dispersion in water containing SDS.... 89

A.8 Dispersion of MWCNTs in water with various concentrations of SDS 90

A.9 Dispersion of MWCNTs in water with various concentrations of SDBS 91

A.10 Dispersion of MWCNTs in water with various concentration of BZT 91

B.1 RMN^{1}H spectra of RAFT dispersant PSAA 95

B.2 TEM picture of CNT encapsulated in a polymer (entry 1) 98

B.3 TEM picture of CNT encapsulated in a polymer (entry 1) 99

B.4 TEM picture of CNT encapsulated in a polymer (entry 1) 100

B.5 TEM picture of CNT encapsulated in a polymer (entry 2) 101

B.6 TEM picture of CNT encapsulated in a polymer (entry 2) 102

B.7 TEM picture of CNT encapsulated in a polymer (entry 3) 103

B.8 TEM picture of CNT encapsulated in a polymer (entry 3) 104

B.9 TEM picture of CNT encapsulated in a polymer (entry 5) 105

B.10 TEM picture of CNT encapsulated in a polymer (entry 5) 106

B.11 TEM picture of CNT encapsulated in a polymer (entry 6) 107
B.12 TEM picture of CNT encapsulated in a polymer (entry 6) 108
B.13 TEM picture of CNT encapsulated in a polymer (entry 6) 109
B.14 TEM picture of CNT encapsulated in a polymer (entry 7) 110
B.15 TEM picture of CNT encapsulated in a polymer (entry 7) 111
B.16 TEM picture of CNT encapsulated in a polymer (entry 8) 112
B.17 TEM picture of CNT encapsulated in a polymer (entry 8) 113
B.18 TEM picture of CNT encapsulated in a polymer (entry 8) 114
B.19 TEM picture of CNT encapsulated in a polymer (entry 9) 115
B.20 TEM picture of CNT encapsulated in a polymer (entry 9) 116
B.21 TEM picture of CNT encapsulated in a polymer (entry 9) 117
B.22 TEM picture of CNT encapsulated in a polymer (entry 9) 118
B.23 TEM picture of CNT encapsulated in a polymer (entry 10) 119
B.24 TEM picture of CNT encapsulated in a polymer (entry 11) 120
B.25 TEM picture of CNT encapsulated in a polymer (entry 11) 121
B.26 TEM picture of CNT encapsulated in a polymer (entry 12) 122
B.27 TEM picture of CNT encapsulated in a polymer (entry 12) 123
B.28 TEM picture of CNT encapsulated in a polymer (entry 12) 124
B.29 TEM picture of CNT encapsulated in a polymer (entry 12) 125
B.30 Picture of the result of the (failed) encapsulation experiment 126
B.31 TEM picture of MWNT prior encapsulation (PAA) 127
B.32 TEM picture of MWNT prior encapsulation (PAA) 128
B.33 TEM pictures of MWNT prior encapsulation (PAABA) 129
B.34 TEM pictures of MWNT prior encapsulation (PSAA) 130
B.35 Raman spectra of SWNT dispersions 131
B.36 Deconvoluted spectrum (sample 9) 132
B.37 Representative Gel Permeation Chromatogram (sample 9) 133

LISTE DES TABLEAUX

Tableau — Pages

2.1 Characterization of the CNTs before and after washing treatment 35

2.2 Adsorption isotherms of various surfactants on washed MWCNTs and SWCNTs in water 41

2.3 Influence of SDS concentration on the peak positions of RBM in Raman spectra (λ = 514nm) 43

3.1 Encapsulation Reactions 63

A.1 Conditions for each isotherm 72

B.1 Intensity (absolute and then relative to the tallest peak) of the D (1342 cm^{-1}), the G1 and G2 (1565 cm^{-1} and 1589 cm^{-1}) Raman bands 131

LISTE DES ABRÉVIATIONS, SIGLES ET ACRONYMES

AFM	*microscopie à force atomique*
ATRP	*atom transfer radical polymerization*
BET	*Brunauer-Emmett-Teller*
BzT	*benzethonium chloride*
CNT	*nanotube de carbone*
CTA	*agent de transfert de la polymerisation RAFT*
CVD	*dépôt chimique en phase vapeur*
DLVO	*la théorie de Derjaguin, Landau, Verwey et Overbeek*
DSC	*calorimétrie différentielle à balayage*
DWNT	*nanotube de carbone doubleparois*
GPC	*chromatographie à perméation de gel*
HPLC	*chromatographie liquide à haute performance*
HPLC-MS	*chromatographie liquide à haute performance – spectroscopie de masse*
MET	*microscopie électronique à transmission*
MWNT	*nanotube de carbone multiparois*
NMP	*nitroxide-mediated polymerization*
PAA	*polyacide acrylique*
PAABA	*poly(acide acrylique-co-butyle acrylate)*
PMMA :	*polyméthacrylate de méthyle*
PSAA	poly(styrène-*co*-acide acrylique)
RAFT	*Reversible Addition-Fragmentation chain Transfer*
RBM	*radial breathing mode*
SDBS	*sodium dodécyl benzène sulfonate*
SDS	*sodium dodécylsulfate*
SWNT	*nanotube de carbone monoparoi*
Tg	*transition vitreuse*
Tx-100	*triton x-100*

RÉSUMÉ

Depuis leur découverte, les nanotubes de carbone (CNT) ont connu de nombreux succès en raison de leurs performances mécaniques, électriques et thermiques exceptionnelles. L'exploitation de ces propriétés requiert néanmoins de pouvoir isoler les CNT, de les manipuler et de les localiser au sein d'un matériau d'architecture plus ou moins complexe. Pour cela, il est souvent nécessaire de disperser les CNT en raison de leur très grande insolubilité dans tout solvant. De nombreuses stratégies de dispersion reposent sur la stabilisation des CNT par des tensioactifs. Cependant, très peu d'études visent à déterminer les forces colloïdales mises en jeu, un des paramètres clés de la dispersion. Ainsi, la dispersion des CNT reste souvent un art plutôt qu'un processus bien contrôlé et maîtrisé. Dans cette étude, le mécanisme d'adsorption en milieu aqueux de quatre tensioactifs usuels a été clarifié, en particulier grâce à la détermination de leur isotherme d'adsorption. En se basant sur les résultats d'adsorption, des dispersions concentrées et sans agrégats de CNT ont été préparées et ensuite utilisées pour la formulation des nanocomposites polymériques.

Une seconde méthode de dispersion est basée sur l'encapsulation des CNT par une écorce polymérique. Alors que la majorité de telles méthodes requiert la modification covalente des CNT, ce qui entraîne la détérioration des propriétés des CNT, nous présentons une méthode de dispersion et d'encapsulation des CNT qui ne nécessite pas de modification covalente de leur surface. Cette méthode se base sur l'adsorption physique des polymères préparés par polymérisation par transfert de chaîne de type addition et fragmentation, appelée polymérisation RAFT. Cette procédure d'encapsulation est versatile et permet la formation d'une couche polymérique homogène et continue sur la surface des CNT.

Mots clés : nanotubes de carbone (CNT) ; dispersion ; isotherme d'adsorption ; encapsulation ; polymérisation RAFT.

CHAPITRE I

INTRODUCTION

Cette introduction débute par la présentation générale des nanotubes de carbone. Une mise en contexte historique sera abordée, suivie de la description des différentes structures des nanotubes de carbone. Les principales méthodes de synthèse seront ensuite présentées en commençant par la décharge d'arc électrique suivi de l'ablation laser et du dépôt chimique en phase vapeur (CVD). Ensuite, les différentes propriétés physico-chimiques dont leur résistance mécanique, leur conductions thermique et électrique seront passées en revue. L'exploitation de ces propriétés exceptionnelles donne naissance à de nombreuses applications potentielles, en particulier dans le domaine des nanocomposites fonctionnels. Dans l'ensemble de ce manuscrit, nous avons utilisé les abréviations usuelles CNT, SWNT, et MWNT pour désigner respectivement les nanotubes de carbone, nanotubes monoparois de carbone, et les nanotubes multiparois de carbone. Ces abréviations correspondent aux acronymes anglais de carbon nanotubes, single walled carbon nanotubes et multi walled carbon nanotubes.

Pour préparer ces nanocomposites, il est nécessaire de disperser les CNT. Dans notre travail, le milieu dispersant est l'eau. Aussi, les principes de la stabilité colloïdale dans l'eau seront présentés. Ce projet de recherche ayant beaucoup utilisé le concept d'isotherme d'adsorption, nous rappellerons les principales caractéristiques de ceux-ci.

Enfin, une portion de notre travail a consisté en l'encapsulation de CNT par une couche de polymère, en utilisant la méthode de polymérisation radicalaire par transfert de chaînes, appelée polymérisation RAFT. Cette technique récente de polymérisation radicalaire contrôlée sera aussi présentée dans ce chapitre.

1.1 Introduction des nanotubes de carbone

Les différentes formes allotropiques du carbone lui confèrent de nombreuses propriétés, qui peuvent être exploitées de manière différente dans plusieurs domaines. Pendant plus de 6000 années, le carbone a été utilisé pour la réduction des oxydes métalliques [1]. Le carbone a connu sa première utilisation massive lors de la révolution industrielle au XIX^{e} siècle en Europe puis en Amérique sous forme de charbon. Puis, l'exploitation du carbone issu de la pétrochimie a connu un essor remarquable. Ce n'est qu'en 1985, suite à la découverte des fullerènes par Kroto, Smalley et Curl qu'une nouvelle forme de carbone a été découverte [2]. Quelques années plus tard, les écrits d'Iijima en 1991 ont popularisé les nanotubes de carbone [3-4]. En 2004, l'isolation du graphène par Geim et Novoselov pousse à son apogée la recherche sur les nanostructures de carbone [5].

De nos jours, les nanotubes de carbone (CNT) occupent un rôle important dans la recherche sur les nanostructures avec des ramifications dans de nombreux domaines de la recherche et de la technologie, que ce soit en physique, en chimie, en ingénierie, en biologie et en médecine. De nombreux manuscrits attribuent la découverte des CNT à S. Iijima en 1991 [3]. Cependant, cette affirmation est trompeuse et omet de citer tous les scientifiques qui ont contribué à la compréhension de ces nano filaments de carbone avant cette citation [6]. La première observation des CNT par la microscopie électronique à transmission (MET) remonte en 1952 par Radushkevich et Lukyanivich dans un journal de physico-chimie russe [7]. Cependant, l'accès aux documents scientifiques russes par la communauté occidentale pendant la guerre froide était souvent très limité. De plus, la méconnaissance de cette première découverte des CNT est renforcée par la langue de publication du manuscrit. Ce n'est qu'en 1976 que la première observation des CNT fut rapportée en occident par Oberlin *et al* [8]. Cependant, la technologie de la MET ne permettait pas alors d'obtenir un grossissement suffisant pour déduire le nombre de parois du CNT. Il faut attendre 1991 [3] pour qu'Iijima confirme la structure des nanotubes à parois multiples (MWNT) obtenus par décharge électrique. Puis en 1993, la première observation des nanotubes à paroi simple (SWNT) a été rapportée simultanément par Iijima et Ichihashi [4] affiliés à NEC Corporation (*Nippon Denki Kabushiki Gaisha)* et par Bethune *et al* [9] de IBM (*International Business Machines Corporation*). Des lors, l'intérêt sur les CNT n'a cessé de croître.

1.2 La structure des CNT

Structurellement, les SWNT peut être considérés conne un enroulement d'un feuillet monoatomique de graphite appelé graphène (Figure 1) avec un diamètre approximatif de 1nm et qui peut atteindre une longueur d'ordre millimétrique. La figure ci-dessous représente le repliement sur elle-même du feuillet de graphène pour former un SWNT [10].

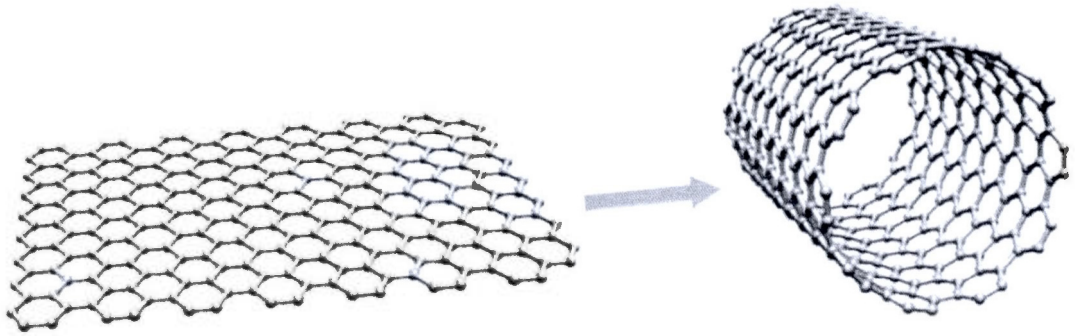

Feuillet de graphène **SWNT**

Figure 1.1 Enroulement du feuillet de graphène pour former un SWNT [10].

Le principe de construction des SWNT à partir du graphène est schématisé sur la figure 2. Deux entiers, m et n, suffisent à définir la structure de celui-ci. A partir de ces deux entiers, on peut définir le vecteur $\vec{C}$ suivant :

$$\vec{C} = n\vec{a}_1 + m\vec{a}_2 \qquad (1)$$

où $\vec{a}_1$ et $\vec{a}_2$ sont deux vecteurs unitaires bordant deux cotés d'un hexagone. En joignant un point quelconque à un point distant de $\vec{C}$, alors la feuille de graphène enroulée sur elle-même forme un SWNT. Un paramètre important est l'angle θ formé par les vecteurs $\vec{C}$ et $\vec{a}_2$. Quand les entiers $n = m$ et que θ = 30 degrés, le SWNT est sous la forme « chaise ». Quand $m = 0$ et que l'angle θ = 0 degrés, le SWNT adopte une structure « zigzag ». Lorsque l'angle θ est compris entre 0 et 30 degrés et les entiers $n > m > 0$, le SWNT est

chiral. Les propriétés électrique, mécanique et optique sont fortement dépendantes de la chiralité des SWNT, comme décrit en dans le *chapitre 1.4*.

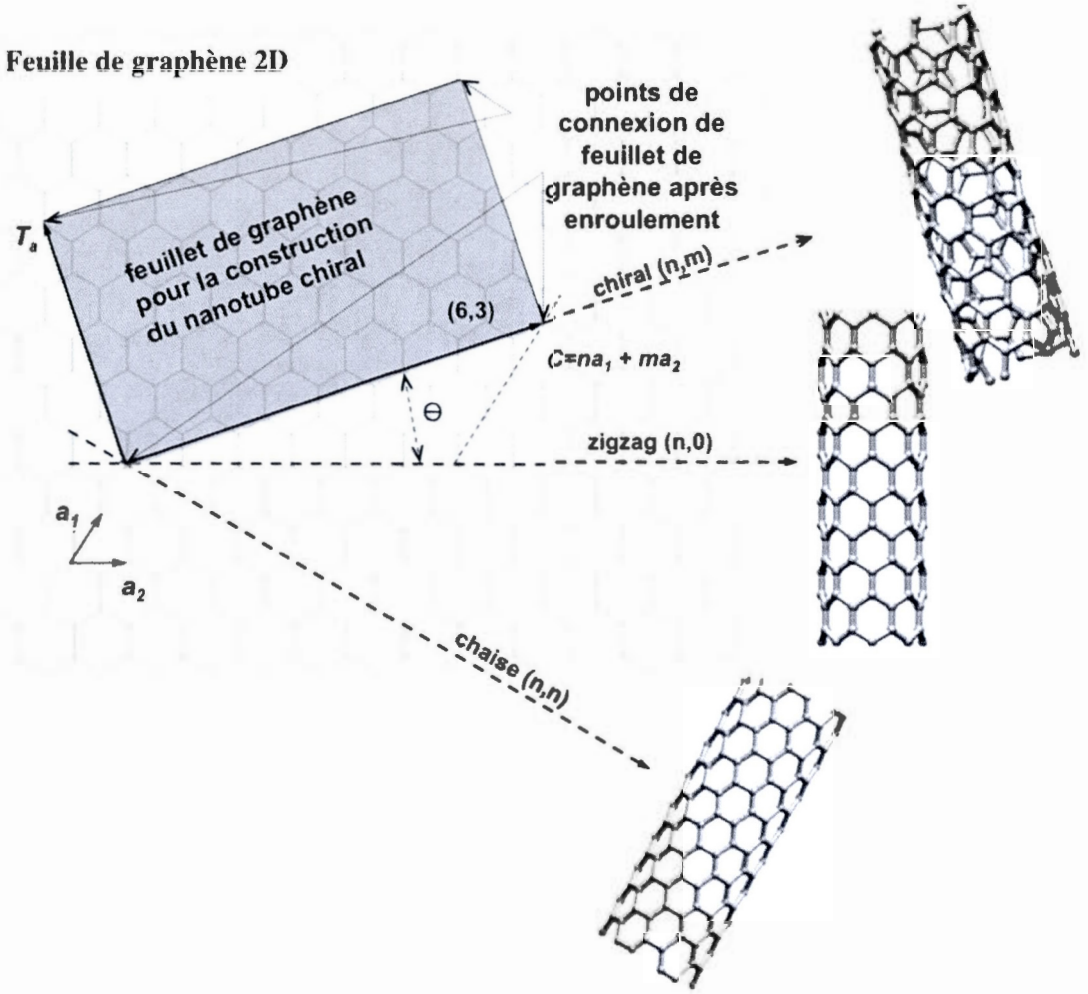

Figure 1.2 Les différentes formes des SWNT construites à partir du feuillet de graphène selon le vecteur $\vec{C}$ [10].

Les MWNT sont constitués de plusieurs SWNT concentriques. Ce type d'enroulement permet aux MWNT d'atteindre un diamètre de l'ordre d'une dizaine de nanomètres. Cependant, les MWNT ne sont pas chiraux en raison des variétés géométriques de chacun des tubes de SWNT le constituant. Ainsi, les MWNT possèdent une combinaison des propriétés des SWNT et ont plusieurs avantages par rapport ce derniers. Par exemple, ils offrent une meilleure stabilité thermique et leur rigidité est accrue. Le modèle le plus

simple des MWNT est sans doute celui des nanotubes à double parois (*de l'acronyme anglais double-walled nanotubes* DWNT) dans lequel seuls deux tubes de SWNT sont enroulés l'un dans l'autre (Figure 3) [10].

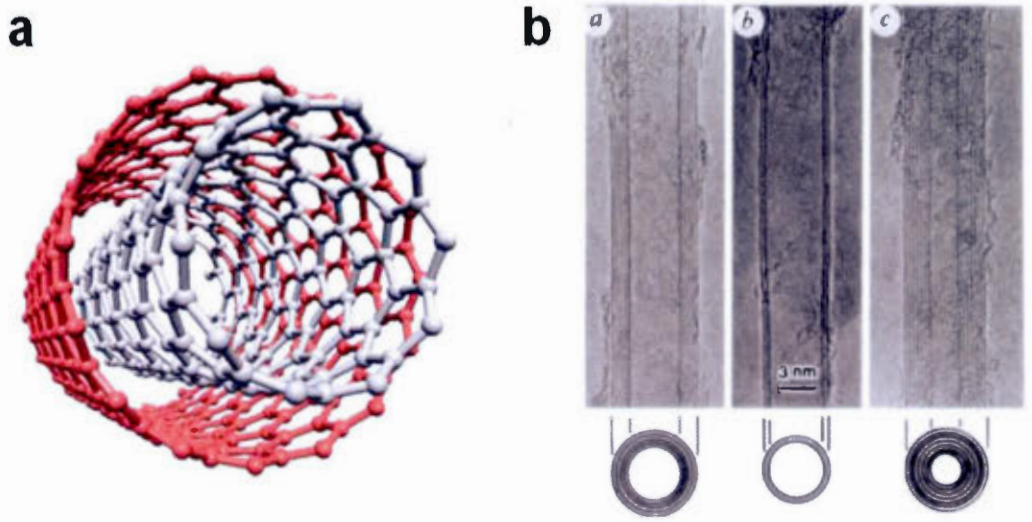

Figure 1.3 a DWNT comme modèle simple de MWNT [10], b observation par TEM des MWNT [3].

Au delà des structures de base des CNT, une panoplie de carbones nanoformes avec différents empaquetages ou enroulements ont été rapportés. Afin de faciliter la nomenclature de chacun des formes, l'arbre généalogique des CNT ci-dessous (Figure 4) résume les relations topologiques entre chacun d'eux [11].

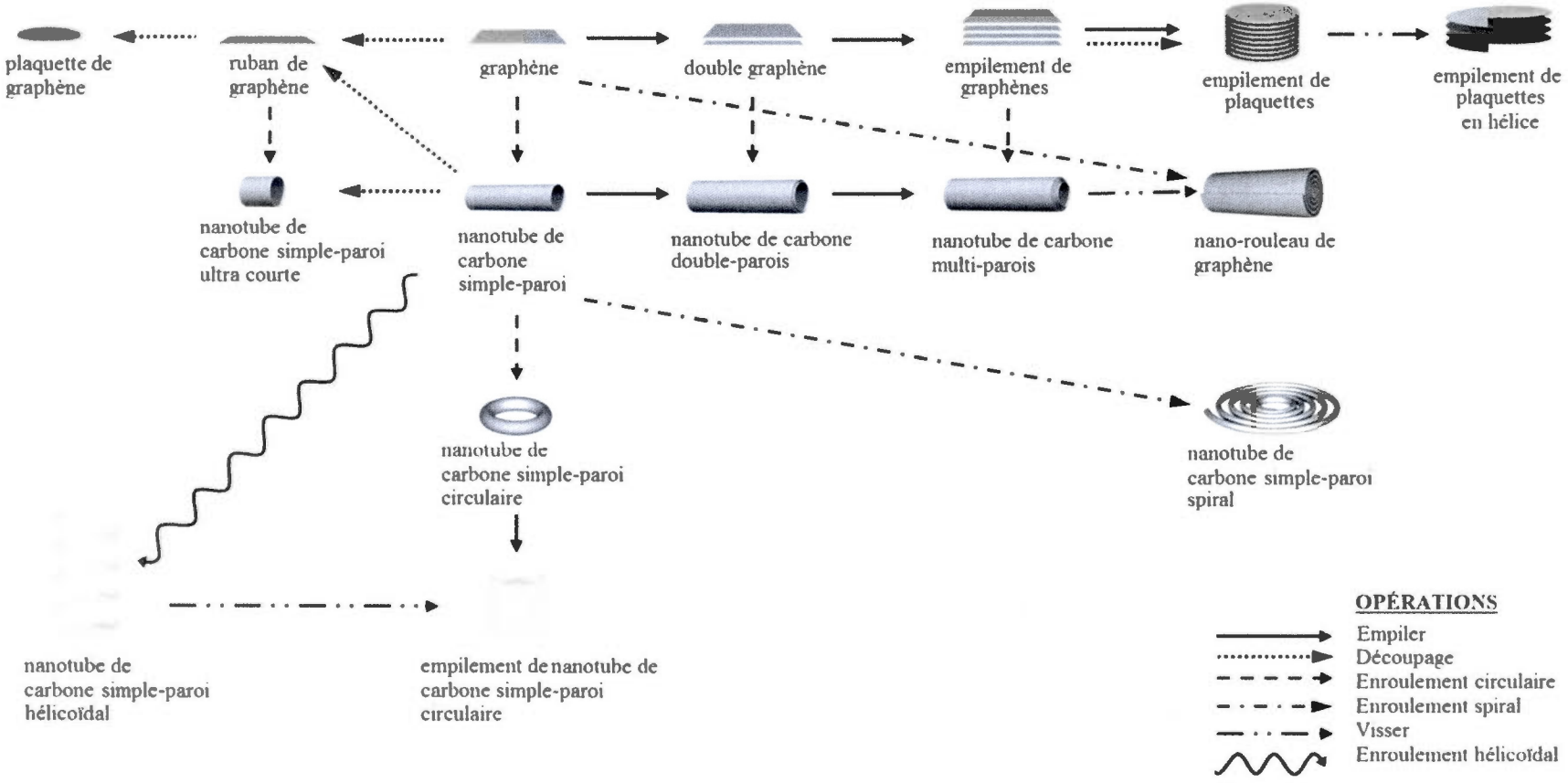

Figure 1.4 Arbre généalogique des nanotubes primaires montrant les relations topologique entre eux [11]

1.3 La synthèse des CNT

Les CNT peuvent être synthétisés par divers procédés qui ont tous des ingrédients communs incontournable: une source de carbone sous forme solide ou gazeux, un catalyseur métallique nanoparticulaire et une source d'énergie souvent sous forme de chaleur. La plupart de ces techniques dérivent de celles utilisées pour la production des fullerènes. Ainsi, les synthèses des CNT peuvent être regroupées en trois principales catégories: la décharge d'arc, l'ablation laser et la déposition chimique en phase vapeur (CVD). Chacun de ces techniques possèdent leurs avantages et leurs inconvénients.

1.3.1 Décharge d'arc

La décharge d'arc est la première méthode de production des CNT reportée par Iijima en 1991 [3]. C'est la technique qui utilise la température la plus élevée, supérieure à 1700°C, et qui créée le moins de défauts structurels lors de la croissance des tubes. Dans ce procédé, une décharge d'arc électrique est générée entre deux électrodes de graphite sous une atmosphère d'Hélium ou d'Argon. La haute température conduit à la sublimation du carbone et à une croissance des CNT sur la cathode (Figure 5). La croissance des CNT par décharge d'arc peut être réalisée avec ou sans catalyseurs métalliques. D'une manière générale, les MWNT peuvent être obtenus sans catalyseur. Par contre, les anodes à base de métaux de transition (Nickel, Cobalt, Palladium, Argent, Platine...) sont souvent utilisées pour la production des MWNT [12].

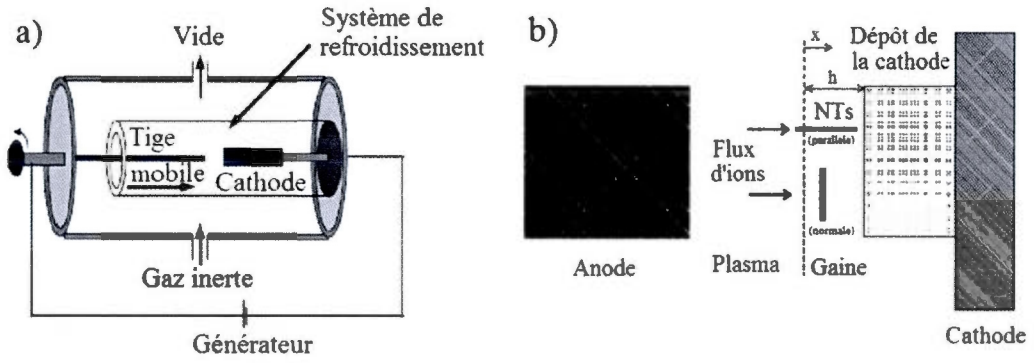

Figure 1.5 a Représentation schématique de la méthode par décharge d'arc utilisée à l'Université de Montpellier, b Décharge d'arc et formation de CNT sur les électrodes [12].

1.3.2 Ablation laser

L'ablation laser est la seconde méthode utilisée pour la production des CNT. Cette technique est connue pour permettre de meilleurs contrôles sur la structure des CNTs ainsi produits. Les premiers SWNT ont été développés par Smalley *et al* en 1995 [13] par cette technique. Son principe consiste à évaporer du graphite par une irradiation laser sous atmosphère inerte. Le réarrangement des fragments de carbone en présence des catalyseurs métalliques tels que le Nickel ou le Cobalt permet ainsi l'obtention des CNT de haute qualité. L'ensemble de la synthèse est réalisée dans un tube en quartz à une température de l'ordre de 1200°C (Figure 6) [12].

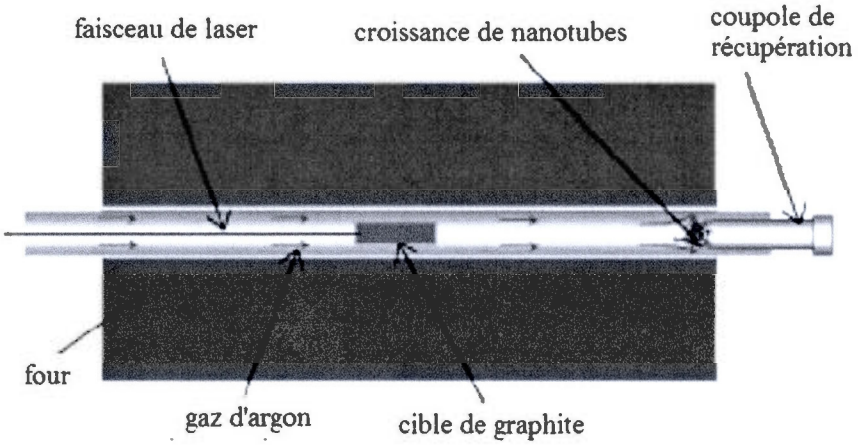

Figure 1.6 Représentation schématique de la méthode d'ablation laser [12] .

1.3.3 Dépôt chimique en phase vapeur (CVD)

Le dépôt chimique en phase vapeur (CVD) est la technique standard pour la production des CNT en grande quantité. Malgré la présence des impuretés dans le produit final, cette méthode est plus souvent utilisée par les industriels en raison de son coût de production plus faible. La technique consiste à véhiculer une source de carbone gazeuse tels l'acétylène, l'éthylène, l'éthanol ou le méthane par un gaz inerte dans un four entre 500 à 1000°C. La précipitation et le réarrangement des carbones à la surface des catalyseurs métallique permettent une croissance tubulaire des CNT. Ainsi les CNT obtenus vont dépendre du type et de la taille du catalyseur, le temps et la température de croissance ainsi que la source de carbone choisie. Par exemple, l'obtention des MWNT par la

méthode de CVD nécessite une dispersion nanoparticulaire des catalyseurs métallique de l'ordre de 1-3nm [12].

1.3.4 Autres méthodes et purification des CNT

En dehors des trois principales méthodes principales citées ci-dessus, la production des CNT peut être réalisée par d'autres techniques plus exotiques. Citons, par exemple, l'utilisation du four solaire [14], la méthode de la torche à plasma [15-16], l'électrolyse [17] ou la pyrolyse solide [18].

Cependant la production des CNT est toujours accompagnée de la présence des impuretés dont les catalyseurs métallique et le carbone amorphe. Aussi, les CNT peuvent être recuits à haute température [19] ou être oxydés en milieu acide [20-21] afin d'éliminer les produits secondaires indésirables. De plus, dans un même échantillon, les dimensions et les structures des SWNT sont souvent très variables. Ainsi Hersam *et al* [22-25] ont développé des méthodes de séparation des CNT par ultracentrifugation à gradient de densité. Les CNT peuvent être isolés en fonction de leur taille ainsi que de leur structure électronique. La figure ci-dessous (Figure 7) montre un exemple de l'isolation des SWNT semi-conducteurs et métalliques par rapport aux DWNT. Ainsi la purification et la séparation des CNT permettent l'isolation des SWNT de haute pureté.

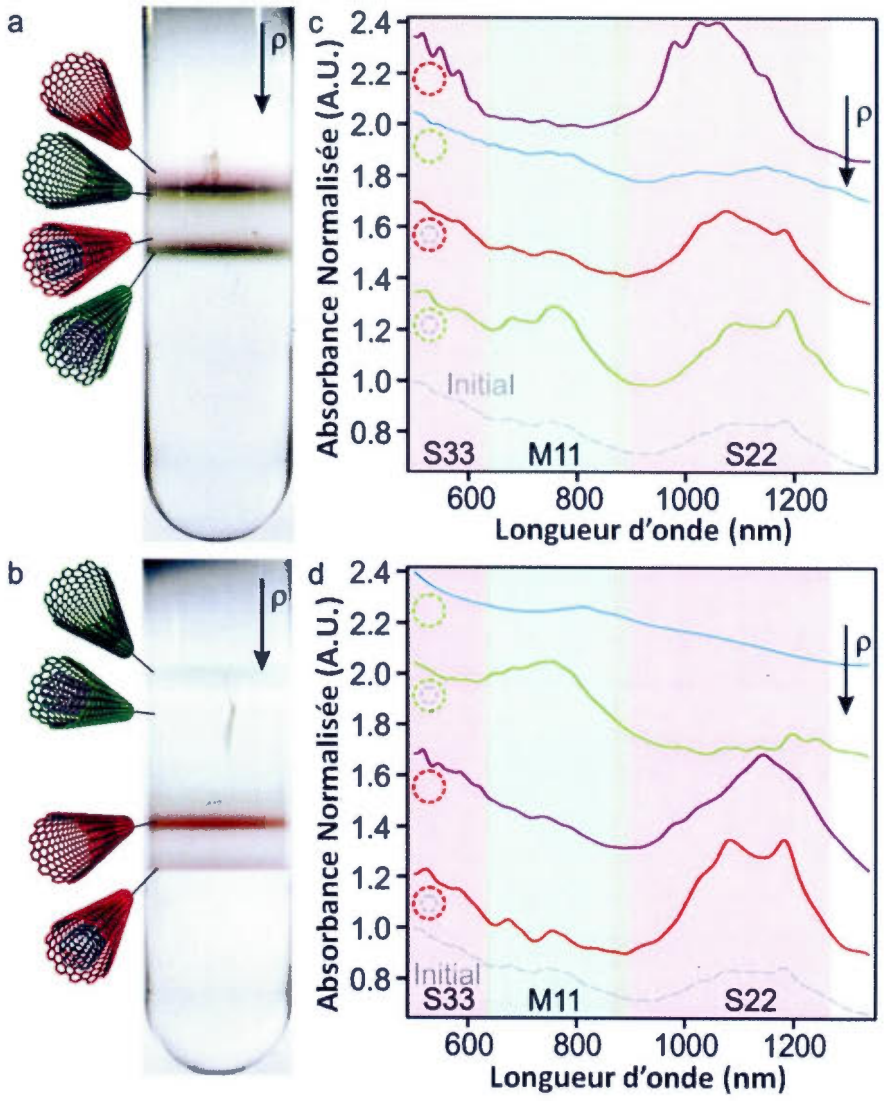

Figure 1.7 Séparation des SWNT/DWNT par ultracentrifugation à gradient de densité. (a) isolation du SWNT et du DWNT. (b) isolation du SWNT métallique du semi-conducteur. (c,d) Spectres d'absorbance de chacun des tubes correspondants [22].

1.4 Propriétés et applications des CNT

Depuis le papier d'Iijima [3], les nanomatériaux à base de carbone ont fait l'objet d'études dans de nombreux domaines en raison de leurs propriétés exceptionnelles mécaniques, électriques, photoélectriques et thermiques. Les CNT peuvent être d'excellents conducteurs de courant à cause de la présence d'électrons π tout au long du tube.

L'absence de dissipation par effet Joule permet aux CNT de supporter une densité de courant supérieure à $10^9 A/cm^2$ [26-27]. Le caractère semi-conducteur des SWNT est caractérisé par une bande interdite de 0,25 à 1,81 eV en fonction de leur chiralité [28]. Les CNT sont également de bons conducteurs de phonons. Une conductivité thermique de 200 W/mK a été mesurée par Hone *et al* [29]. En comparaison au graphite, les CNT ont également une résistance mécanique supérieure. Les mesures traction effectuées par microscopie à force atomique (AFM) montrent un module de Young variant entre 0,27 et 0,95 TPa pour les MWNT [30].

Compte tenu des propriétés exceptionnelles des CNT, ces derniers sont souvent utilisés comme renforcement mécanique, semi-conducteur électrique et conducteur thermique. Sur cette base, de nombreuses applications industrielles ont été développées: renforcement mécanique de matrices polymériques, incorporation dans des dispositifs électroniques, stockage d'hydrogène, dispositifs à émission de champs, capteurs et sondes... [31].

1.5 Dispersion des CNT

De nombreuses applications potentielles ont été proposées pour les CNT [12, 32]. Comme la synthèse de ces nanomatériaux est réalisée principalement par la croissance de carbone en phase solide (section 1.3), ce « matériau insoluble », tel que qualifié par Iijima,[3] est très peu soluble dans la plupart des solvants conventionnels. Or, les applications nécessitent souvent une bonne séparation des chacun des tubes dans une matrice solide ou liquide, ainsi de nombreux effort sont consacrés à la dispersion des CNT en milieu aqueux et organique. La fonctionnalisation chimique a été largement employée pour la solubilisation des CNT [33]. Cependant, cette modification de surface par des liaisons covalentes détériore les propriétés intrinsèques des CNT, en particulier pour les SWNT. Une méthode alternative est basée sur les interactions non covalentes entre les tensioactifs et la surface des CNT [34]. Cependant les dispersions des CNT dans l'eau comme tout autre système colloïdal sont des états thermodynamiquement métastables. Les CNT sont séparés du liquide par une interface solide/liquide d'où la présence d'une tension superficielle. Cette dernière tend de minimiser la surface de

contact avec le solvant afin de réduire l'énergie totale du système. Ainsi, tout processus de dispersion colloïdale se termine par une floculation des CNT. L'insertion des dispersants amphiphiles à l'interface CNT/liquide permet justement de réduire cette tension superficielle. La stabilité colloïdale des CNT relève le défi principal dans l'application industrielle de ces nanomatériaux. Le choix des tensioactifs doit être optimisé afin de répondre aux contraintes imposées par le procédé industriel. Par exemple, le cisaillement mécanique, la variation de température, l'ajout des ions et le séchage sont des processus qui mènent facilement à une floculation des CNT. Un dispersant de CNT en milieu aqueux doit en général comprendre deux composantes: une partie hydrophile qui stabilise la dispersion dans le solvant et une partie hydrophobe qui est adsorbée à la surface des CNT.

1.5.1 Stabilisation des CNT

Les deux principaux mécanismes de stabilisation sont : la stabilisation électrostatique et la stabilisation stérique

En milieu aqueux, les répulsions créées par les tensioactifs anioniques, et moins couramment cationiques, sont définies comme la stabilisation électrostatique. Avec le tensioactif chargé, les CNT sont recouverts d'une couche électrique formée par la charge de celui-ci et de son contre ion. Il est en général admis que les deux surfaces chargées négativement se repoussent, ce qui est à l'origine de la stabilisation électrostatique [35]. En fait, une analyse plus récente montre que lorsque deux surfaces chargées s'approchent, l'énergie électrostatique de l'ensemble du système avec leur contre ions est attractive. Cependant l'approche de ces deux surfaces résulte en une zone où la concentration de charges est très grande, ce qui thermodynamiquement défavorable (l'eau va essayer de diluer les charges par effet osmotique) [36]. Ce phénomène de pression osmotique constitue alors une barrière énergétique qui est à l'origine de la métastabilité colloïdale prédis par la théorie de Derjaguin, Landau, Verwey et Overbeek (DLVO). Selon cette théorie, qui se base sur l'explication 'ancienne' que les surfaces chargées négativement se repoussent, les forces mises en jeu entre les CNT sont à la fois attractives et répulsives. L'énergie totale V_T du système peut être décrite comme étant la

somme de la contribution attractive V_A, répulsive V_R ainsi que le potentiel de répulsion de Born V_B.

$$V_T = V_A + V_R + V_B \quad (2)$$

A très courte distance, les électrons orbitalaires forment un mur de potentiel appelé répulsion de Born (V_B). L'énergie potentielle de cette répulsion varie selon une expression de fonction $1/D^{14}$ où D représente la distance qui sépare les deux surfaces. Ainsi, la répulsion de Born est négligeable dans les systèmes colloïdaux où la séparation de surface est de l'ordre de quelques nanomètres, mais se fait sentir à une distance de 1 Angstrom ou moins. La stabilité colloïdale dépend principalement de l'équilibre entre l'attraction de Van der Waals (V_A) et le potentiel de répulsion électrostatique (V_R) d'expression :

$$V_R = \frac{64\pi c_0 r k_B T}{K^2} \gamma^2 e^{-KD} \quad (3)$$

c_0 concentration en électrolytes (mol/L)

K^{-1} longueur de Debye (m)

γ tension superficielle (N/m)

La théorie de DLVO suggère que l'énergie totale d'interaction entre deux colloïdes est la somme de toutes les interactions qui sont représentées dans la figure suivante (Figure 8).

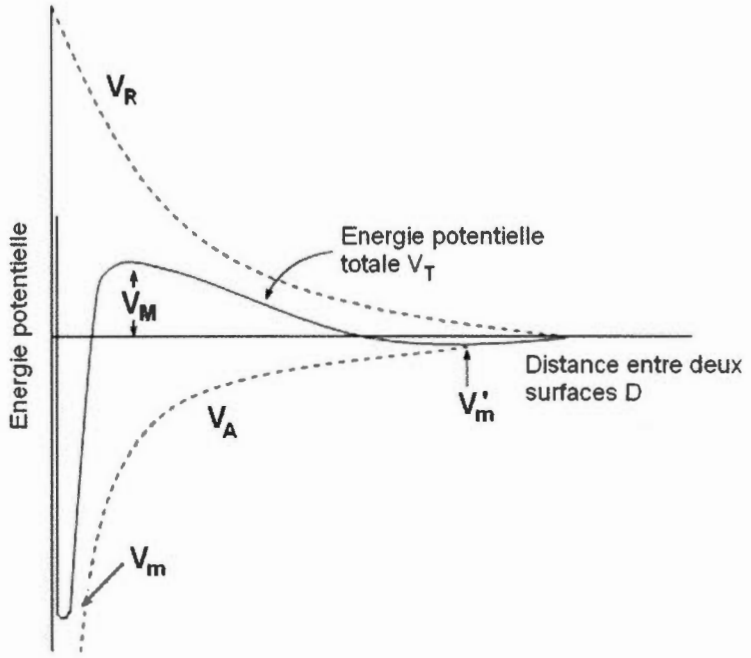

Figure 1.8 Diagramme du potentiel total d'interaction entre 2 surfaces en fonction de la distance D.

Le premier minimum sur la courbe, appelé minimum primaire (V_m) représente la distance d'approche minimale entre les deux surfaces. C'est un état thermodynamiquement stable où la floculation des CNT est irréversible - il se situe à une distance de l'ordre de 1 nm (suivant les conditions). Le maximum primaire (V_M) constitue la barrière énergétique de flocculation - le système est stable si cette barrière est largement supérieur à l'énergie thermique, d'une manière générale, lorsque V_M est supérieur à $10k_BT$ (k_B = 1,38.10^{-23} J/K). Le minimum secondaire (V_m') reflète la décroissance exponentielle de la répulsion électrostatique qui se caractérise par une floculation réversible. Ce minimum est souvent très peu profond par rapport à l'énergie thermique, et par conséquent, les colloïdes sont libres d'en sortir. Néanmoins, il est bon de se rappeler que deux colloïdes, même dans un état de stabilité colloïdale, ont tendance à se rapprocher afin de se trouver dans un minimum secondaire. Ce phénomène est souvent observé, par exemple en microscopie électronique, on observe plus souvent des particules formant des 'amas' ou des 'colliers' que des particules isolées. En diffusion dynamique de la lumière, il est souvent nécessaire

d'agiter le milieu (au moyen d'un bain sonicateur) afin de séparer les particules qui sont piégées dans ce minimum secondaire. La distance caractéristique de ce minimum secondaire dépend des conditions, en particulier de la force ionique - elle peut être de quelques nanomètres jusqu'à des dizaines de nanomètres, par exemple dans le cas des cristaux colloïdes. Ainsi, les principales forces qui assurent la dispersion dépendent des conditions ioniques de la phase aqueuse. L'ajout d'ions en solution réduit significativement la pression osmotique de la surface chargée et permet ainsi à l'agrégation des CNT en solution. En effet, l'introduction d'ions diminue la longueur de Debye, K^{-1}, résultant en un écrantage de la surface, ce qui favorise le rapprochement des CNT. Néanmoins, l'ajout d'ions peut provoquer des effets plus complexes. En effet, des simulations informatiques [37] et nos mesures expérimentales [38] (voir chapitre II) ont démontré qu'en présence des sels, l'adsorption des tensioactifs anioniques est plus importante à la surface des CNT car l'écrantage diminue la répulsion électrostatique entre deux tensioactifs adjacents, ce qui permet de diminuer leur distance de séparation.

Dans les cas de la stabilisation stérique, les dispersants utilisés en milieu aqueux portent à la fois des groupements apolaires et des groupements polymériques polaires (en général non ionisés). Lors de la dispersion, la partie hydrophobe est adsorbée sur le CNT, alors que la partie hydrophile est orientée vers le solvant. Ainsi, les macromolécules déployées jouent le rôle de 'pare-chocs' et tendent à maintenir les CNT séparés. Cette stabilisation résulte d'un phénomène mécanique. Cela signifie que les forces de répulsion n'apparaissent que lorsque les deux surfaces entrent en contact. Lorsque les couches polymériques s'interpénètrent, un effet osmotique causé par la forte concentration locale de polymère provoque une diffusion de solvant ce qui tend à séparer de nouveau les surfaces. Un second effet, élastique, est causé par la compression de la couche de polymère, ce qui conduit à une diminution de l'entropie des chaînes suite à la baisse du nombre de conformations qu'elles peuvent atteindre. Ces deux effets constituent ainsi la barrière énergétique d'une stabilisation stérique. Cependant, la couche stérique doit être suffisamment épaisse pour que l'interaction de Van der Waals soit négligeable à cette distance. La figure ci-dessous (Figure 9) représente le potentiel de stabilisation par effet stérique en fonction de la distance entre deux surfaces.

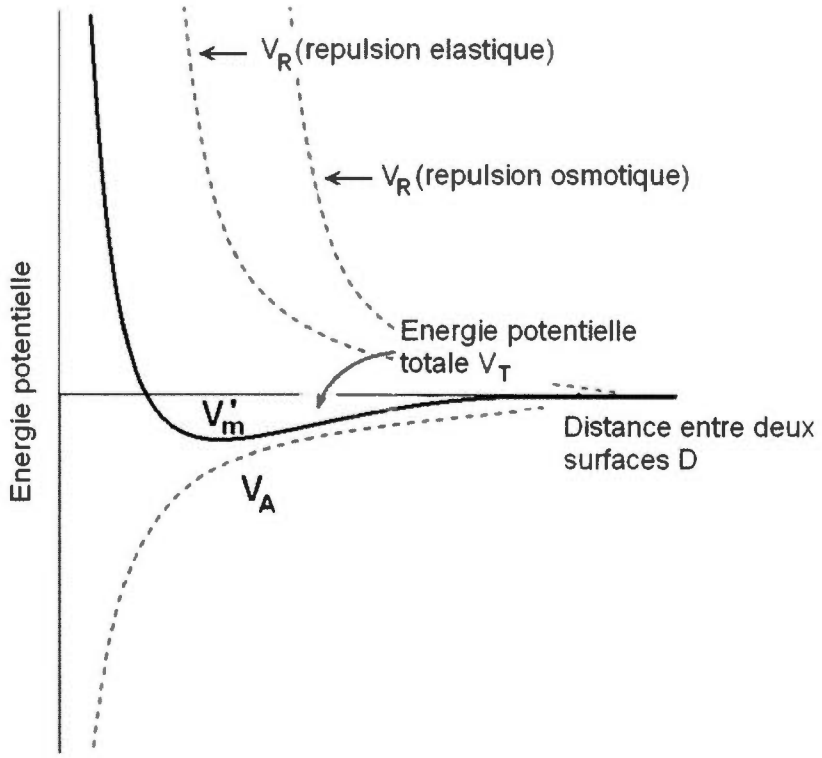

Figure 1.9 Diagramme du potentiel total de répulsion stérique entre 2 surface en fonction de la distance D.

Le mode de stabilisation stérique permet d'offrir une stabilité colloïdale en présence de solutions concentrées en électrolytes. De plus, dans certains cas, la floculation d'un système pourvu d'une stabilisation stérique efficace est réversible et le système peut être alors thermodynamiquement stable.

Notons enfin l'existence d'une stabilisation électrostérique, qui se produit lorsque des polymères amphiphiles avec une partie hydrophile chargée plusieurs fois sont utilisés pour stabiliser le système.

1.5.2 Adsorption des tensioactifs

La théorie de la stabilité colloïdale est principalement décrite par des phénomènes de répulsion électrostatique et stérique. Pour cela, il faut que le tensioactif, ou plus généralement le dispersant, soit adsorbé à la surface du CNT. Comme les parois des CNT sont essentiellement constituées de carbone d'hybridation sp^2, l'interaction entre les

surfaces graphitiques et les dispersants est principalement de type hydrophobe dans l'eau, mais les interactions π–π peuvent aussi jouer un rôle. Pour un tensioactif, il existe un équilibre entre deux états, libre et adsorbé. L'isotherme d'adsorption le plus simple, dit isotherme de Langmuir, traduit la présence de cet équilibre :

$$\Gamma = \frac{\Gamma_S \, C_{free}}{C_{free} + a} \qquad (4)$$

dans lequel Γ et Γ_s sont respectivement les taux de couverture de la surface de CNT en présence de la concentration C_{free} de tensioactif libre et lorsque la surface est saturée. La constante a, en $mol.L^{-1}$, est la constante d'équilibre de désorption. Elle est égale à la concentration de tensioactif nécessaire pour couvrir 50% de la surface du CNT. Plus cette constante est grande, moins le tensioactif présente d'affinité pour la surface [39].

Le modèle d'adsorption de Langmuir est le plus simple, et ne s'applique que lorsqu'un seul type de site d'adsorption et une seule molécule de dispersant sont présents dans le système. A l'exemple du dodécylsulfate de sodium (SDS), des études de modélisation [37] ont démontré que le tensioactif anionique s'adsorbe avec le groupement alkyle le long de la paroi des SWNT. Cependant, à plus haute concentration, le SDS forme des hémi-micelles sur la surface, en particulier pour les SWNT en raison de leur rayon de courbure plus élevé. La figure ci-dessous (Figure 8) modélise l'adsorption du SDS à la surface des CNT en fonction de leur rayon de courbure [37].

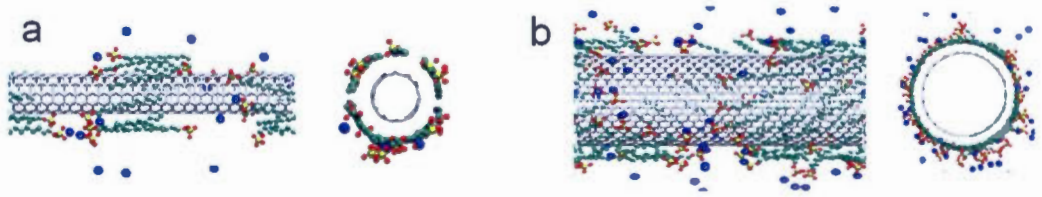

Figure 1.10 Adsorption des SDS sur les nanotubes (a) SWNT de diamètre 1,2nm. (b) SWNT de diamètre 15 nm [37].

D'après la littérature [34], les MWNT semblent être plus stable en présence des dispersants polymériques qu'avec des tensioactifs classiques. En effet, les longues

chaines hydrophobes permettent de s'enrouler le long du tube malgré le grand rayon de courbure du tube. Ainsi, la longueur et la structure de la chaine alkyle sont des paramètres importants de l'adsorption. De plus, les dispersants contenants des groupements aromatiques sont plus adhérents sur la surface des CNT de par la présence d'interactions π–π. Ainsi, la comparaison entre le SDS et le sodium dodécyl benzène sulfonate (SDBS) sur les SWNT a démontré que les chaînes alkyle portant des groupements phényle possèdent une meilleure efficacité d'adsorption [40]. Les principales études sur la dispersion des CNT par les tensioactifs sont décrites dans l'introduction du chapitre II. Ce chapitre est un article qui vient de paraître dans le journal « Carbon ».

Selon la littérature [41], l'adsorption des tensioactifs non-ioniques due aux interactions hydrophobes est principalement endothermique. Cette variation de température se manifeste par l'augmentation de l'entropie ΔS causée par l'expulsion des molécules d'eau à la surface des CNT. Cependant, la variation d'entropie semble être inversée en présence des tensioactifs anioniques et cationiques. Ce phénomène peut être expliqué par la formation de la double couche chargée où la diffusion des contre-ions contribue à la diminution de l'entropie ΔS sur l'ensemble du système.

1.6 Polymérisation RAFT

Malgré la simplicité de sa préparation, une dispersion de CNT en milieu aqueux est souvent influencée par des paramètres physico-chimiques qui mènent à sa floculation. Ainsi de nouvelles stratégies se sont développées pour préparer des nanomatériaux hybrides fonctionnels à base de CNT. Une de ces stratégies consiste à encapsuler les CNT par une écorce polymérique. Dans le chapitre III, nous allons présenter une technique d'encapsulation des CNT via le procédé de polymérisation contrôlée appelée Reversible Addition-Fragmentation chain Transfer (RAFT). L'introduction du chapitre III, qui est une publication du Journal of Polymer Science - Polymer Chemistry, présente les principales voies d'encapsulation des CNT par des polymères. Dans ce paragraphe nous allons introduire les principales caractéristiques de la polymérisation RAFT.

La polymérisation RAFT est la technique la plus récente de polymérisation radicalaire vivante ou contrôlée [42]. Elle permet de synthétiser des polymères d'architecture contrôlée de faible polymolécularité et elle s'applique à un grand nombre de monomères fonctionnels tel que l'acétate de vinyle [43] ou l'acide acrylique [44].

La technique a été développée par l'équipe de CSIRO (*Commonwealth Scientific and Industrial Research Organisation*) sous la direction de Rizzado en 1998 [43]. Le procédé de RAFT emploie une approche de croissance des chaînes différente par rapport aux deux autres techniques, la nitroxide-mediated polymerization (NMP) et à l'atom transfer radical polymerization (ATRP). Contrairement à l'ATRP et à la NMP où la croissance des chaînes est basée sur un équilibre rapide entre un état actif et un état dormant, la polymérisation RAFT utilise un équilibre de transfert réversible aussi appelé transfert dégénératif (Schéma 1). Au départ, les chaines sont amorcées par un amorceur radicalaire usuel. Des chaînes en croissance vont donc apparaitre, et réagir avec un agent de transfert spécifique appelé agent RAFT. Le choix de l'agent RAFT est tel que la chaine transférée après réaction avec l'agent RAFT est elle-même un agent RAFT. Ainsi la concentration d'agent RAFT dans le domaine demeure constante. Les agents de transfert RAFT contiennent tous une fonction thiocarbonylthio (schéma 1). Lors du transfert, une chaîne en croissance (Pn•) s'additionne sur la fonction thiocarbonylthio pour former un radical intermédiaire. Celui-ci se fragmente pour générer un groupe partant (R•) qui permet à son tour de continuer la propagation (Pm•). Comme la fonction thiocarbonylthio est un excellent agent de transfet, l'équilibre entre P_n• et P_m• est rapide. Il existe donc un équilibre entre chaines transférées et chaines actives, ce qui permet à toutes les chaines de croitre en même temps, à condition que la proportion de chaînes vivantes injectées dans le système tout au long de la réaction par la décomposition de l'amorceur demeure faible par rapport à la quantité d'agent RAFT. Lorsque cette condition est respectée, toutes les chaînes croissent en même temps, et donc leur indice de polymolécularité est bas.

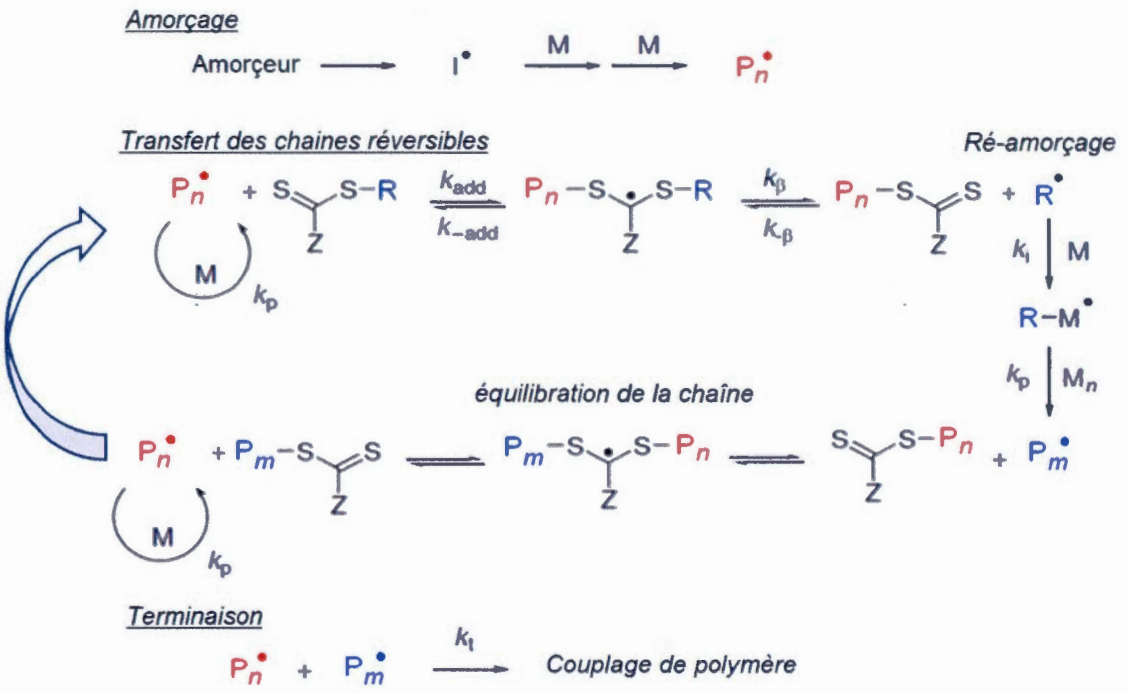

Figure 1.11 Mécanisme réactionnel de la polymérisation RAFT [44].

Des études cinétiques [46] sur la polymérisation RAFT ont démontré que malgré la complexité de la croissance des chaînes, la vitesse de la propagation peut être résumée en une cinétique d'ordre 1. Cependant, la vitesse est grandement réduite comparée aux polymérisations classiques et elle nécessite un apport d'énergie additionnel afin de favoriser le départ du groupe partant. La vitesse de polymérisation est également dépendante de la nature du groupement Z porté par l'agent RAFT. Ainsi, de nombreux groupement Z ont été synthétisé : dithioesters aromatiques et aliphatiques, trithiocarbonates, xanthates et dithiocarbamates. Plus le groupement Z stabilise le radical intermédiaire, plus la fragmentation est lente, et plus la cinétique de polymérisation est lente. Par contre, plus le radical intermédiaire est stable, meilleur est l'agent de transfert RAFT. Aussi, il existe un compromis entre cinétique de polymérisation et caractère contrôlé de la polymérisation : les polymérisations les plus lentes donnant lieu au meilleur contrôle (Figure 11). La figure ci-dessous (Figure 11) [45] représente l'activité relative de l'agent de transfert (CTA) selon l'effet stabilisant du groupement activateur (Z). On voit ainsi que les meilleurs groupements stabilisateurs sont les dithioesters

aromatiques, suivi des trithiocarbonates. Ce sont ces derniers que nous allons utiliser dans notre travail.

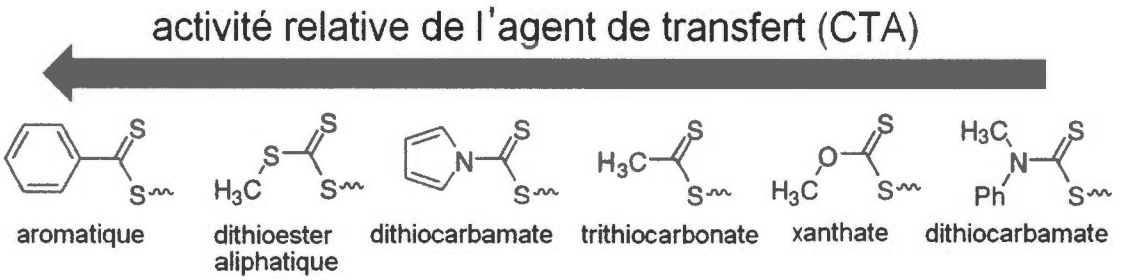

Figure 1.12 L'activité relative du CTA en fonction du groupement activateur (Z) [45].

La polymérisation RAFT peut être employée comme une polymérisation vivante - pour cela, il faut que toutes les chaînes croissent en même temps, et que le nombre de chaînes reste constant. Cette dernière condition se produit lorsque la concentration d'amorceur est faible (en général, inférieur à 10%) par rapport à la concentration d'agent RAFT. Suivant ce mécanisme, le laboratoire Claverie a dans le passé mis au point des conditions permettant la formation de polymères vivants de polyacide acrylique [47-48], et de copolymères d'acide acrylique et d'acrylate de butyle [49-50]. Si la concentration d'amorceur est élevée, alors la polymérisation donne lieu à la formation d'un mélange de chaines mortes et vivantes. La polymérisation RAFT est souvent utilisée pour la formation de copolymères diblocs. Dans ce cas, on démarre la polymérisation du deuxième monomère avec un agent RAFT macromoléculaire formé du premier monomère. Lorsque l'on travaille en présence d'un excès d'amorceur (afin d'avoir une cinétique de polymérisation acceptable), alors la polymérisation résulte en la formation de copolymères diblocs mélangés avec des homopolymères formés par le second monomère. Notre travail a été effectué dans ces conditions : aussi, il est normal que les polymères que nous avons formé n'aient pas des indices de polydispersité faibles.

1.7 Bibliographie

[1] Schmidt P, Avery DH. Complex Iron Smelting and Prehistoric Culture in Tanzania. Science, 1978;201(4361):1085-9.

[2] Kroto HW, Heath JR, O'Brien SC, Curl RF, Smalley RE. C60: Buckminsterfullerene. Nature. 1985;318(6042):162-3.

[3] Iijima S. Helical microtubules of graphitic carbon. Nature. 1991;354(6348):56-8.

[4] Iijima S, Ichihashi T. Single-shell carbon nanotubes of 1-nm diameter. Nature. 1993;363(6430):603-5.

[5] Geim AK. Graphene: Status and prospects. Science. 2009;324(5934):1530-4.

[6] Monthioux M, Kuznetsov VL. Who should be given the credit for the discovery of carbon nanotubes? Carbon. 2006;44(9):1621-3.

[7] Radushkevich L, Lukyanovich V. Zh Phys Khim. 1952;26:88.

[8] Oberlin A, Endo M, Koyama T. Filamentous growth of carbon through benzene decomposition. Journal of Crystal Growth. 1976;32(3):335-49.

[9] Bethune DS, Kiang CH, De Vries MS, Gorman G, Savoy R, Vazquez J, et al. Cobalt-catalysed growth of carbon nanotubes with single-atomic-layer walls. Nature. 1993;363(6430):605-7.

[10] Prasek J, Drbohlavova J, Chomoucka J, Hubalek J, Jasek O, Adam V, et al. Methods for carbon nanotubes synthesis - Review. Journal of Materials Chemistry. 2011;21(40):15872-84.

[11] Suarez-Martinez I, Grobert N, Ewels CP. Nomenclature of sp 2 carbon nanoforms. Carbon. 2012;50(3):741-7.

[12] Paradise M, Goswami T. Carbon nanotubes – Production and industrial applications. Materials & Design. 2007;28(5):1477-89.

[13] Guo T, Nikolaev P, Thess A, Colbert DT, Smalley RE. Catalytic growth of single-walled manotubes by laser vaporization. Chemical Physics Letters. 1995;243(1–2):49-54.

[14] Journet C, Bernier P. Production of carbon nanotubes. Applied Physics A: Materials Science & Processing. 1998;67(1):1-9.

[15] Smiljanic O, Larouche F, Sun X, Dodelet JP, Stansfield BL. Synthesis of single-walled carbon nanotubes (C-SWNTs) with a plasma torch: A parametric study. Journal of Nanoscience and Nanotechnology. 2004;4(8):1005-13.

[16] Chen C-K, Perry WL, Xu H, Jiang Y, Phillips J. Plasma torch production of macroscopic carbon nanotube structures. Carbon. 2003;41(13):2555-60.

[17] Hsu WK, Li J, Terrones H, Terrones M, Grobert N, Zhu YQ, et al. Electrochemical production of low-melting metal nanowires. Chemical Physics Letters. 1999;301(1–2):159-66.

[18] Li YL, Yu YD, Liang Y. A novel method for synthesis of carbon nanotubes: Low temperature solid pyrolysis. Journal of Materials Research. 1997;12(7):1678-80.

[19] Bandow S, Asaka S, Zhao X, Ando Y. Purification and magnetic properties of carbon nanotubes. Applied Physics A: Materials Science & Processing. 1998;67(1):23-7.

[20] Rinzler AG, Liu J, Dai H, Nikolaev P, Huffman CB, Rodríguez-Macías FJ, et al. Large-scale purification of single-wall carbon nanotubes: process, product, and characterization. Applied Physics A: Materials Science & Processing. 1998;67(1):29-37.

[21] Stobinski L, Lesiak B, Kövér L, Tóth J, Biniak S, Trykowski G, et al. Multiwall carbon nanotubes purification and oxidation by nitric acid studied by the FTIR and electron spectroscopy methods. Journal of Alloys and Compounds. 2010;501(1):77-84.

[22] Green AA, Hersam MC. Properties and Application of Double-Walled Carbon Nanotubes Sorted by Outer-Wall Electronic Type. ACS Nano. 2011;5(2):1459-67.

[23] Antaris AL, Seo J-WT, Green AA, Hersam MC. Sorting Single-Walled Carbon Nanotubes by Electronic Type Using Nonionic, Biocompatible Block Copolymers. ACS Nano. 2010;4(8):4725-32.

[24] Green AA, Hersam MC. Ultracentrifugation of single-walled nanotubes. Materials Today. 2007;10(12):59-60.

[25] Arnold MS, Green AA, Hulvat JF, Stupp SI, Hersam MC. Sorting carbon nanotubes by electronic structure using density differentiation. Nature nanotechnology. 2006;1(1):60-5.

[26] Collins PG, Hersam M, Arnold M, Martel R, Avouris P. Current saturation and electrical breakdown in multiwalled carbon nanotubes. Physical Review Letters. 2001;86(14):3128-31.

[27] Yao Z, Kane CL, Dekker C. High-field electrical transport in single-wall carbon nanotubes. Physical Review Letters. 2000;84(13).

[28] Si HG, Wang YX, Yan YL, Zhang GB. Structural, Electronic, and Thermoelectric Properties of InSe Nanotubes: First-Principles Calculations. The Journal of Physical Chemistry C. 2012;116(6):3956-61.

[29] Hone J, Llaguno MC, Biercuk MJ, Johnson AT, Batlogg B, Benes Z, et al. Thermal properties of carbon nanotubes and nanotube-based materials. Applied Physics A: Materials Science & Processing. 2002;74(3):339-43.

[30] Yu MF, Lourie O, Dyer MJ, Moloni K, Kelly TF, Ruoff RS. Strength and breaking mechanism of multiwalled carbon nanotubes under tensile load. Science. 2000;287(5453):637-40.

[31] Baughman RH, Zakhidov AA, De Heer WA. Carbon nanotubes - The route toward applications. Science. 2002;297(5582):787-92.

[32] Coleman JN, Khan U, Blau WJ, Gun'ko YK. Small but strong: A review of the mechanical properties of carbon nanotube-polymer composites. Carbon. 2006;44(9):1624-52.

[33] Homenick CM, Lawson G, Adronov A. Polymer grafting of carbon nanotubes using living free-radical polymerization. Polymer Reviews. 2007;47(2):265-90.

[34] Britz DA, Khlobystov AN. Noncovalent interactions of molecules with single walled carbon nanotubes. Chemical Society Reviews. 2006;35(7):637-59.

[35] Somasundaran P, Yu X, Krishnakumar S, Markovic B. Colloid Systems and Interfaces - Stability of Dispersions through Polymer and Surfactant Adsorption. Handbook of Surface and Colloid Chemistry, Second Edition: CRC Press; 2002.

[36] Cabane B. La stabilité colloïdale des latex. Les latex synthétiques: Lavoisier; 2006.

[37] Tummala NR, Striolo A. SDS Surfactants on Carbon Nanotubes: Aggregate Morphology. ACS Nano. 2009;3(3):595-602.

[38] Zhong W, Claverie JP. Probing the carbon nanotube-surfactant interaction for the preparation of composites. Carbon. 2013. 51:72-84

[39] Rosen MJ. Adsorption of Surface-Active Agents at Interfaces: The Electrical Double Layer. Surfactants and Interfacial Phenomena: John Wiley & Sons, Inc.; 2004. p. 34-104.

[40] Islam MF, Rojas E, Bergey DM, Johnson AT, Yodh AG. High Weight Fraction Surfactant Solubilization of Single-Wall Carbon Nanotubes in Water. Nano Letters. 2003;3(2):269-73.

[41] Wittrock C, Kohler H-H, Seidel J. Adsorption Enthalpies of Cationic and nonionic Surfactant on Silica Gel. 1. Isoteric Determination of Adsorption Enthalpies. Langmuir, 1996;12:5550-6.

[42] Barner-Kowollik C. Introduction. Handbook of RAFT Polymerization: Wiley-VCH Verlag GmbH & Co. KGaA; 2008. p. 1-4.

[43] Chiefari J, Chong YK, Ercole F, Krstina J, Jeffery J, Le TPT, et al. Living Free-Radical Polymerization by Reversible Addition−Fragmentation Chain Transfer: The RAFT Process. Macromolecules. 1998. 31(16):5559-62.

[44] Lai JT, Filla D, Shea R. Functional polymers from novel carboxyl-terminated trithiocarbonates as highly efficient RAFT agents. Macromolecules. 2002; 35(18):6754-6.

[45] Moad G, Barner-Kowollik C. The Mechanism and Kinetics of the RAFT Process: Overview, Rates, Stabilities, Side Reactions, Product Spectrum and Outstanding Challenges. Handbook of RAFT Polymerization: Wiley-VCH Verlag GmbH & Co. KGaA; 2008. p. 51-104.

[46] Junkers T, Lovestead TM, Barner-Kowollik C. The RAFT Process as a Kinetic Tool: Accessing Fundamental Parameters of Free Radical Polymerization. Handbook of RAFT Polymerization: Wiley-VCH Verlag GmbH & Co. KGaA; 2008. p. 105-49.

[47] Llauro MF, Loiseau J, Boisson F, Delolme F, Ladavière C, Claverie J. Unexpected end-groups of poly(acrylic acid) prepared by RAFT polymerization. Journal of Polymer Science, Part A: Polymer Chemistry. 2004;42(21):5439-62.

[48] Loiseau J, Doërr N, Suau JM, Egraz JB, Llauro MF, Ladavière C, et al. Synthesis and characterization of poly(acrylic acid) produced by RAFT polymerization. Application as a very efficient dispersant of CaCO3, Kaolin, and TiO2. Macromolecules. 2003;36(9):3066-77.

[49] Das P, Claverie JP. Synthesis of single-core and multiple-core core-shell nanoparticles by RAFT emulsion polymerization: Lead sulfide-copolymer nanocomposites. Journal of Polymer Science, Part A: Polymer Chemistry. 2012;50(14):2802-8.

[50] Das P, Zhong W, Claverie JP. Copolymer nanosphere encapsulated CdS quantum dots prepared by RAFT copolymerization: Synthesis, characterization and mechanism of formation. Colloid and Polymer Science. 2011;289(14):1519-33.

CHAPITRE II

ARTICLE SCIENTIFIQUE (FULL PAPER)

Probing the carbon nanotube-surfactant interaction for the preparation of composites

Weiheng Zhong, Jerome P. Claverie*

NanoQAM, Quebec Center for Functional Materials, Department of Chemistry, University of Quebec in Montreal, Succ Centre Ville, PO Box 8888, Montreal, QC, H3C3P8, Canada. Fax: 514 9874054 E-mail: claverie.jerome@uqam.ca

* claverie.jerome@uqam.ca

Carbon

Volume 51, January 2013, pages 72-84

Cet article de recherche porte sur l'étude des interactions entre les nanotubes de carbone (CNT) avec les tensioactifs usuels en milieu aqueux. Les isothermes de Langmuir sont tracés pour des tensioactifs anioniques, cationiques et non-ioniques. Les résultats expérimentaux nous montrent que l'adsorption des tensioactifs dépend de la température et de la présence des électrolytes. Mais d'autres paramètres tels le diamètre des CNT, la structure et la taille du tensioactif influencent aussi la stabilité colloïdale de la dispersion. Avec l'optimisation de la méthode de dispersion, des films de CNT sont préparés en présence de nanoparticules polymériques. Des mesures de conductivité sur ces films permettent de déduire le seuil de percolation du réseau de CNT au sein d'une matrice solide.

Ce chapitre est formé par un papier publié au journal « Carbon ». Les deux auteurs de cet article sont moi-même et Prof. Jérôme Claverie. Dans ce chapitre, tout le travail expérimental a été effectué par moi-même. Le manuscrit (incluant le matériel supplémentaire, Appendice A) a été rédigé par Jérôme Claverie et moi-même.

Abstract

Adsorption isotherms of four different surfactants, sodium dodecyl sulfate (SDS), sodium dodecyl benzyl sulfonate, benzethonium chloride and Triton X-100 were measured on multi-wall carbon nanotubes (MWCNT) in water. With the surfactant SDS, the isotherms were also measured on single-wall carbon nanotubes (SWCNT) as well as on MWCNT under various ionic strength and temperature conditions. The nature of the polar head had only little influence on adsorption which was mainly driven by hydrophobic interactions. However, the outcome of the dispersion experiment was dependent on the purity of the carbon nanotubes. Using these results, it was possible to prepare concentrated colloidaly stable dispersions of MWCNTs in water ($c = 32$ g/L). Conducting MWCNT/polymer composite films could then readily be prepared by simple formulation of the MWCNTs with a polymeric dispersion.

2.1 Introduction

Since the landmark paper by Ijima [1], carbon nanotubes (CNTs) have attracted tremendous attention due to their unique mechanical, electrical and thermal properties [2]. The exploitation of such properties has been a driving force for the preparation of composites whereby CNTs are dispersed within a solid matrix [3]. The characteristics of such composites are highly dependent on how well the CNTs are dispersed [4], with direct significance on electrical percolation threshold [5] and [6], mechanical properties [7], durability [8] and esthetical aspect [9]. Numerous strategies have been proposed to form CNT/polymer composites [10], many of which involve dispersing the CNTs into a liquid first, and later mixing the liquid dispersion to the solid matrix. When added to a liquid, CNTs will not spontaneously disperse: a mechanical device such as a sonicator or a microfluidizer needs to be used to overcome the van der Waals forces which hold the CNT bundles together [11]. This step is necessary, but it is not sufficient to insure long term colloidal stability of the liquid dispersion: this role is imparted to a stabilizing molecule. Numerous such stabilizers have been proposed in recent literature [12]. Despite this flurry of activity, few reports concentrate on determining colloidal forces which are at play during dispersion [13]. To our knowledge, key parameters such adsorption enthalpy and entropy of the stabilizer have not been experimentally determined, even for

the most simple and ubiquitous stabilizers such as common surfactants. Thus, the dispersion of CNTs often remains an art rather than a well-controlled and understood process. Uddin et al. [14] and Striolo et al. [15] and [16] used molecular simulations to predict the surface coverage of CNTs by the surfactants sodium dodecyl sulfate, SDS, and sodium dodecyl benzene sulfonate, SDBS. Using dissipative particle dynamics as a mesoscale modeling technique, Angelikopoulos et al. [17] and [18] studied the interaction of SDBS with CNT surfaces and highlighted the differences between the adsorption on isolated CNTs and on bundles of CNTs. Clark et al. [19] have experimentally determined several factors favoring the formation of a stable low-concentration CNT dispersion which could be filtered. Shin et al. [20] compared various surfactants, and found Igepal to be able to stabilize CNT dispersions of higher concentration. Several experimental methods have been used in the past in order to study the surfactant adsorption at a CNT surface. For example, Islam et al. [21] analyzed dried samples of aqueous dispersions of CNTs by atomic force microscopy to distinguish between bundles and isolated CNTs, and thus demonstrated that sonication did not significantly promote tube fragmentation. Grossiord et al. [22], Utsumi et al. [23], and Matarredona et al. [24] demonstrated that surface tension measurement can be used to measure the surface coverage at saturation of single-wall CNTs, SWCNTs. Using also a surface tension measurement, Sa and Kornev [25] were recently able to construct the adsorption isotherm of SDS on SWCNTs. Bai et al. [26] recently reported adsorption isotherms of non-ionic surfactants on CNTs after separation of the CNTs from the aqueous phase by centrifugation and titration of the residual surfactant in the aqueous phase. Chappell et al. [27] have measured the settling rate of CNTs with various surfactants and humic acid in water. Finally, Utsumi et al. [23] correlated the dispersion state of single wall CNT to radial breathing mode (RBM) in Raman spectra.

In this paper, we analyze the mechanism of adsorption of four usual surfactants (SDS, SDBS, Triton X-100, Tx-100, and benzethonium chloride, BzT) on CNT dispersed in water in order to determine the driving force for the stabilization of CNT dispersion in aqueous media. For this purpose, we have built adsorption isotherms that is to say the curves linking the amount of dispersant adsorbed at the surface of the CNT to the amount of dispersant free in water. In contrast to already published adsorption isotherms, we have

employed an equilibrium dialysis technique which does not require separation of the CNT from the free surfactant by either drying [21] centrifugation [23] and [26] or by filtration [24], as any of these processes conceptually result in a change of the partitioning between adsorbed and free surfactant. This technique allowed us to work at CNT concentrations greater or equal than 1 g/L, concentrations at which most optical method are precluded due to the opacity of the medium. We then demonstrate how these results can be exploited to prepare concentrated and aggregate-free dispersions of CNT which were formulated into CNT/polymer composites.

2.2 Experimental

2.2.1 Materials

Multiwall carbon nanotubes (MWCNT, Baytubes® C 150 P) were graciously supplied by Bayer Material Science whereas SWCNTs (KH SWCNT80) were graciously offered by the company KH chemicals. Nanopure water ($\sigma = 18.2$ M Ω cm) was obtained from Milli-Q Plus system. Surfactant Tx-100 (EMD), SDBS (technical grade, Acros Organic) and BzT (Sigma–Aldrich) were used without purification whereas SDS (ACS grade, Sigma–Aldrich) was purified by recrystallization in order to remove the impurity dodecanol [28]. In short, 30 g of SDS was dissolved in 150 mL solution of benzene and ethanol (50:50 v:v) under reflux. The solution was then cooled to room temperature, and SDS crystals were then collected by vacuum filtration and dried in vacuum overnight at 70 °C. The procedure was repeated three times. Dialysis membranes, Fisherbrand membranes with a MWCO cutoff of 12,000–14,000 g/mol and Spectro membranes (MWCO = 50,000 g/mol), were obtained respectively from Fisher Scientific and Spectrum Labs. They were conditioned using the procedure recommended by the manufacturer. Sonication was performed with a Branson ultrasonic sonifier (450 W nominal power) equipped with a 19 mm (3/4″) diameter solid horn.

2.2.2 CNT purification

The purification procedure was identical for MWCNT and SWCNT, and was adapted from Musumeci et al. [29]. CNTs (200 mg) were suspended in 100 mL of a 1 mol/L HCl aqueous solution and dispersed by sonication for 5 min (amplitude 20%). The suspension

was then centrifuged at 3500 rpm for 10 min at room temperature and the CNTs were then collected and separated from the supernatant. This procedure was repeated 5 times. The procedure was then repeated using nanopure water instead of the acidic solution, until the pH of the supernatant was neutral. The CNTs were then dried overnight in an air-convection oven at 70 °C.

2.2.3 CNT dispersion

In a vial containing 20 mg of CNT was added 20 mL of a stock solution of surfactant at the appropriate concentration (tables consigning the values of each concentration can be found in the Supplementary content section). The suspension was stirred using a small magnetic stir bar while being immersed in an ice bath (0 °C) and was sonicated at 40% amplitude during 5 min. The role of the ice-bath is to prevent a large temperature increase during sonication. Magnetic stirring during sonication is necessary to allow the entire volume to be homogeneously sonicated. Care was used to introduce the sonicator tip in such a way that it did not touch the magnetic stir bar.

2.2.4 Determination of CNT porosity by Brunauer Emmett Teller (BET)

The adsorption isotherms were measured on ca. 40 mg of CNT with a QuantaChrome Autosorb-1 instrument using N_2 at 77 K as sorbent. The samples were outgassed under vacuum at room temperature for 12 h. The Brunauer-Emmett-Teller (BET) surface area was calculated from the adsorption branch in the relative pressure range from 0.05 to 0.10 Torr.

2.2.5 Transmission electron micrography (TEM)

The dispersed CNT sample was diluted with ultrapure water in order to reach a concentration of approx 0.01 g/L. A 20 µL drop of the diluted dispersion was deposited on a Cu/carbon grid (mesh 200). The grid was dried overnight and analyzed with a Jeol JEM-2100F microscope equipped with a field emission gun running at 200 kV.

2.2.6 Conductimetry

Conductimetric measurements were realized with a Copenhagen CDM80 conductimeter, in a Teflon thermostated cell (25 ± 0.1 °C) and calibrated with a 10^{-2} mol/L solution of KCl. Water used for the preparation and the dispersion of CNT was Nanopure, with a measured conductimetry of less than 5 μS cm^{-1}. CNT concentration was set at 0.1 g/L for all experiments.

2.2.7 Determination of adsorption isotherm by dialysis and HPLC quantification

The determination of C_{free}, the concentration of surfactant free in solution, was performed by HPLC. For this purpose, to a volume $V = 20$ mL of CNT dispersion containing the surfactant at a concentration C_0, was added a sealed dialysis bag containing a volume $V_{dial} = 1$ mL of ultrapure water (Fig. 1). The ensemble was gently stirred on an orbital shaker until the concentration of surfactant in the dialysis bag, as measured by HPLC, remained constant. For anionic and cationic surfactants (SDS, SDBS and BzT) a porous membrane with MWCO = 12,000–14,000 g/mol was used whereas for the non-ionic surfactant (Tx-100) a porous membrane with MWCO = 50,000 g/mol was chosen. For all surfactants, it was found that equilibrium was reached in less than 4 h at room temperature, thus, in order to allow sufficient time, dispersions and dialysis bags were stirred for 24 h. The content of the dialysis bag was analyzed by HPLC, resulting in the determination of the surfactant concentration in the dialysis bag, C_{dial}. The free surfactant concentration in the CNT compartment, C_{free}, was equal to C_{dial}, since equilibrium was reached.

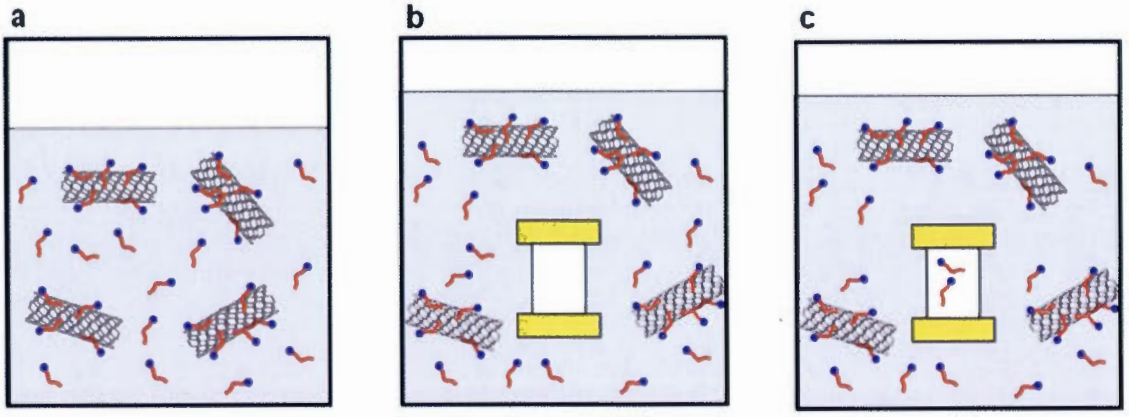

Fig. 2.1 Determination of the concentration of free surfactant. (a) The determination is performed on a volume V = 20 mL of CNT dispersed by a surfactant (total concentration C_0). (b) A dialysis bag containing a volume V_{dial} = 1 mL of water is introduced in the dispersion. (c) When equilibrium is reached, the concentration of free (i.e. not adsorbed) surfactant is the same on both sides of the bag.

During this process, part of the surfactant was also trapped on the dialysis membrane. This amount, $n_{hold\text{-}up}$, in mol, was determined in a separate experiment by performing a blank experiment in which CNT-free surfactant solutions of various concentrations were dialyzed. Thus, the total concentration of surfactant in the CNT compartment was determined as

$$C_{total} = \frac{C_0 V - n_{hold-up} - C_{dial} V_{dial}}{V} \quad (1)$$

The determination of the surfactant concentration in the dialysis bag, C_{dial} was performed by HPLC, using specific methods for each surfactant.

For SDS, the HPLC method was adapted from Zahrobsky et al. [30]. The SDS sample was eluted at 1 mL/min with a mixture of acetonitrile (30%) and a 0.3 mmol/L aqueous solution of *N*-methyl pyridinium iodide [31] (70%) on a C18 Phenomenex Spherex Column (250 × 4.6 mm). The analyte was detected by UV–VIS detector at 258 nm.

For SDBS, the HPLC method was adapted from Nakae and Kunihiro [32]. Each sample was eluted at 1 mL/min with acidic water (83 mL of 60% ACS perchloric acid, qsp 1 L) on a Agilent Zorbax SB-C8 5 µm (4.6 × 150 mm) column, using a UV–VIS detector set at 225 nm. With this method, SDBS appeared under the form of four separate peaks (Fig. 5) which were identified by a method of solid-phase extraction SPE – liquid chromatography coupled mass spectrometry LC–MS [33].

For BzT, the HPLC method was adapted from Takeoka et al. [34]. A 90:10 v:v mixture of methanol and a 0.1 mol/L aqueous solution of sodium perchlorate ($NaClO_4$) was prepared. This solution was acidified with phosphoric acid until pH 3, and used as eluent (1 mL/min) on a C18 Phenomenex Spherex Column (250 × 4.6 mm) column, using a UV–VIS detector set at 215 nm.

For Tx-100, the HPLC method was adapted from Yang et al. [35] Each sample was eluted at 1 mL/min with a 80:20 v:v mixture of methanol and water on Agilent Zorbax SB-C8 5 µm (4.6 × 150 mm) column, using a UV–VIS detector set at 224 nm.

2.2.8 CNT film preparation

The polymer nanoparticles were prepared by a miniemulsion polymerization process. Butyl acrylate (BA) and methyl methacrylate (MMA) were first filtered through basic alumina to remove the inhibitor, and acrylic acid (AA) was distilled under reduced pressure before use. MMA, BA and AA (resp 16 g, 16 g and 1.6 g) were mixed with 70 mL of water containing 0.24 g of SDS (3 g/L).This mixture was then sonicated using the high-power sonicating probe (5 min, 10%). A white stable miniemulsion was obtained, to which 10 mL of a 8.3 g/L potassium persulfate aqueous solution was added. The mixture was sparged with nitrogen for 30 min, and was then stirred and heated to a temperature of 80 °C for 6 h. The solid content of the nanoparticle dispersion, measured by a thermogravimetric balance, was found to be 23%. The average nanoparticle size, as measured by dynamic light scattering, was found to be 97.6 nm (polydispersity = 0.08). Then, SDS was slowly added to the dispersion so as to reach a total surfactant concentration of 8 g/L. This was necessary so as to saturate the nanoparticle surface with SDS before adding the CNTs [36]. If SDS was not added, agglomeration occurred when

the CNT dispersion was added, due to the migration of the SDS from the CNT surface to the polymer nanoparticle surface. A dispersion of washed MWCNT in water (32 g/L) containing SDS (8 g/L) was prepared using the protocol described in Section 2.3. An aliquot of the CNT dispersion was then added to the polymer nanoparticle dispersion so as the ratio CNT:polymer to be comprised between 0.01:1 and 0.1:1 w:w. Then, 1 mL of this mixture was dropped onto a 35 mm PE Petri dish and dried in air overnight. The continuous black shiny films were gently detached by lifting. Conductivity was determined by a four point probe measurement.

2.2.9 Raman characterization of the SWCNT dispersions

Raman spectra ranging from 170 cm^{-1} to 400 cm^{-1} were acquired on a Renishaw RM 3000 confocal microscope equipped with a laser of wavelength 514 nm. A drop of the dispersion to analyze was dropped on an aluminum foil surface, and was covered with a cover glass. The position of the RBM bands were then analyzed using the software Peakfit from Systat. Spectra and their respective deconvolutions can be found in the Supplementary content section.

2.3 Results and discussion

Our initial studies on surfactant adsorption were hardly reproducible (see below). We quickly discovered that CNT impurities strongly influence the outcome of the dispersion. Indeed, CNTs contain metallic residues (most commonly Fe, Y, Ni, Co) which are remnants from their synthesis [37]. In aqueous medium, metallic multivalent cations (Fe^{2+}, Fe^{3+}, Y^{3+}, Ni^{2+}, etc...) can leach out from unpurified CNTs, as shown by conductimetric measurement (Table 1). It will be seen below that these metallic ions strongly interfere with the adsorption of surfactants. An acidic wash was found to efficiently remove extractable metal ions: once washed, the MWCNT aqueous suspension conductivity is comparable to the conductivity of Nanopure water (Table 1). However, this treatment does not remove all metallic impurities, as shown by TEM-EDS (Fig. 2). Metallic particles which are partially or fully embedded into carbonaceous shells remain untouched. These particles are shielded from the aqueous environment, and thus do not leach metallic ions. Porosity measurement by BET indicates that the acidic washes

did not noticeably alter the CNT surface (the increase in BET surface is within instrumental precision). The fact that the acidic wash was not detrimental to the CNT was also confirmed by TEM observation (Fig. 2).

Table 2.1 - Characterization of the CNTs before and after washing treatment.

CNT	Tube median diameter (nm)[a]	Tube median length (nm)[a]	Conductivity[b] ($\mu S.cm^{-1}$)		BET surface ($m^2.g^{-1}$)	
			before washing	after washing	before washing	after washing
MWCNT	10 - 15	200 - 1000	7.23	4.87	189.7	198.6
SWCNT	1.1 - 1.3	5000 - 50000			527.2	552.5

a. Manufacturer information. b. CNT concentration: 0.1 g/L (water 25°C). Conductivity of water measured at 4.0 $\mu S.cm^{-1}$

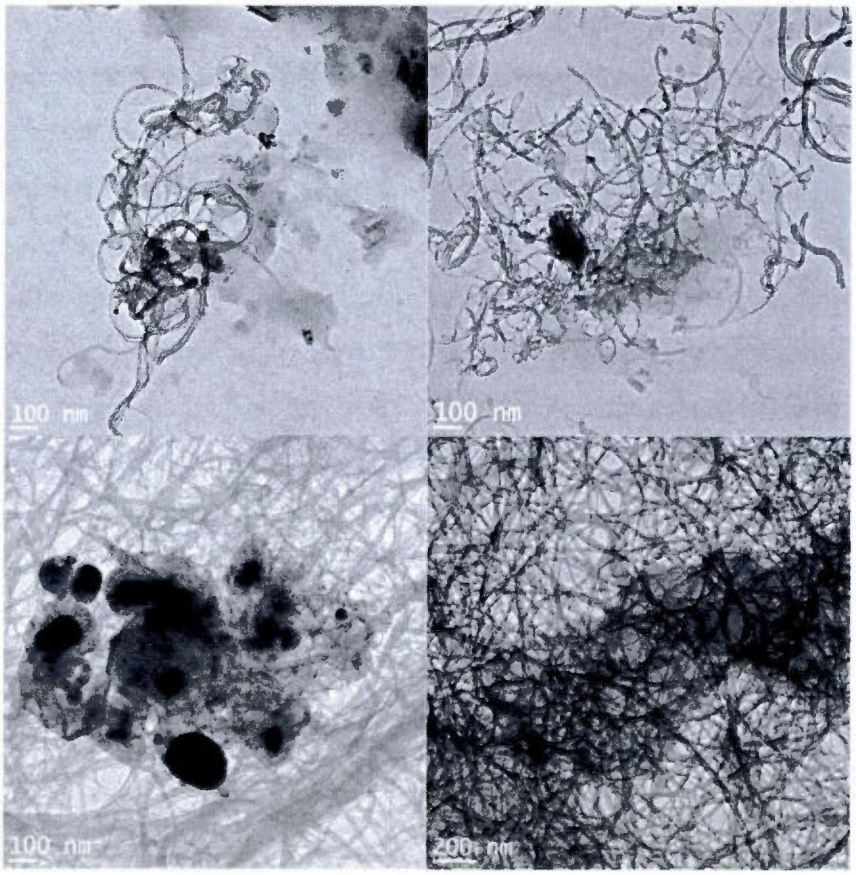

Fig. 2.2 - TEM of the MWCNTs (top) and SWCNTs (bottom) before (left) and after (right) washing.

2.3.1 Nanotube dispersion

The dispersion was performed by sonication of the CNTs in neutral water in the presence of surfactant. It has been reported that sonication may damage CNT [38, 39] but the extent of damage is moderate unless the sonication is performed under highly acidic conditions [40].

As mentioned above, we are interested in probing the dispersion of CNT at relatively 'high' concentrations. At such concentrations, the resulting dispersion is totally opaque, and thus is not suitable for light scattering experiments [10], zeta potential measurement [41], microscopy observations [21], by tensiometry [25] or spectrophotometric measurements [19]. Due the extremely rapid equilibrium dynamics of the surfactant between adsorbed and free states, the sample cannot be diluted without immediately altering the partitioning between free and adsorbed surfactant. This precludes the use of any experiment where the sample concentration would have to be diluted, even transiently. Furthermore, during drying of the sample (for example for TEM or AFM experiments), evaporation of water again leads to a change of concentration and a rapid redistribution of the surfactant. Hence, observations of dried samples cannot be used to infer about the state of dispersion in the liquid state. Even if perfectly dispersed, a concentrated CNT solution sample cannot be filtered on a syringe filter (filter pore size of 0.45 μm or 0.22 μm) because the tubes are entangled. Thus, the number of techniques one can use to judge of the quality of the dispersion is very limited.

Visual inspection of the dispersion (Fig. 3) is of course a rapid method to assess the quality of the dispersion. In Fig. 3, the minimal surfactant concentration to obtain a stable SWCNT dispersion can be clearly identified at $C = 2.75\ 10^{-3}$ mol/L in an aqueous saline environment, whereas it is lower (around $C = 1.0\ 10^{-3}$ mol/L) in pure water. However, this experiment does not yield any information on the coverage of the CNT surface by the surfactant, nor does it indicate the partitioning between adsorbed surfactant and free surfactant (C_{free}).

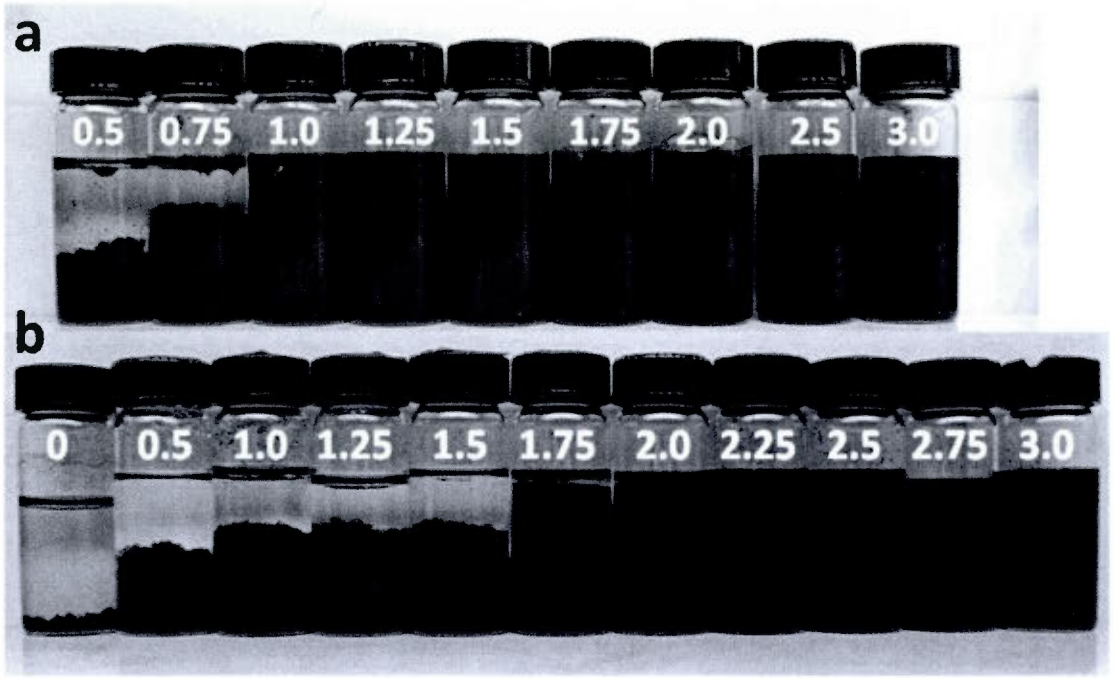

Fig. 2.3 - Dispersion of SWCNTs (1 g/L) (a) in water and (b) in saline solution (NaCl = 50 10^{-3} mol/L) with various concentration of SDS (x10^{-3} mol/L).

2.3.2 Building adsorption isotherms

Adsorption isotherms are convenient tools to study the adsorption of any surfactant on a surface. It is well known that close to the cmc of a surfactant, not only surfactant unimers, but also micellar or premicellar organizations [42] can adsorb on graphite [43]. This results in typical two-step (LS) adsorption isotherms where the first plateau corresponds to the formation of a monolayer of adsorbed unimers, whereas the second plateau corresponds to the adsorption of hemimicelles [44]. When the total surfactant concentration is kept below cmc, adsorption of surfactant unimers shows a Langmuir-type behavior, as expressed by

$$\Gamma = \frac{\Gamma_s C_{free}}{C_{free} + a} \qquad (2)$$

where Γ is the surface coverage of surfactant, in mol/m^2, Γ_s is the saturation coverage, which corresponds to the value of Γ when a continuous monolayer of unimers is adsorbed at the surface and a is the desorption equilibrium constant (unit mol/L) which also corresponds to the surfactant concentration necessary to cover 50% of the surface. In the

case of Tx-100, which has a low cmc (0.22 10^{-3}mol/L), micelles are formed at low surfactant concentration and therefore, one should consider a two plateau adsorption isotherm (0.22 × 10^{-3} mol/L), micelles are formed at low surfactant concentration and therefore, one should consider a two plateau adsorption isotherm

$$\Gamma = \frac{\Gamma_{s1} C_{free}}{C_{free} + a_1} + \frac{\Gamma_{s2} C_{free}}{C_{free} + a_2} \quad (3)$$

where 1 and 2 represent respectively the adsorption of the unimers and of the hemimicelles on the CNT surface.

Experimentally, Γ values are obtained from

$$\Gamma = \frac{\left(C_{total} - C_{free}\right) V}{S\, w_{CNT}} \quad (4)$$

where S is the specific surface of the CNT (as determined by BET), w_{CNT} is the amount of CNT in grams used for the experiment, and V is the dispersion volume in litres. The concentration C_{free} has been determined by HPLC titration of the surfactant (see experimental section). The values of Γ_s and a were obtained upon fitting the curve $\Gamma = f(C_{free})$ (Fig. 4), using Sigma-Plot automated non-linear regression routine for Langmuir isotherms. Each experimental measurement has been repeated at least three times. The sensitivity of our model analysis was also assessed. For example, Fig. 4b shows two fits of the same experimental points, one obtained by SigmaPlot (plain line, Γ_s = 3.11 μmol/m^2 and a = 5.88 10^{-4} mol/L), and another one (dashed line) for which the values of Γ_s = 2.80 μmol/m^2 and a = 3.10 10^{-4} mol/L were obtained by a so-called double-reciprocal linear plot. Both curves are visually acceptable fits of the experimental data but the plain line is in fact a better fit, based on χ^2 value. Thus, one can infer that the saturation coverage is known obtained with a numerical accuracy of 15% and the desorption constant, a, with an accuracy of 40%. From the value of Γ_s, one can compute the surface area occupied per polar head group at saturation, which is an indication of the packing of the surfactant in the adsorbed monolayer (Table 2). Provided both water and surfactant occupy equal areas on the surface, and both surface and bulk phase exhibit ideal behavior, then the desorption constant a can be expressed by

$$a = e^{\Delta G^0 / RT} \quad (5)$$

where ΔG^{o} is the free energy of adsorption. Therefore, from adsorption studies carried at different temperatures, the adsorption enthalpy ΔH^{o} and entropy ΔS^{o} can be determined. Fig. 4 illustrates the adsorption isotherms of anionic surfactants SDS and SDBS, cationic surfactant BzT and non-ionic surfactant Tx-100 under various conditions. The main characteristics of the adsorption isotherms are consigned in Table 2.

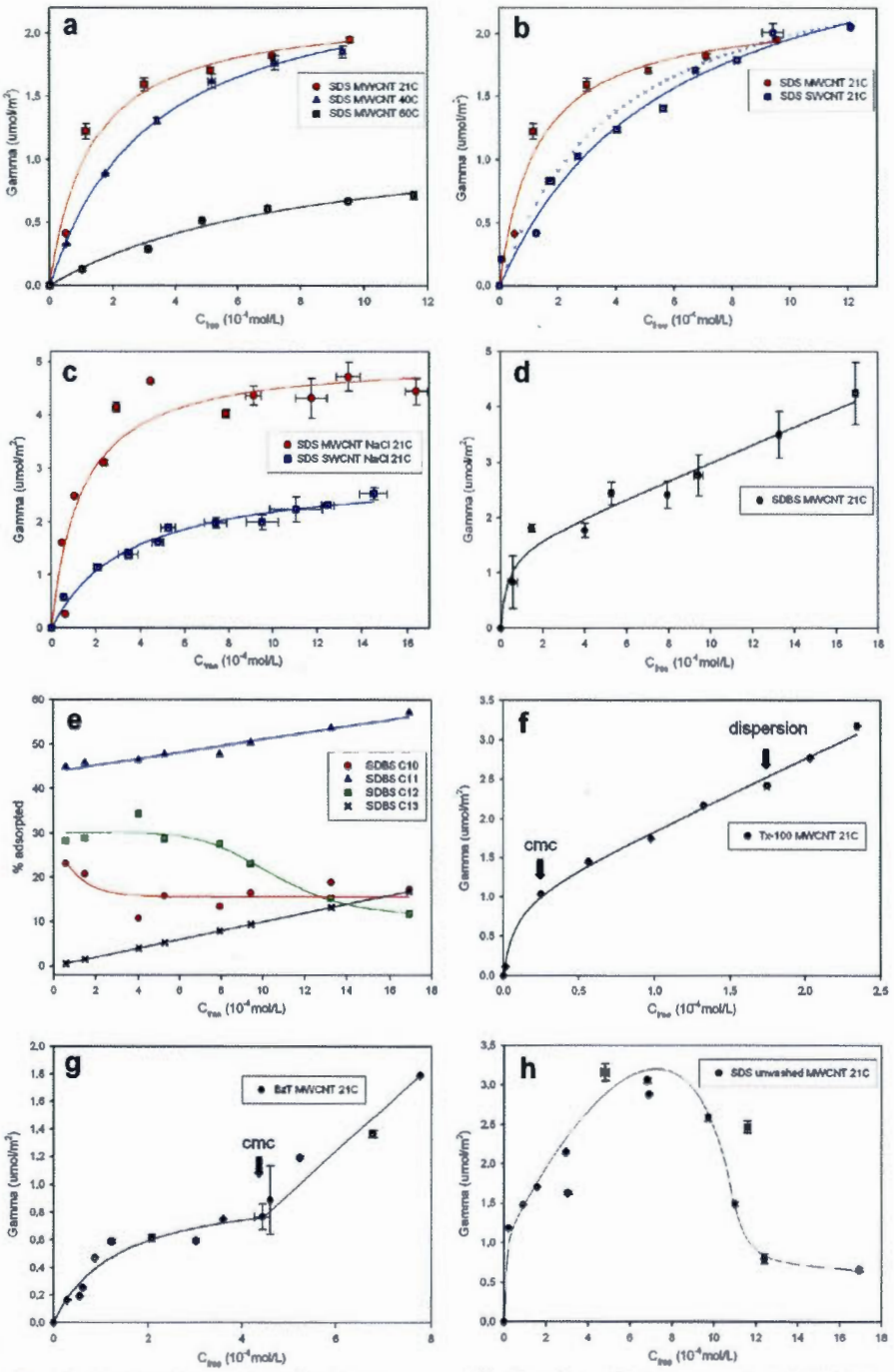

Fig. 2.4 - Surfactant adsorption isotherms on CNTs (1 g/L in water) (a) SDS on washed MWCNTs at various temperatures. (b) SDS on washed SWCNTs and MWCNTs. (c) SDS on washed SWCNTs and MWCNTs in NaCl solution (C = 50 10^{-3}mol/L). (d) SDBS on washed MWCNTs. (e) Composition of the adsorbed layer vs free surfactant concentration. (f) Tx100 on washed MWCNTs. (g) BzT on washed MWCNTs. (h) SDS on unwashed MWCNTs. Isotherms a, b, c, and g (up to C_{free} = 4.2 10^{-3}mol/L): the plain line is the fit of the experimental data by equation (2). Isotherms d and f: the plain line is the fit of the experimental data by equation (3). Graph e and isotherms h: the line is to guide the eye only.

Table 2.2 - Adsorption isotherms of various surfactants on washed MWCNTs and SWCNTs in water

CNT	Surfactant	Exp. Conditions	Γs (μmol/m²)	*a* (10^{-4} mol/L)	Surface area per head group (Å²/molecule)
MWCNT	SDS	21°C	2.20 ± 0.15	1.30 ± 0.33	75.47 ± 4.82
		40°C	2.53 ± 0.07	3.17 ± 0.24	65.62 ± 1.77
		60°C	1.26 ± 0.19	8.17 ± 2.42	131.77 ± 17.27
		21°C [a]	5.09 ± 0.38	1.34 ± 0.43	32.62 ± 2.27
SWCNT	SDS	21°C	3.11 ± 0.28	5.88 ± 1.22	53.39 ± 4.41
		21°C [a]	2.94 ± 0.16	3.46 ± 0.58	56.47 ± 2.91
MWCNT	SDBS	21°C	1.44 ± 0.46	0.33 ± 0.47	115.30 ± 21.50
	Tx-100		1.01 ± 0.16	0.07 ± 0.05	164.39 ± 22.48
	BzT		0.98 ± 0.12	1.31 ± 0.40	169.42 ± 18.48

a: NaCl concentration 50.10^{-3} mol/L

As shown in Fig. 4 (a), the adsorption isotherm of SDS on washed MWCNT is essentially Langmuir type. At room temperature, the experimental values for the coverage at saturation is Γ_s = 2.2 μmol/m² for SDS on MWCNT which corresponds to a surface area of 75 Å² per SDS head group. The desorption equilibrium constant *a* increases with increasing temperature, as expected from the contribution of thermal energy to SDS mobility and aqueous solubility: the surfactant becoming more soluble in water at high temperature is less likely to adsorb on the MWCNT surface. Using equation 5, the adsorption enthalpy and entropy were calculated as respectively ΔH = -38.4 kJ/mol and ΔS = -55.9 J/mol/K. The adsorption enthalpy corresponds well with the SDS adsorption enthalpy measured on graphite, -41.5 kJ/mol [43]. Thus, the adsorption of SDS on MWCNT is similar to the adsorption of SDS on graphite: at the length scale of SDS, the MWCNT surface appears to be flat and graphite-like.

In comparison to MWCNT, efficient dispersion of SWCNT is more difficult, the main reason being that, at equivalent mass, larger quantities of surfactants are necessary to saturate the SWCNT surface owing to its higher specific surface (Table 1). Interestingly, the values of the surface area per head group at saturation (53.4 Å²/molecule) corresponds well with the calculated value (48 Å²/molecule) recently reported for SDS adsorption on a 12,12 SWCNT by Tummala and Striolo [15], and obtained by molecular dynamics. In comparison to MWCNT, the desorption constant *a* is much larger for

SWCNT: the affinity of SDS for the curved SWCNT surface is lower. The most stable conformation of the SDS alkyl chain being the planar zigzag conformation, adsorption onto a curved surface will require an additional positive enthalpic cost in order the SDS molecule to adopt a bent conformation. In other words, unlike for MWCNT, the SDS molecule 'feels' the curvature of the SWCNT surface. In the presence of salt (NaCl 0.05 mol/L), the coverage at saturation Γ_s on MWCNT is found to increase, resulting from the screening of repulsive electrostatic interactions between negatively charged SDS molecules by Na^+ cations. Interestingly, the desorption constant, a, remains unchanged, in good agreement with the fact that the driving force for adsorption/desorption at low surface coverage is the interaction of the hydrophobic alkyl chain with the MWCNT surface – such interaction is insensitive to the presence of NaCl in the aqueous phase. Importantly, although it is possible to adsorb larger amounts of SDS on MWCNT surface by adding salt to the aqueous phase, this does not translate into an improvement of colloidal stability (as illustrated in Fig. 3). As predicted by the classical DLVO theory [45], by screening electrostatic interactions with NaCl, the Debye length decreases and the nanotubes can be in closer contact, and eventually become aggregated. The reduced influence of ionic strength on the desorption equilibrium constant, a, and its strong influence on colloidal stability should be taken as a cautionary tale on the value of visual inspection experiments. In Fig. 3, samples appear to be well-dispersed in pure water at surfactant concentrations as low as 2.0×10^{-3} mol/L. At this concentration, less than 50% of the surface is covered by surfactant (see below). However, in saline solution, dispersion is acceptable only when the total surfactant concentration is above 2.5×10^{-3} mol/L (corresponding to 80% of the surface covered by surfactant). Thus, visual inspections should not be used to assess the capacity of a surfactant to adsorb onto the CNT surface, since aggregation can occur at vastly different surface coverages, depending on experimental conditions (Table 3).

Table 2.3 - Influence of SDS concentration on the peak positions of RBM in Raman spectra ($\lambda = 514nm$)

SWCNT	RBM band position (cm^{-1})				
	RBM 1	RBM 2	RBM 3	RBM 4	RBM 5
Dry	189.5	207.6	nd	nd	nd
Dispersed in water	195.6	209.7	246.9	261.2	270.1
SDS 0.5mM	192.8	209.5	250.2	261.1	270.4
SDS 1.5mM	192.9	210.3	249.2	259.7	271.5
SDS 3.0mM	192.7	208.9	249.8	263.8	276.0
SWCNT diameter[a] (nm)	1.35	1.17	0.97	0.92	0.88

[a] Estimated from $\nu_{RBM} = 234/d + 10$

The curve of SDBS adsorption onto MWCNT (Fig. 4d) does not obey a simple Langmuir type isotherm. Yet, this isotherm was realized with surfactant concentrations far below cmc, therefore, the adsorption of hemi-micelles can be ruled out. Although SDBS is widely used for CNT dispersion, it is often overlooked that SDBS is not a pure compound, but a mixture of four aryl sulfonates with various chain lengths, later called SDBS C10, SDBS C11, SDBS C12 and SDBS C13, as shown in Fig. 5. The SDBS surfactant used in this study contained 25.3% of SDBS C10, 44.2% of SDBS C11, 26.5% of SDBS C12 and 4.0% of SDBS C13. HPLC conditions allowed us the independent quantification of each of these compounds (Fig. 4e and inset of Fig. 5). At low surfactant concentration, the composition of the adsorbed layer corresponds to the surfactant composition as all surfactant is adsorbed and none is free in solution. When increasing the total surfactant concentration, the surface becomes enriched in the most hydrophobic compounds, SDBS C13 and SDBS C12 to the expense of SDBS C10 and SDBS C11 which have been displaced and released to the aqueous phase (Fig. 4e). Therefore, the isotherm represented in Fig. 4d is in fact the overlay of a single-plateau Langmuir adsorption isotherm and a rising curve corresponding to the displacement of the less hydrophic compounds by more hydrophobic ones. Accordingly, Fig. 4d was fitted by a double-plateau adsorption isotherm, which lead to a surface area of 115 $Å^2$ per adsorbed polar head, in good agreement with the 117 $Å^2$ value obtained by atomistic simulation [16]. Interestingly, the desorption constant, a (0.33 10^{-4} mol/L), is significantly lower than for SDS (1.3 10^{-4}). This can be explained by the fact that SDBS, with 16 to 19

carbons in its hydrophobic tail, is more hydrophobic than SDS, and also by the presence of π-stacking interactions between the aryl group of SDBS and the CNT.

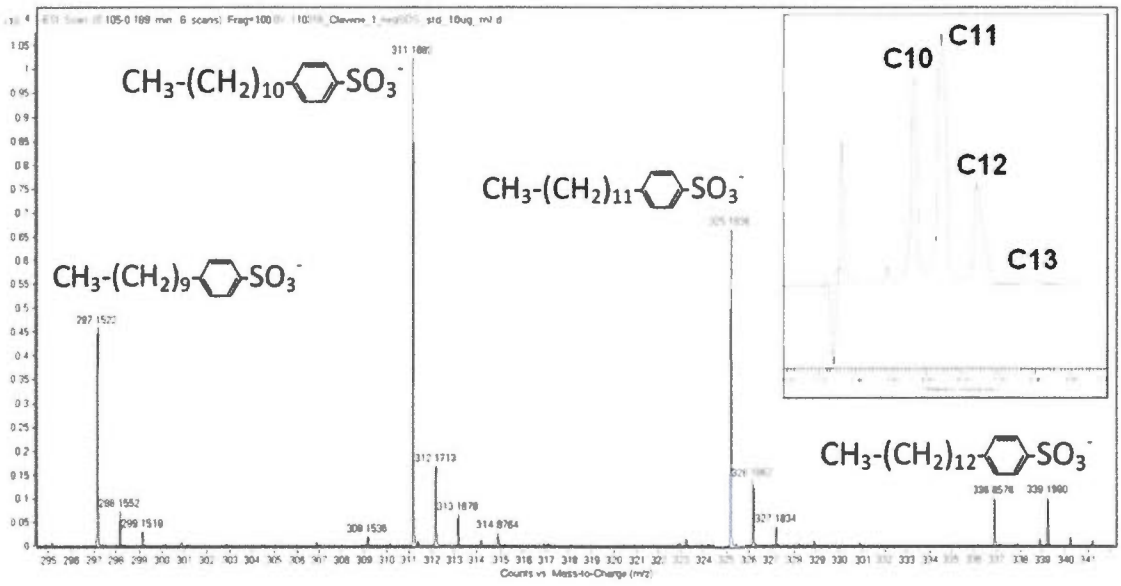

Fig. 2.5 - Composition of SDBS surfactant by HPLC-MS. Inset: HPLC chromatogram showing the separation of the four constituents of SDBS.

Two other surfactants were assessed for this study, cationic BzT and non-ionic Tx-100. Desorption constants, *a*, are not very different from those of anionic surfactants, indicating that there is only a small influence of the nature of the polar head on adsorption mechanism (adsorption is mainly driven by hydrophobic interactions). In the case of Tx-100, the experimental curve was fitted by a double-plateau isotherm because this surfactant has a very low cmc. Yet, the dispersion is only colloïdaly stable when C_{free} =7.52.10^{-4} mol/L, which is largely past cmc. At concentrations so high above cmc, one should wonder whether unimers or micellar aggregates are adsorbed at the surface, a question with is beyond the scope of this paper. For BzT, the adsorption of unimers (Fig. 4g, C_{free} < 4.2 10^{-3} mol/L) is clearly differentiated from the adsorption of micellar aggregates (C_{free} > 4.2 10^{-3} mol/L), as shown by a break in the adsorption plateau.

Fig. 4h presents an isotherm measured on an unwashed MWCNT sample. As mentioned above, divalent and trivalent metallic cations are responsible for the observed departure from Langmuir type isotherm. The experimental curve (Fig. 4h) encompasses two

separate phenomena, adsorption of SDS unimers and deposition of water-insoluble $M(SDS)_x$ compounds (where M = Fe or Co and x = 2 or 3). At low SDS concentration, both adsorbed unimers and precipitated $M(SDS)_x$ are on the surface of the CNT, resulting in abnormally high saturation coverage (Γ up to 3 $\mu mol/m^2$, in comparison to Γ_s = 2.2 $\mu mol/m^2$ for unimer adsorption on washed MWCNT). At higher SDS concentration, there is a sufficiently high SDS concentration for $M(SDS)_x$ to be redispersed into the aqueous phase, resulting in an apparent decrease in Γ (as schematized in Fig. 6b). The displacement of adsorbed $M(SDS)_x$ by SDS unimers is also observed by conductimetry (Fig. 6). In the absence of MWCNT, the conductivity vs SDS concentration curve (Fig. 6a) is constituted of two straight lines which intersect at cmc. In the presence of washed MWCNT, the same curve is obtained although a portion of SDS is adsorbed on the MWCNT surface. This phenomenon has already been observed by Esumi et al. [46] and it indicates that conductimetry cannot be used to determine free surfactant concentrations and adsorption isotherms. By contrast, on unwashed MWCNT, a sudden surge (indicated by an arrow) in the conductivity vs SDS concentration, indicates that an excess of ionic species is freed in solution when a sufficiently high surfactant concentration is present. Thus, we have here illustrated the prominent role of metallic cationic impurities on the adsorption of SDS on MWCNT.

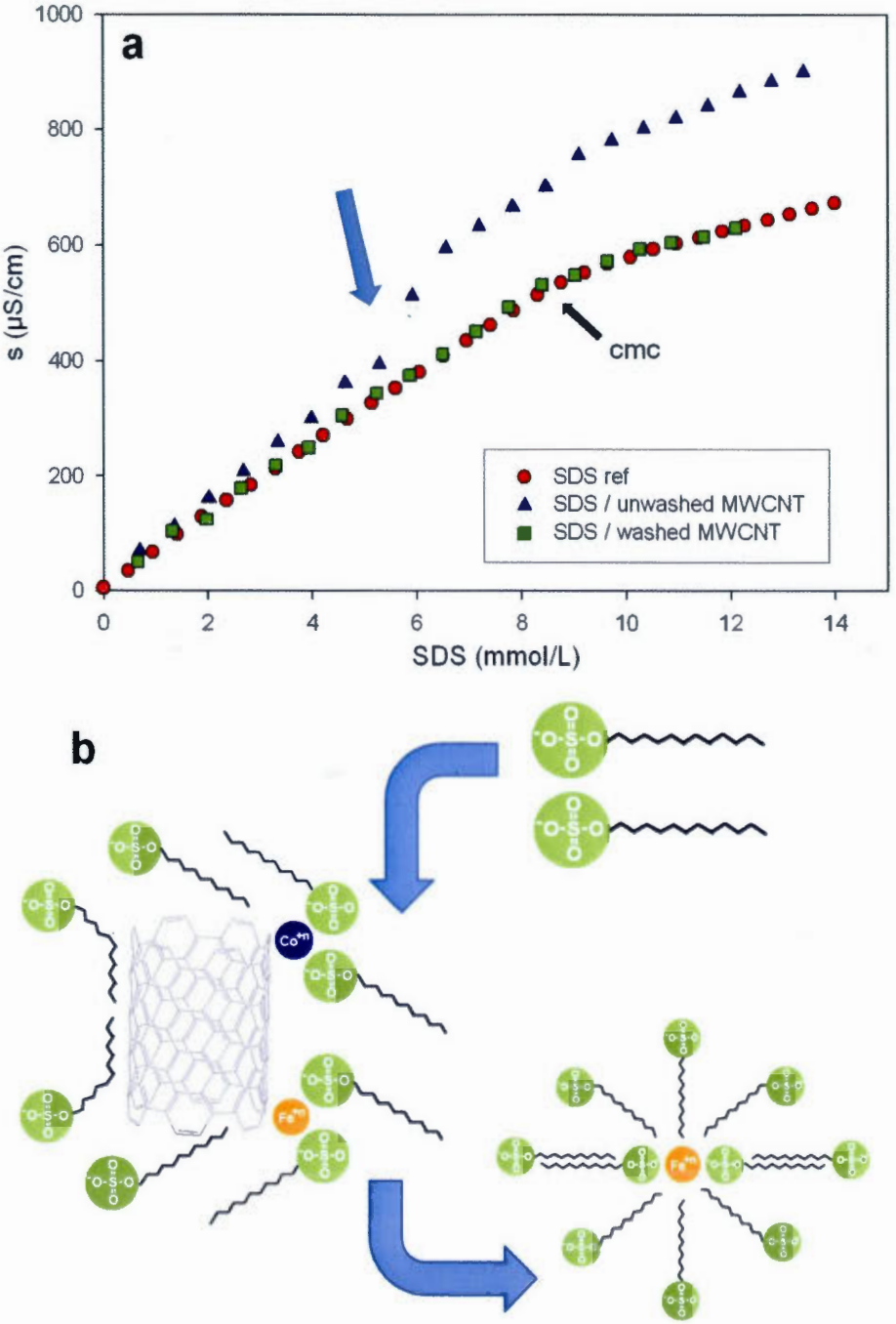

Fig. 2.6 - (a) Conductivity vs SDS concentration in the absence of MWCNTs (●), in the presence of washed MWCNTs (■) and in the presence of unwashed MWCNTs (▲). (b) Displacement of deposited $M(SDS)_x$ by SDS at a concentration indicated by the blue arrow in (a).

In this paper, we have studied the adsorption of the surfactant at the CNT/water interface and its partitioning between both phases. In short, the dispersion has been characterized from the point of view of the surfactant. Using visual inspections, we also are able to determine whether the dispersion is colloidally stable or not. However, it remains to determine whether the CNT is dispersed under a unimer form, or under the form of a bundle. At CNT concentrations of 1 g/L and above, this is a difficult question to answer, due to the opacity of the dispersion which strongly limits the choice of techniques available. For SWCNT dispersions, and based on the work of Utsumi et al. [23] it is possible to monitor the position of the radial breathing mode bands, RBM, in Raman spectra to assess whether individual tubes or aggregates are present. In comparison to the position of the RBM for the dry aggregated sample, the sample dispersed in water (no surfactant) shifts to a higher wavenumber, which is due to the presence of H-bonded water molecules which are directly in contact with the carbon surface (Table 3). Once the surfactant is present, the RBM peaks shift to a lower wavenumber as water is displaced by the surfactant. Since the RBM peak in surfactant solutions is at a higher wavenumber than the RBM peak in the aggregated SWCNT, these observations are, according to Utsumi et al. [23], consistent with the fact that the SWCNT are isolated. However, in order to probe the state of aggregation of SWCNT, the position of RBM is not as effective a tool as the fluorescence yield and the position of the fluorescent peak observed in absorption spectra [47] and [48]. Unfortunately, as mentioned above, the latter method is not applicable at a concentration of 1 g/L (see Supplementary content for the absorption spectrum).

Understanding the factors controlling the dispersion is of prime importance in the fabrication of films and composites containing CNTs. In order to apply our results, we have endeavored to prepare conducting polymeric aqueous coatings. For this purpose, a concentrated solution (32 g/L) of washed MWCNT in water was dispersed using SDS as surfactant. At such high MWCNT concentration in water, visual inspection of the dispersion becomes excessively difficult because of the opacity of the medium, and therefore, it is nearly impossible to know whether the chosen surfactant concentration is satisfactory or not. Using the values of Γ_s and a (Table 2), one can calculate the surfactant concentration necessary to cover 99% of the MWCNT surface: $C_{free} = 0.014$ mol/L and

0.013 mol/L of SDS is adsorbed on the MWCNT, resulting in C_{total} = 0.027 mol/L = 8 g/L. Thus, stable MWCNT dispersions were prepared using SDS surfactant at a total concentration of 8 g/L and mixed to a dispersion of acrylic polymer nanoparticles. It was important to ensure that the SDS concentration is similar in the MWCNT and in the polymer nanoparticle dispersions so as to avoid a possible redistribution of surfactant when both samples are mixed, possibly leading to colloidal destabilization of MWCNT. Once applied onto a flat surface, water evaporates from the joined MWCNT and polymer dispersion (Fig. 7a) and polymer spheres deform into a dodecahedral packed array with MWCNT confined at the interface [49] and [50]. Due to the broad Tg of the polymer which ranges from 17 °C to 60 °C, as measured by DSC, polymer chain interdiffusion from one particle to another can occur at room temperature thus leading to the formation of a continuous film. Using this procedure, films containing varying concentrations of MWCNT could be prepared by adjusting the relative amount of polymer and MWCNT dispersions. The resulting films are always smooth and devoid of aggregates to the eye (Fig. 7b – observations by electronic microscopy have not been done), and are black and shiny for MWCNT concentrations greater than 1 wt%. The conductivity of these films were measured using a four-point probe assembly, yielding a percolation threshold of 4.5% (Fig. 7c) which corresponds to the percolation calculated threshold of a composite in which MWCNT are fully dispersed, as calculated by Zeng et al. [51]. By contrast, when lower amounts of surfactant was used, or when the surfactant concentration in the polymer dispersion was not adjusted to the surfactant concentration in the MWCNT dispersion, then the presence of CNT aggregates could be visually observed (film surface not smooth) and the measured conductivity was lower.

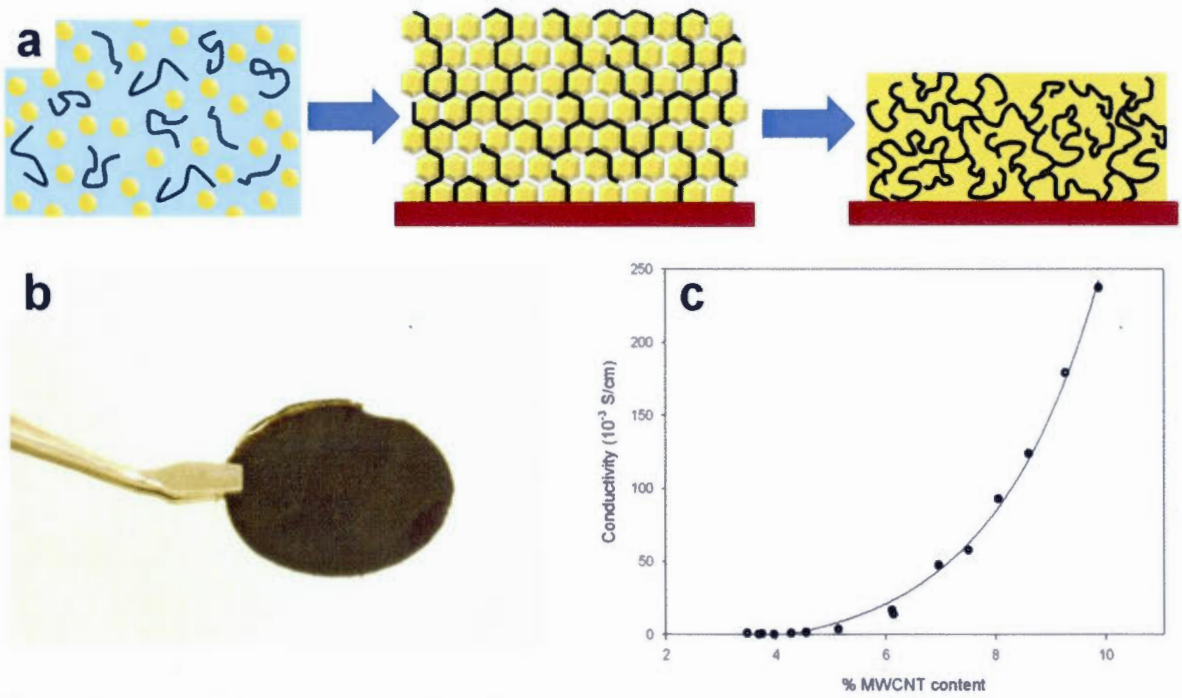

Fig. 2.7 - (a) Scheme of the film formation process using aqueous dispersions of MWCNTs and polymer nanoparticles (yellow spheres). (b) Picture of the resulting film. (c) Conductivity vs amount of MWCNTs in the CNT/polymer composite (wt%).

The successful preparation of conducting coatings clearly illustrates the importance of carefully optimizing surfactant concentration in both CNT dispersion and polymer dispersion when preparing a CNT polymer composite. Such optimization can only be done after precise determination of the adsorption isotherm of the surfactant on the CNT surface. Practically, once Γ_s and a parameters are known, it is possible to calculate the relative surface coverage, Γ/Γ_s, for any experiment performed with a given surfactant molar concentration C_{total}, and CNT weight concentration, C_{CNT}. From Eqs. (2) and (4), one derives

$$C_{free} = \frac{C_{total} - \Gamma_s S C_{CNT} - a + \sqrt{(\Gamma_s S C_{CNT} + a - C_{total})^2 + 4 C_{total} a}}{2} \qquad (6)$$

and, once C_{free} determined, the value of Γ/Γ_s can be directly calculated using Eq. (2).

Fig. 8a and b illustrates the dependence of Γ/Γ_s with the surfactant concentration, C_{total}, for MWCNT and SWCNT dispersed with SDS in water at 25 °C (C_{CNT} = 1 g/L). The relative surface coverage increases with the surfactant concentration, as expected. The

vertical lines delimitate the domains of colloidal stability, as determined by visual inspections (Fig. 3). Under these conditions, the MWCNT is stable when 90% of its surface is covered, where the SWCNT is stable as soon as 45% is covered. We currently have no explanation to account for this fact. On the left axes of the same graphs, the proportion of the surfactant which is adsorbed is indicated. It is also important to realize that achieving a stable colloidal suspension can only be achieved at a significant price, since a significant proportion (at least 70% for MWCNT and 40% for SWCNT) of the surfactant is free in water and does not participate to the colloidal stabilization. In fact, the surfactant free in solution contributes to an increase of ionic strength, and therefore to a decrease of the Debye length and a possible colloidal destabilization. Thus, colloidal stability is the result of a compromise: high surfactant concentrations are necessary to cover most of the CNT surface, but it is also less efficient as the surfactant is mostly free in water.

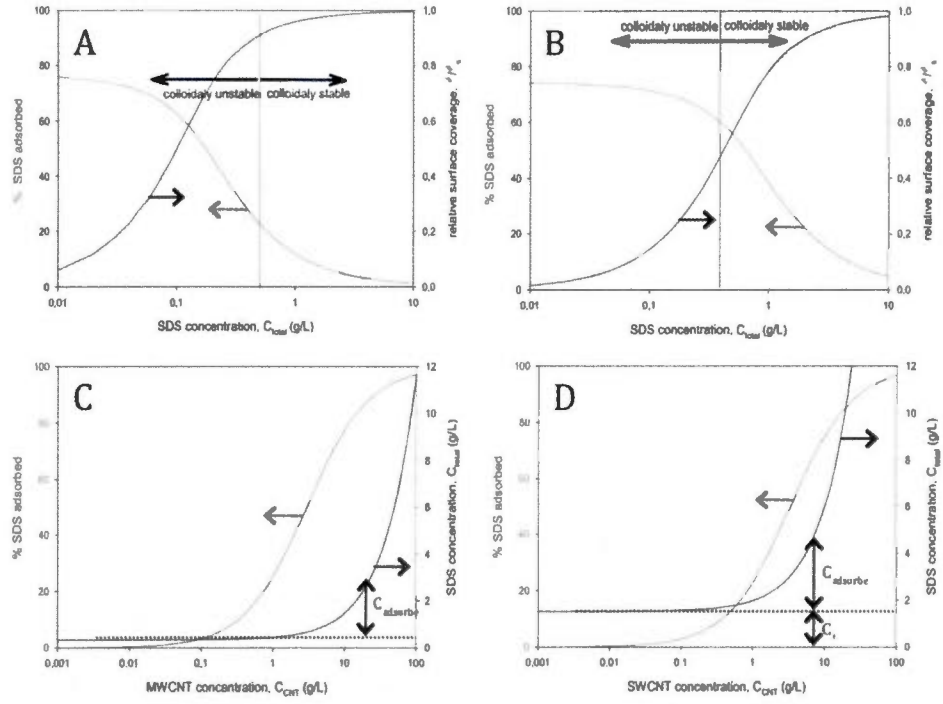

Fig. 2.8 – Top: Proportion of SDS adsorbed and relative surface coverage vs the total SDS concentration for MWCNT (A) and SWCNT (B) dispersions at 1 g/L. Bottom : Total concentration of SDS and proportion of SDS adsorbed necessary to cover 90% of the surface vs MWCNT (C) and of SWCNT (D) concentration.

With the values of Γ_s and a in hand, it is also possible to predict the surfactant concentration necessary to cover 90% of the surface at a given CNT concentration (Fig. 8c and d) – a coverage which we believe should be sufficient to ensure colloidal stability under most conditions. One striking feature of a Langmuir isotherm is that the concentration of surfactant free in solution, C_{free}, only depends on Γ/Γ_s, and not on the CNT concentration (as clearly shown in Eq. (2)). Thus, in order $\Gamma/\Gamma_s = 0.9$, $C_{free} = 0.9/0.1\ a = 9\ a$, and C_{total} which is by definition greater than C_{free} must be greater than $9\ a$ (horizontal dashed line in Fig. 8c and d). This characteristic appears under the form of a plateau in the SDS vs CNT concentration curve at low CNT concentrations (Fig. 8c and d). Consequently, covering 90% of the CNT surface when the CNT is at low concentration ($C_{CNT} < 0.01$ g/L) requires a very large surfactant concentration (0.33 g/L for MWCNT and 1.52 g/L for SWCNT), most of it being free in water. These curves can also be used to understand the influence of the cmc on the adsorption behavior of surfactants on CNT. Indeed, surfactant concentrations (C_{total}) greater than cmc (2.3 g/L for SDS in water at 21 °C) are often used to disperse CNTs. However, this does not mean that micelles are present in the dispersion: a portion of the surfactant is adsorbed at the surface, with the consequence that the effective surfactant concentration in water is much lower. For example, when the surface of a 20 g/L SWCNT suspension is covered at 90% (Fig. 7c), $C_{free} = 1.52$ g/L (below cmc). Such dispersion is achieved with 10.4 g/L of surfactant which is far above cmc. Thus, only the value of C_{free}, and not the value of C_{total}, should be compared to the cmc.

2.4 Conclusions

In this study, surface area per head group at saturation and desorption constants were measured for a variety of surfactants on MWCNTs and SWCNTs in water. Using these values, it was shown that a concentrated (32 g/L) dispersion of MWCNT in water could be achieved, and used for the preparation of a MWCNT/polymer composite. Although dispersion of CNTs in water is routinely performed by numerous researchers, to our knowledge, there were, prior to this study, no guidelines to help determine the required amount of surfactant for common surfactants such as SDS or SDBS and we envision that by using a and Γ_s values, one should be able to rationally determine the necessary

amount. Furthermore, this study also clearly demonstrates the role of the CNT preparation and conditioning, as metallic impurities are strongly affecting the adsorption/precipitation behavior of the surfactant on the CNT surface. In an ongoing study, we are determining how these impurities affect SDS adsorption for CNTs issued from a variety of commercial suppliers, and, more specifically, whether these impurities improve or deteriorate the colloidal stability of the CNT dispersion. Last, this study also exemplifies the danger of using visual assessment to judge of the ability of a surfactant to form a stable dispersion.

Acknowledgments

We wish to thank CM2 laboratory (Mr J.P. Masse) for technical help with TEM experiments and Dr. L. Sleno for SPE LC-MS analysis of SDBS.

References

[1] Iijima S. Helical microtubules of graphitic carbon. Nature 1991;354(6348):56–8.
[2] Vilatela JJ, Khare R, Windle AH. The hierarchical structure and properties of multifunctional carbon nanotube fibre composites. Carbon 2012;50(3):1227–34.
[3] Jung H, An SY, Jang DM, Kim JM, Park JY, Kim D. A multi-wall carbon nanotube/polymethyl methacrylate composite for use in field emitters on flexible substrates. Carbon 2012;50(3):987–93.
[4] Sahoo NG, Rana S, Cho JW, Li L, Chan SH. Polymer nanocomposites based on functionalized carbon nanotubes. Progr Polym Sci 2010;35(7):837–67.
[5] Liu Q, Tu J, Wang X, Yu W, Zheng W, Zhao Z. Electrical conductivity of carbon nanotube/poly(vinylidene fluoride) composites prepared by high-speed mechanical mixing. Carbon 2012;50(1):339–41.
[6] White KL, Shuai M, Zhang X, Sue HJ, Nishimura R. Electrical conductivity of well-exfoliated single-walled carbon nanotubes. Carbon 2011;49(15):5124–31.
[7] Behabtu N, Green MJ, Pasquali M. Carbon nanotube-based neat fibers. Nano Today 2008;3(5–6):24–34.
[8] Casagrande T, Lawson G, Li H, Wei J, Adronov A, Zhitomirsky I. Electrodeposition of composite materials containing functionalized carbon nanotubes. Mater Chem Phys 2008;111(1):42–9.
[9] Bokobza L. Multiwall carbon nanotube elastomeric composites: a review. Polymer 2007;48(17):4907–20.
[10] Kim HS, Park WI, Kang M, Jin HJ. Multiple light scattering measurement and stability analysis of aqueous carbon nanotube dispersions. J Phys Chem Solids 2008;69(5–6):1209–12.
[11] Strano MS, Moore VC, Miller MK, Allen MJ, Haroz EH, Kittrell C, et al. The role of surfactant adsorption during ultrasonication in the dispersion of single-walled

carbon nanotubes. J Nanosci Nanotechnol 2003;3(1–2):81–6.
[12] Wang H. Dispersing carbon nanotubes using surfactants. Curr Opin Colloid Interf 2009;14(5):364–71.
[13] Vaisman L, Wagner HD, Marom G. The role of surfactants in dispersion of carbon nanotubes. Adv Colloid Interf 2006;128–130:37–46.
[14] Uddin NM, Capaldi FM, Farouk B. Molecular dynamics simulations of carbon nanotube dispersions in water: effects of nanotube length, diameter, chirality and surfactant structures. Comput Mater Sci 2012;53(1):133–44.
[15] Tummala NR, Striolo A. SDS surfactants on carbon nanotubes: aggregate morphology. ACS Nano 2009;3(3):595–602.
[16] Suttipong M, Tummala NR, Kitiyanan B, Striolo A. Role of surfactant molecular structure on self-assembly: aqueous SDBS on carbon nanotubes. J Phys Chem C 2011;115(35):17286–96.
[17] Angelikopoulos P, Bock H. The differences in surfactant adsorption on carbon nanotubes and their bundles. Langmuir 2010;26(2):899–907.
[18] Angelikopoulos P, Gromov A, Leen A, Nerushev O, Bock H, Campbell EEB. Dispersing individual single-wall carbon nanotubes in aqueous surfactant solutions below the cmc. J Phys Chem C 2010;114(1):2–9.
[19] Clark MD, Subramanian S, Krishnamoorti R. Understanding surfactant aided aqueous dispersion of multi-walled carbon nanotubes. J Colloid Interf Sci 2011;354(1):144–51.
[20] Shin JY, Premkumar T, Geckeler KE. Dispersion of singlewalled carbon nanotubes by using surfactants: are the type and concentration important? Chem Eur J 2008;14(20):6044–8.
[21] Islam MF, Rojas E, Bergey DM, Johnson AT, Yodh AG. High weight fraction surfactant solubilization of single-wall carbon nanotubes in water. Nano Lett 2003;3(2):269–73.
[22] Grossiord N, Schoot Pvd, Meuldijk J, Koning CE. Determination of the surface coverage of exfoliated carbon nanotubes by surfactant molecules in aqueous solution. Langmuir 2007;23(7):3646–53.
[23] Utsumi S, Kanamaru M, Ohkubo T, Honda H, Kanoh H, Tanaka H, et al. RBM band shift-evidenced dispersion mechanism of single-wall carbon nanotube bundles with NaDDBS. J Colloid Interf Sci 2007;308(1):276–84.
[24] Matarredona O, Rhoads H, Li Z, Harwell JH, Balzano L, Resasco DE. Dispersion of single-walled carbon nanotubes in aqueous solutions of the anionic surfactant NaDDBS. J Phys Chem B 2003;107(48):13357–67.
[25] Sa V, Kornev KG. Analysis of stability of nanotube dispersions using surface tension isotherms. Langmuir 2011;27(22):13451–60.
[26] Bai Y, Lin D, Wu F, Wang Z, Xing B. Adsorption of Triton X-series surfactants and its role in stabilizing multiwalled carbon nanotube suspensions. Chemosphere 2010;79:362–7.
[27] Chappell MA, George AJ, Dontsova KM, Porter BE, Price CL, Zhou P, et al. Surfactive stabilization of multi-walled carbon nanotube dispersions with dissolved humic substances. Environ Pollut 2009;157:1081–7.
[28] Umlong IM, Ismail K. Micellization behaviour of sodium dodecyl sulfate in different electrolyte media. Colloid Surf A 2007;299(1–3):8–14.

[29] Musumeci AW,Waclawik ER, Frost RL. A comparative study of single-walled carbon nanotube purification techniques using Raman spectroscopy. Spectrochim Acta A 2008;71(1):140–2.
[30] Zahrobsky M, Camporese D, Rist Ø, Carlsen PHJ. HPLC analysis of aliphatic sulfonate surfactants using ion-pair detection. Molecules 2005;10(9):1179–89.
[31] Wu J, Lan Z, Wang D, Hao S, Lin J, Huang Y, et al. Gel polymer electrolyte based on poly(acrylonitrile-co-styrene) and a novel organic iodide salt for quasi-solid state dye-sensitized solar cell. Electrochim Acta 2006;51(20):4243–9.
[32] Nakae A, Kunihiro K. Separation of homologous alkylbenzenesulphonates by high-performance liquid chromatography. J Chromatogr 1978;152(1):137–44.
[33] Lara-Martin PA, Gomez-Parra A, Gonzalez-Mazo E. Development of a method for the simultaneous analysis of anionic and non-ionic surfactants and their carboxylated metabolites in environmental samples by mixed-mode liquid chromatography–mass spectrometry. J Chromatogr A 2006;1137(2):188–97.
[34] Takeoka G, Dao L, Wong RY, Lundin R, Mahoney N. Identification of benzethonium chloride in commercial grapefruit seed extracts. J Agr Food Chem 2001;49(7):3316–20.
[35] Yang K, Zhu L, Zhao B. Minimizing losses of nonionic and anionic surfactants to a montmorillonite saturated with calcium using their mixtures. J Colloid Interf Sci 2005;291(1):59–66.
[36] Loiseau J, Ladaviere C, Suau JM, Claverie J. Dispersion of calcite by poly(sodium acrylate) prepared by reversible addition-fragmentation chain transfer (RAFT) polymerization. Polymer 2005;46(19):8565–72.
[37] Ge C, Lao F, Li W, Li Y, Chen C, Qiu Y, et al. Quantitative analysis of metal impurities in carbon nanotubes: efficacy of different pretreatment protocols for ICPMS spectroscopy. Anal Chem 2008;80(24):9426–34.
[38] Nepal D, Kim DS, Geckeler KE. A facile and rapid purification method for single-walled carbon nanotubes. Carbon 2005;43(3):660–2.
[39] Mukhopadhyay K, Dwivedi CD, Mathur GN. Conversion of carbon nanotubes to carbon nanofibers by sonication. Carbon 2002;40(8):1373–6.
[40] Aviles F, Cauich-Rodrı´guez JV, Moo-Tah L, May-Pat A, Vargas- Coronado R. Evaluation of mild acid oxidation treatments for MWCNT functionalization. Carbon 2009;47(13):2970–5.
[41] Sun Z, Nicolosi V, Rickard D, Bergin SD, Aherne D, Coleman JN. Quantitative evaluation of surfactant-stabilized singlewalled carbon nanotubes: dispersion quality and its correlation with zeta potential. J Phys Chem C 2008;112(29):10692–9.
[42] Cui X, Mao S, Liu M, Yuan H, Du Y. Mechanism of surfactant micelle formation. Langmuir 2008;24(19):10771–5.
[43] Kiraly Z, Findenegg GH, Klumpp E, Schlimper H, Dekany I. Adsorption calorimetric study of the organization of sodium n-decyl sulfate at the graphite/solution interface. Langmuir 2001;17(8):2420–5.
[44] Rosen MJ. Surfactants and interfacial phenomena. 3rd ed. John Wiley & Sons; 2004, p. 464-9.
[45] Adamson AW, Gast AP, editors. Physical chemistry of surfaces. 6th ed. Wiley; 1997, p. 784-6.

[46] Esumi K, Hayashi H, Koide Y, Suhara T, Fukui H. Adsorption of metal ion and aromatic compounds by anionic surfactantcoated particles of titanium dioxide. Colloid Surf A 1998;144(1–3):201–6.

[47] Moore VC, Strano MS, Haroz EH, Hauge RH, Smalley RE, Schmidt J, et al. Individually suspended single-walled carbon nanotubes in various surfactants. Nano Lett 2003;3(10):1379–82.

[48] Britz DA, Khlobystov AN. Noncovalent interactions of molecules with single walled carbon nanotubes. Chem Soc Rev 2006;35:637–59.

[49] Vandervorst P, Lei CH, Lin Y, Dupont O, Dalton AB, Sun YP, et al. The fine dispersion of functionalized carbon nanotubes in acrylic latex coatings. Prog Org Coat 2006;57(2):91–7.

[50] Jurewicz I, Worajittiphon P, King AAK, Sellin PJ, Keddie JL, Dalton AB. Locking carbon nanotubes in confined lattice geometries – a route to low percolation in conducting composites. J Phys Chem B 2011;115(20):6395–400.

[51] Zeng X, Xu X, Shenai PM, Kovalev E, Baudot C, Mathews N, et al. Characteristics of the electrical percolation in carbon nanotubes/polymer nanocomposites. J Phys Chem C 2011;115(44):21685–90.

CHAPITRE III

ARTICLE SCIENTIFIQUE (COMMUNICATION)

A versatile encapsulation method of non-covalently modified carbon nanotubes by RAFT polymerization

Weiheng Zhong, Jules Nguendia Zeuna, Jerome P. Claverie*

NanoQAM, Quebec Center for Functional Materials, Department of Chemistry, University of Quebec in Montreal, Succ Centre Ville, PO Box 8888, Montreal, QC, H3C3P8, Canada. Fax: 514 9874054 E-mail: claverie.jerome@uqam.ca

* claverie.jerome@uqam.ca

Journal of Polymer Science Part A: Polymer Chemistry

Volume 50, Issue 21, November 2012, pages 4403–4407

Dans cet article, l'encapsulation des nanotubes de carbone (CNT) a été réalisée en milieu aqueux via l'utilisation de polymères-dispersants préparés par polymérisation RAFT. Les oligomères hydrosolubles dont le polyacide acrylique (PAA), le polyacide acrylique-*co*-acrylate de butyle (PAABA) et le polystyrène-*co*-acide acrylique (PSAA) ont été synthétisés par la polymérisation RAFT. Des mesures d'isotherme d'adsorption sont ensuite réalisées avec les nanotubes de carbone à parois simple (SWNT) et à parois multiples (MWNT) sur chacun de ces polymères-dispersants. Par la suite, une écorce polymérique est générée à la surface des CNT par polymérisation en émulsion. Les observations en microscopie électronique à transmission ont confirmé qu'une couche de polymère homogène de l'ordre de 5 nm s'est formée sur la surface des CNT. Les résultats expérimentaux ont démontré la versatilité de cette méthode qui ne requiert pas la modification covalente de la surface des CNT.

Ce chapitre est formé par un papier publié au « Journal of Polymer Science Part A: Polymer Chemistry ». Les trois auteurs de cet article sont moi-même, Jules Nguendia Zeuna et Prof. Jérôme Claverie. Dans ce chapitre, j'ai réalisé toutes les synthèses des polymères-dispersants ainsi que tous les encapsulations des CNT. Jules Nguendia Zeuna, étudiant en maîtrise, et moi-même ont mesuré les isothermes d'adsorption. Le manuscrit (incluant le matériel supplémentaire, Appendice B) a été rédigé par Jérôme Claverie et moi-même.

ABSTRACT

Single-wall carbon nanotubes (SWNT) and multi-wall carbon nanotubes (MWNT) are coated by a uniform polymeric shell via a two-step encapsulation process which does not involve any covalent modification of the sp^2 conjugated skeleton. In a first step, the tubes are dispersed in water using a dispersant prepared by Reversible Addition-Fragmentation chain Transfer (RAFT) polymerization. In the second step, the polymer shell is generated by emulsion polymerization. This procedure is shown to be efficient for a variety of dispersants and polymer shells, demonstrating the versatility of this encapsulation process.

KEYWORDS Dispersion, Reversible Addition Fragmentation chain Transfer (RAFT), Emulsion Polymerization, Carbon Nanotube, Encapsulation

Since the landmark paper by Iijima,[1] carbon nanotubes (CNTs) have been intensely scrutinized in reason of their exceptional electrical, thermal, and mechanical properties. To fully exploit these properties, it is generally necessary to overcome the lack of solubility and the propensity of CNTs to form aggregates.[2] Several well-established strategies exist to generate colloidally stable dispersions of CNTs in a liquid continuous phase, by either covalent grafting or noncovalent adsorption of surface-active groups.[3] Among surface active groups which have been considered, polymers have been intensely scrutinized because they are usually more efficient than small molecule to improve colloidal stability and they further pave the way for the fabrication of CNT/polymer nanocomposites. Covalently grafted polymers have been introduced either by a "grafting to" approach, for example, by free radical[4, 5] or click[6] coupling, or by a "grafting from" approach, for example by derivatizing the CNT surface with a nitroxide,[7] an atom transfer radical polymerization (ATRP) macroinitiator[8] or a reversible addition-fragmentation chain transfer (RAFT)[9] agent and by subsequently growing polymer chains of controlled length. For the noncovalent approach, polymers bearing pyrene or porphyrin groups have been shown to form strong π–π interactions[10, 12] with the CNT surface and to efficiently allow the supramolecular functionalization of CNTs. The

noncovalent approach does not introduce sp^3 hybridized carbons on the CNT (these defects are associated with a deterioration of the thermal and electrical properties), however, its scope is limited to polymers forming strong π–π interactions. We here present an efficient and versatile method which maintains the integrity of the CNT (no covalent attachment of the polymer to the surface), but which could be applied to the large variety of polymers which can be prepared by radical polymerization.

Hawkett's group[13, 14] and our group[15] recently reported a versatile two-step method for the encapsulation of inorganic nanoparticles in water. Nanoparticles are first dispersed by a dispersant prepared by RAFT polymerization and the resulting dispersion is engaged in an emulsion polymerization, resulting in the formation of core-shell nanoparticles. This method has been recently used in the encapsulation of inorganic nanomaterials, such as Gibbsite[16] or quantum dots.[17, 18] In a patent by Baker et al.[19] it is claimed that CNTs encapsulated in an alkali-swellable polymer layer are obtained when CNT covalently modified with COOH groups are reacted first with an amine containing polymer, then with a dispersant prepared by RAFT polymerization, then with a series of acrylic monomers and finally with styrene. Here, we demonstrate how the general two-step encapsulation method (Scheme 1) can be very simply adapted to coat pristine multiwall carbon nanotubes (MWNT) as well as single-wall carbon nanotubes (SWNT) with a continuous polymer layer in the absence of any covalent linkage between the polymer and the CNT.

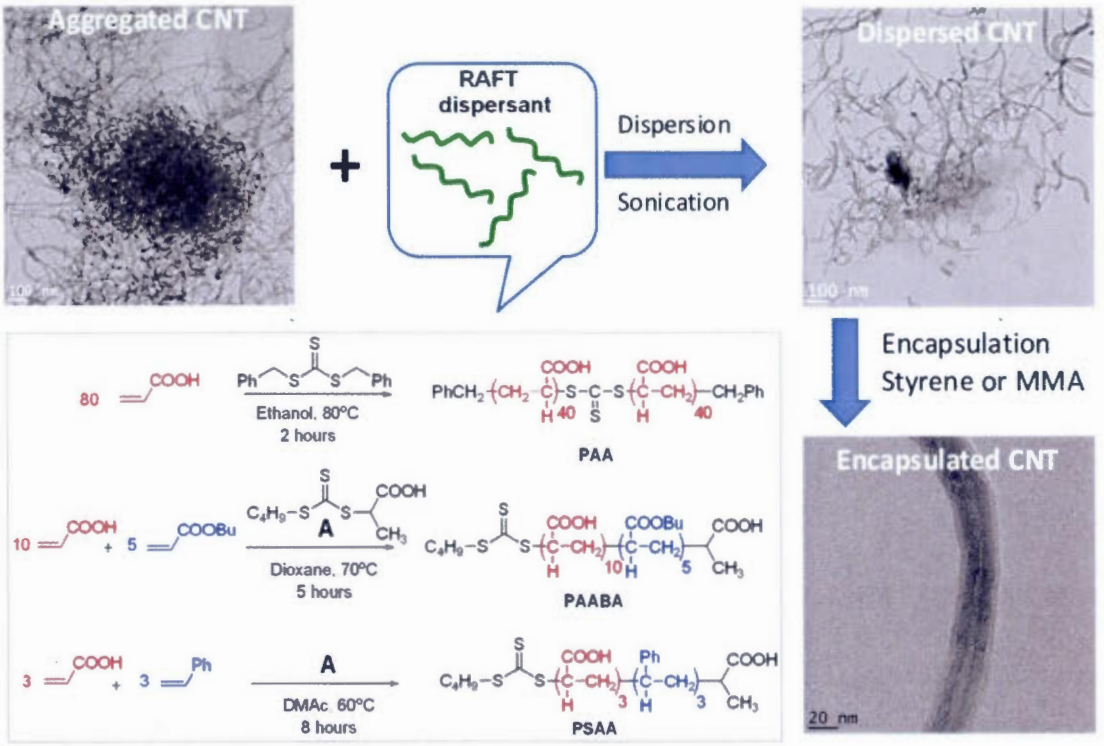

Figure 3.1 Structure of the RAFT dispersants and CNT encapsulation in aqueous medium by RAFT polymerization.

The encapsulation begins with the preparation of a dispersant oligomer or low molecular weight polymer by RAFT polymerization. We have considered three different dispersants (Scheme 1), a symmetrical polyacrylic acid with a number average degree of polymerization of 40 (PAA), a statistical oligomer constituted of five butyl acrylate and 10 acrylic acid units (PAABA) and a statistical oligomer constituted of three styrene units and three acrylic acid units (PSAA). Synthesis and characterization of PAA[15, 20] and PAABA[14] were already reported in the past, whereas PSAA synthesis is described in Supporting Information. PSAA was designed with the idea that it will form π–π interactions with the CNT; however, it will be seen below that, despite their dissimilarities, all the three dispersants lead to equally successful encapsulations of the nanotubes. No further effort was done to tailor the respective number of units of hydrophilic and hydrophobic monomers. Whereas PAA is soluble in water in its acidic form, at least 40% of the COOH groups of PAABA and PSAA must be deprotonated with NaOH to ensure aqueous solubility. Except for the small amount of base used to solubilize the RAFT dispersants PAABA and PSAA, all further steps are performed in

pure water, in the absence of base or buffer. These dispersants are efficient in stabilizing colloidal solutions of CNT in water and in forming solutions devoid of aggregates, as illustrated in Figure 1.

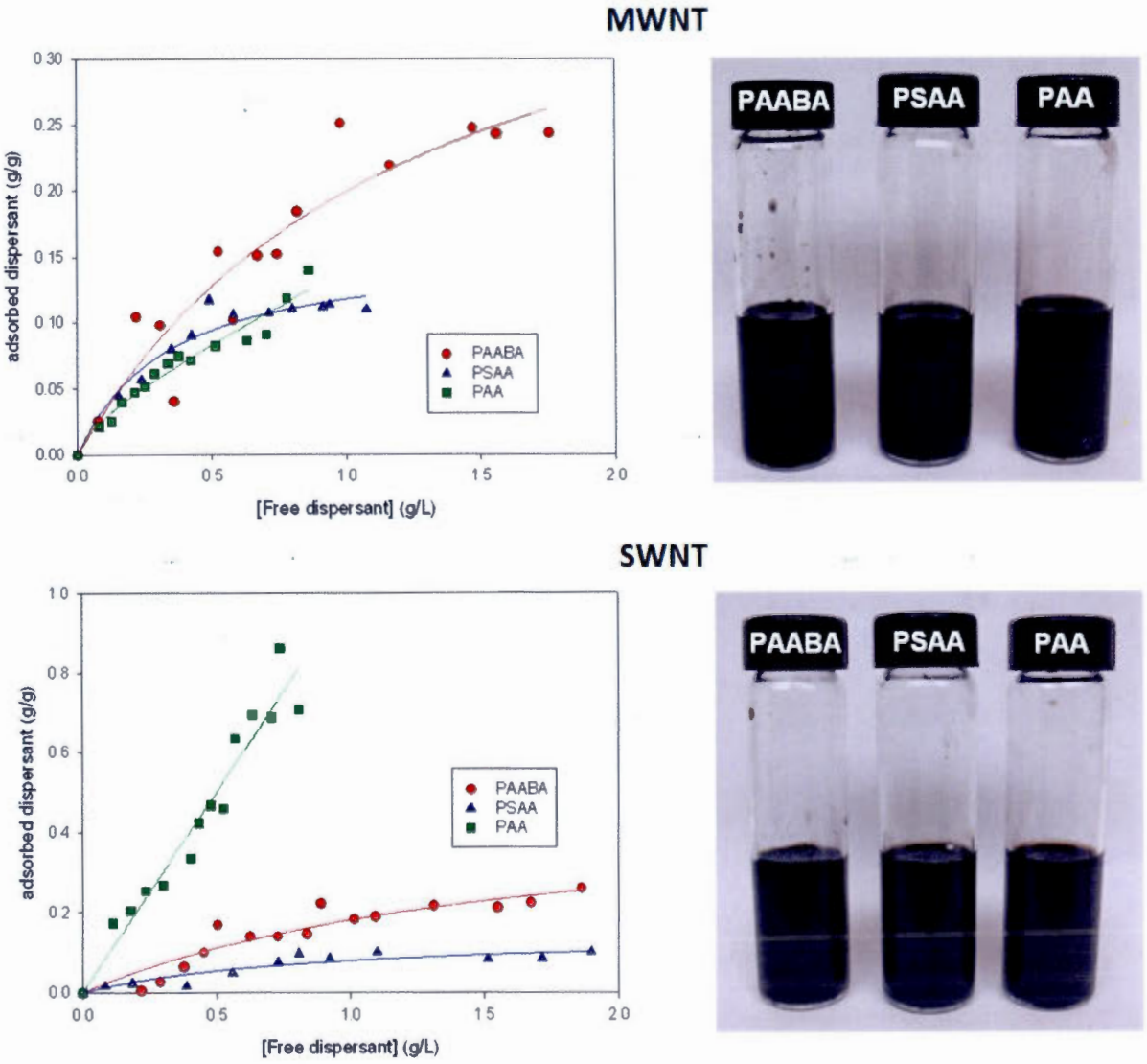

Figure 3.2 Adsorption isotherms (left) and pictures of the CNT dispersed in water (right) with the RAFT dispersants for MWNT (top) and SWNT (bottom). Concentration MWNT = 1 g/L, concentration SWNT = 0.5 g/L. Isotherms for PAABA (40% of the COOH group deprotonated), PSAA (50% of the COOH groups deprotonated), and PAA measured in unbuffered water. For the pictures, the RAFT dispersant concentration was set at 0.5 g/L.

The adsorption isotherm, that is, the graph of adsorbed dispersant per weight of CNT versus the free concentration of dispersant in solution in g/L is shown in Figure 1. All isotherms exhibit a Langmuir behavior whereby the plateau corresponds to the surface concentration at saturation, and the slope at low concentration is related to the affinity of the dispersant for the CNT surface. A remarkable feature of the isotherm curve is the fact that saturation is reached only when a significant amount of dispersant is free in solution, which is indicative of a rather low affinity of the dispersant for the CNT surface, but nonetheless sufficient to ensure colloidal stability. This situation contrasts with the strong binding observed for the adsorption of RAFT PAA on TiO_2 for example.[21, 22] Saturation of CNTs necessitates larger amounts of PAA than PAABA and PSAA, which can be explained by the greater molecular weight of PAA (Mn = 6060 g/mol) than for PAABA (Mn = 1600 g/mol) and PSAA (Mn = 770 g/mol). Furthermore, saturation of SWNT surface requires larger amounts of RAFT dispersant than MWNT which is expected owing to the larger specific surface area of SWNT.

The second step of the process is the encapsulation process via emulsion polymerization. All encapsulation experiments (Table 1) are performed with a total RAFT dispersant concentration of 0.5 g/L (MWNT = 1 g/L, SWNT = 0.5 g/L). During the emulsion polymerization, the RAFT dispersant is extended by styrene or methyl methacrylate (PMMA, Entry 8), resulting in the formation of an asymmetric block copolymer composed of a short surface active block (the dispersant) and a long hydrophobic block (as the quantity of monomer is larger than the dispersant). Since the dispersant is adsorbed at the surface of the CNT, the hydrophobic block effectively forms a continuous shell of polymer around the CNT. In short, the CNT is trapped in a shell of hydrophobic polymer covalently anchored to the dispersant. Importantly, although the use of a RAFT polymerization process is required to allow chain-extension of the dispersant by styrene (or MMA), it is not our intent to prepare polymers with a narrow molecular weight distribution (Table 1). Experimental conditions were chosen so as to favor high conversion and reasonably rapid kinetics (high ratio initiator vs. RAFT dispersant) over control of the molecular weight distribution.

Table 3.1 Encapsulation Reactions

Entry	CNT (g)	Dispersant	Dispersant Weight (g)	Monomer (g)	Shell Thickness (nm)[d] Before Polym	Shell Thickness (nm)[d] After Polym	M_n (g/mol)[e]	PDI[e]
1	MWNT (0.05)	PAABA	0.025	Styrene (0.21)	1.0	4.2	11,800	1.4
2	MWNT (0.05)	PSAA	0.025	Styrene (0.21)	0.9	3.5	27,700	1.6
3	MWNT(0.05)	PAA	0.025	Styrene (0.21)	1.1	6.2	13,900	1.3
4	MWNT(0.05)	RAFT A[a]	0.025	Styrene (0.21)	nd	Flocculated	nd	nd
5	MWNT (0.05)	SDS	0.0125	Styrene (0.21)	nd	0	nd	nd
6	SWNT (0.05)	SDS	0.0125	Styrene (0.21)	nd	0	nd	nd
7	MWNT (0.05)	PAABA	0.025	Styrene (0.63)	1.0	3.3	28,100	1.6
8	MWNT (0.05)	PAABA	0.025	MMA (0.21)	1.0	5.2	13,300	2.3
9	MWNT (0.05)	PSAA	0.025	Styrene (0.21)[c]	0.9	2.1–31.8	9600	1.4
10	SWNT (0.025)	PAABA	0.025	Styrene (0.21)	1.1	4.3	16,100	1.9
11	SWNT (0.025)	PSAA	0.025	Styrene (0.21)	1.0	5.4	28,000	1.6
12	SWNT (0.025)	PAA	0.025	Styrene (0.21)	0.9	5.0	14,300	1.4

All encapsulation reactions were performed at 80 °C in water (50 mL). The monomer was introduced continuously over a period of 4 h.
[a] RAFT agent A.
[b] Not determined (see Scheme 1).
[c] Batch addition.
[d] Determined by TEM.
[e] Determined by GPC.

Evaluation of the encapsulation experiments by transmission electron microscopy (TEM) indicates that both MWNT and SWNT are covered by a continuous shell of polymer (Fig. 2B–F, I–P and numerous other TEM pictures in Supporting Information). Before encapsulation, the shell formed by the RAFT dispersant measures ~1 nm (see Supporting Information) whereas it measures 3–6 nm after encapsulation (Table 1). Interestingly, although their adsorption isotherms are different (Fig. 1), all three dispersants (PAA, PAABA, and PSAA) give quite similar encapsulation results for MWNT (Fig. 2B–F) and SWNT (Fig. 2N–P). The CNTs are well separated over the grid, they are covered with a polymer shell of uniform thickness, and no free polymer particles or uncoated CNTs could be observed. The resulting composites are also colloidaly stable, and no traces of aggregates could be visually observed, even after several weeks.

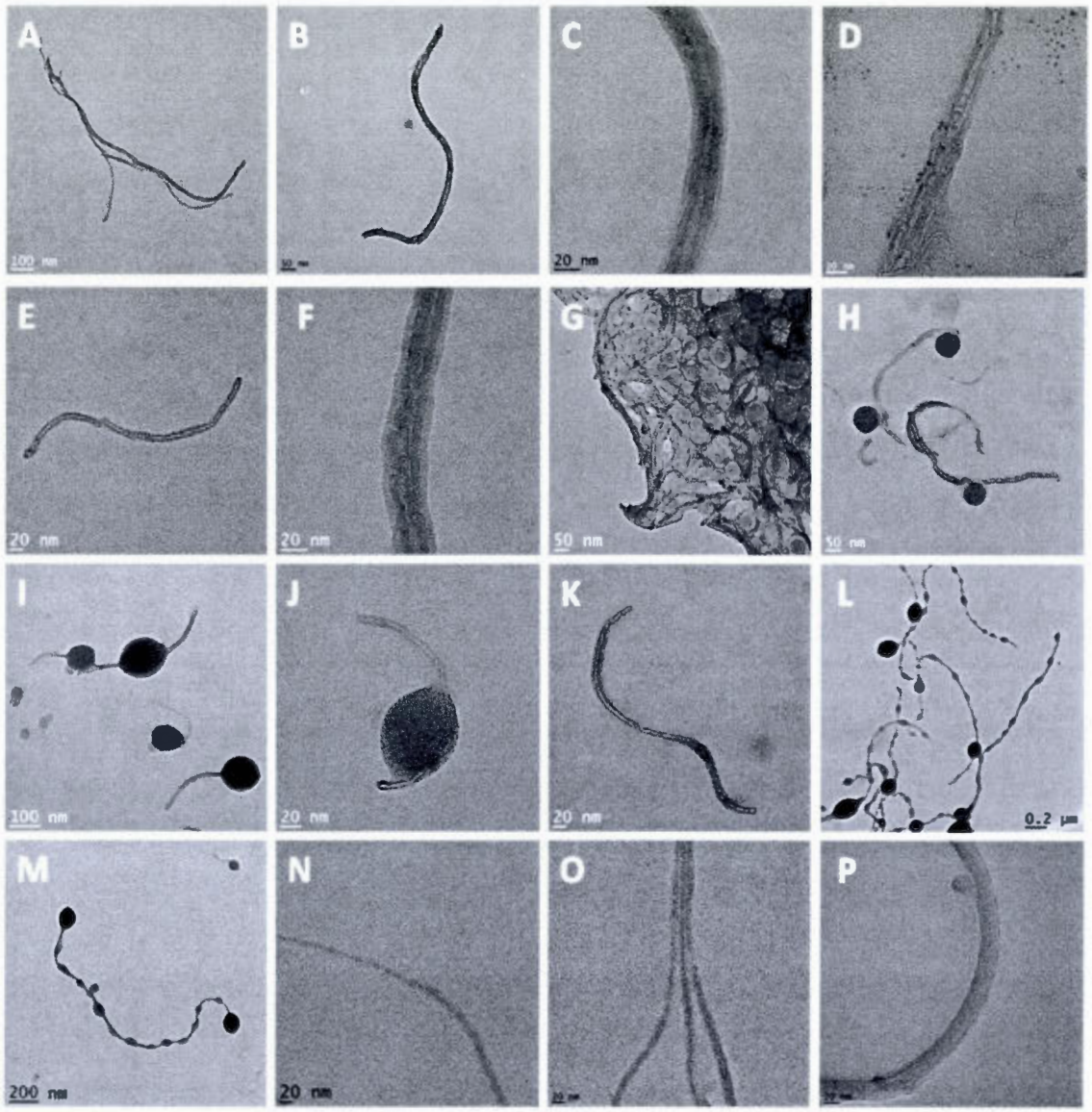

Figure 3.3 TEM of CNT and CNT-polymer nanocomposites. (A) Nude MWNT without any dispersant, (B and C): Entry 1, (D): Entry 2, (E and F): Entry 3, (G and H): Entry 5, (I and J): Entry 6, (K): Entry 8, (L and M): Entry 9, (N): Entry 10, (O): Entry 11, (P): Entry 12.

It has been demonstrated by others that polymeric chains can be covalently grafted on the CNT surface at high temperature via direct addition of a macro radical on a sp^2 carbon.[4, 5] To rule out that in our case the polymer shell is generated by such mechanism, two control experiments were performed. First, the encapsulation experiment (Entry 4) was repeated in the absence of a RAFT dispersant, but by using molecule A (Scheme 1) as

RAFT agent. Unlike all other samples which were colloidaly stable, this experiment led to the formation of CNT aggregates and a partially flocculated polystyrene latex. Then, the experiment (Entry 5, resp. 6) was performed by using a MWNT (resp. SWNT) dispersion stabilized by SDS (no RAFT agent) resulting in the formation of a mixture of polymer-free MWNT and empty polystyrene latex particles (Fig. 2G and H). Interestingly, empty polymer particles were not observed when CNT were dispersed with any of the three RAFT dispersants, indicating the high efficiency of the encapsulation process. As shown in the case of the encapsulation of quantum dots,[17, 18] we believe that free (i.e., not adsorbed) RAFT dispersants lead to empty polymer particles that have a tendency to precipitate on the surface of the CNT.

The process is sensitive to the operating conditions used to introduce the monomer. For experiments 1–3, 8, and 10–12 which yield uniformly coated CNTs, the monomer was introduced over a period of 4 h at a slow rate of 53 mg/h. Introducing the monomer at a faster rate (Experiment 7, 210 mg/h) results in the formation of MWNTs coated with a 3 nm polymer layer in conjunction with larger polymeric domains. Finally, if the monomer is added in a single batch at the onset of the encapsulation reaction (Experiment 9, Fig. 1L and M), the MWNT surface is covered by a polymer shell with thickness undulating between 2 and 32 nm. At low addition rate, the system is under monomer starved conditions, the viscosity of the polymer coat is high and the polymer coat grows uniformly from the outer layer. By contrast, in batch mode, the system is flooded with monomer, resulting in the formation of zones of low viscosity where the polymer is accumulated. The presence of undulations are likely the sign that phase separation phenomena are occurring, at least partially, in batch mode whereas kinetically trapped morphologies are observed with slow addition rates.

The encapsulation process can be implemented with other monomers than styrene, for example, with methyl methacrylate, MMA (as shown in Fig. 2K), clearly underlining the versatility of this method.

The absence of covalent bonds between the polymer and the CNT was established by two separate experiments. First, the polymer was separated from the CNT and analyzed by gel permeation chromatography (Table 1) after dissolution of the dried composite in

THF. This indicates that most of the polymer was not grafted, however, the measurement of the polymer concentration by GPC was too imprecise to assess whether 100% of the polymer was free. In a separate experiment, the SWNT-polymer latexes were analyzed by Raman spectroscopy, as the intensity of the D band at 1339 cm^{-1} is very sensitive to covalent modifications of the surface.[23] The Raman spectra (see Supporting Information) indicate that there is no significant modification of the tubes either when the tube is dispersed with the dispersant, or when the tube is encapsulated in a polymeric layer. For example, the intensity of the D band represents 5.6% for the pristine SWNT in the dry state, it is 6.5% in the colloidal dispersion of SWNT stabilized by PAA and it is 4.7% for sample 12, which has been encapsulated.

To summarize, we have developed a simple and solvent-free encapsulation method which is efficient both for MWNTs and SWNTs. This method, which uses readily accessible and inexpensive monomers, could easily be implemented on a large scale. We expect that the encapsulated CNTs exhibit greater compatibility with polymeric matrices, thus facilitating the preparation of CNT-polymer nanocomposites.

ACKNOWLEDGMENTS

This work is supported by National Science and Engineering Research Council and by NanoQuébec (Quebec Major Infrastructure). We appreciate the cooperation of Mr. Masse of Centre CM^2 of École Polytechnique for TEM measurements and Dr. Cottenye of Université de Montréal for Raman measurements.

REFERENCES AND NOTES

1 Iijima, S. *Nature* **1991**, *354*, 56-58.
2 Howard, W. *Curr. Opin. Colloid. In.* **2009**, *14*, 364-371.
3 Homenick, C. M.; Lawson, G.; Adronov, A. *Polym. Rev.* **2007**, *47*, 265-290.
4 Lou, X.; Detrembleur, C.; Pagnoulle, C.; Jérôme, R.; Bocharova, V.; Kiriy, A.; Stamm, M. *Adv. Mater.* **2004**, *16*, 2123-2127.
5 Liu, Y.; Yao, Z.; Adronov, A. *Macromolecules* **2005**, *38*, 1172-1179.
6 Li, H.; Cheng, F.; Duft, A. M.; Adronov, A. *J. Am. Chem. Soc.* **2005**, *127*, 14518-14524.
7 Dehonor, M.; Varlot-Masenelli, K.; Gonzalez-Montiel, A.; Gauthier, C.; Cavaille, J. Y.; Terrones, H.; Terrones, M. *Chem. Commun.* **2005**, 5349–5351.
8 Yao, Z.; Braidy, N.; Botton, G. A.; Adronov, A. *J. Am. Chem. Soc.* **2003**, *125*, 16015-16024.
9 Cui, H.; Wang, W. P.; You, Y. Z.; Liu, C. H.; Wang, P. H. *Polymer* **2004**, *45*, 8717–8721.
10 Bahun, G. J.; Wang, C.; Adronov, A. *J. Polym. Sci. Pol. Chem.* **2006**, *44*, 1941-1951.
11 Cheng, F.; Imin, P.; Maunders, C.; Botton, G.; Adronov, A. *Macromolecules* **2008**, *41*, 2304-2308.
12 Cheng, F.; Zhang, S.; Adronov, A.; Echegoyen, L.; Diederich, F. *Chem. Eur. J.* **2006**, *12*, 6062-6070.
13 Nguyen, D.; Zondanos, H. S.; Farrugia, J. M.; Serelis, A. K.; Such, C. H.; Hawkett, B. S. *Langmuir* **2008**, *24*, 2140-2150.
14 Nguyen, D.; Such, C.; Hawkett, B. *J. Polym. Sci. Pol. Chem.* **2012**, *50*, 346-352.
15 Daigle, J. C.; Claverie, J. P. *J. Nanomater.* **2008**, DOI:60918410.1155/2008/609184.
16 Ali, S. I.; Heuts, J. P. A.; Hawkett, B. S.; Van Herk, A. M. *Langmuir* **2009**, *25*, 10523-10533.
17 Das, P.; Zhong, W.; Claverie, J. P. *Colloid Polym. Sci.* **2011**, *289*, 1519-1533.
18 Das, P.; Claverie, J. P. *J. Polym. Sci. Pol. Chem.* **2012**, *50*, 2802-2808.
19 Baker, M. P.; Davey, T. W.; Hawkett, B. S.; Nguyen, D. N.; O'Brien, C. C.; Such, C. H. (Univ. Sydney) Patent WO 2011/066608 A1, June 9, 2011.
20 Llauro, M. F.; Loiseau, J.; Boisson, F.; Delolme, F.; Ladaviere, C.; Claverie, J. *J. Polym. Sci., Part A: Polym. Chem.* **2004**, *42*, 5439-5462.
21 Loiseau, J.; Doerr, N.; Suau, J. M.; Egraz, J. B.; Llauro, M. F.; Ladaviere, C.; Claverie, J. *Macromolecules* **2003**, *36*, 3066-3077.
22 Loiseau, J.; Ladaviere, C.; Suau, J. M.; Claverie, J. *Polymer* **2005**, *46*, 8565-8572.
23 Hussain, S.; Jha, P.; Chouksey, A.; Raman, R.; Islam, S. S.; Islam, T.; Choudhary, P. K.; Harsh. *J. Mod. Phys.* **2011**, 2, 538-543.

CHAPITRE IV

CONCLUSION

4.1 Sommaire

Les mesures d'isotherme d'adsorption des tensioactifs sur les CNT dans l'eau nous a permis de déterminer les principales caractéristiques de la dispersion colloïdale. La température et la force ionique sont des facteurs importants qui modifient l'affinité entre les CNT et les tensioactifs ioniques. Cette étude démontre aussi l'influence que la préparation des CNT peut apporter à leur stabilité colloïdale. La présence d'impuretés métalliques issue de la synthèse des CNT favorise la précipitation des tensioactifs lors de la dispersion.

Cette étude propose également une méthode de détermination des conditions optimales d'une dispersion stable de CNT. Les grandeurs clés telle la surface occupée par tête polaire à saturation Γ_S ainsi que la constante de désorption a sont alors mesurés pour chacun des tensioactifs sur les SWNT et les MWNT. L'utilisation des ces valeurs permet de préparer des dispersions des CNT hautement concentrée (32g/L) avec un minimum de tensioactifs. Ces dispersions concentrées peuvent servir par la suite à la réalisation de nanocomposites conducteurs à base de CNT. Le taux de percolation est vérifié par la conduction électrique des nanocomposites ainsi préparés.

L'extension de la méthode d'évaluation de l'isotherme fut ensuite reportée sur les polymères-dispersants de type RAFT. Ces oligomères adsorbées à la surface des CNT peuvent être réamorcées et continuer leur polymérisation en émulsion. Cette méthode d'encapsulation des CNT via la polymérisation RAFT s'adapte à une grande variété d'écorses polymériques.

4.2 Travaux futurs

Plusieurs points importants se sont dégagés de nos études. Tout d'abord, nous avons été surpris par l'influence des impuretés sur les caractéristiques de la dispersion des CNT. En fonction du fournisseur, et de leurs caractéristiques, les nanotubes peuvent contenir jusqu'à 50% d'impureté. Aussi, dans un travail futur, nous proposons de comparer les différents lots de CNT vis-à-vis de leur comportement dans la dispersion, avant et après purification. Il est fort possible de penser que dans certains cas, des impuretés spécifiques aident à la dispersion, c'est-à-dire qu'il soit plus facile de disperser les nanotubes non purifiés que purifiés. Notre étude jette aussi le discrédit sur de nombreuses études faites par le passé. Trop souvent, il nous a été possible de trouver des articles qui affirment que tel ou tel tensioactif est excellent, et cela en se basant uniquement sur des observations visuelles ou sur des analyses d'images de microscopie électronique ou par force atomique à l'état sec. Les auteurs de ces articles ont négligé de purifier les nanotubes et de mesurer les isothermes d'adsorption. La confusion règne dans la littérature sur le rôle de la concentration micellaire critique (cmc). Tout d'abord, comme nous l'avons démontré, il faut toujours utiliser la concentration de tensioactif libre (et non totale) pour calculer la concentration micellaire. D'autre part, ce ne sont pas les micelles qui dispersent les nanotubes, mais bien des tensioactifs « unimères » qui s'adsorbent à la surface. A haute concentration de tensioactif, les hémimicelles peuvent s'adsorber, mais à ce jour, nous ne savons pas si la stabilisation par les hémimicelles est plus ou moins efficace que la stabilisation par le tensioactif unimère. Ceci pourrait faire l'objet d'un travail futur.

Nos travaux démontrent qu'en milieu aqueux, la principale force motrice de la dispersion est l'interaction hydrophobe entre la queue du tensioactif et le nanotube. La nature de la tête polaire est moins importante. La présence de noyaux phényles qui peuvent faire des interactions π-π avec la surface des CNT semble ne pas apporter un avantage majeur quant à la qualité de la dispersion. Récemment, dans le laboratoire, un travail sur la dispersion en milieu organique a été engage, dans ce cas, les interactions π-π semblent jouer un rôle prédominant.

La méthode d'encapsulation que nous avons mise au point est excessivement versatile. Comparée aux méthodes existantes, elle présente des avantages certains : elle est très

facile à mettre en œuvre, elle me nécessite aucun solvant toxique et elle est assez rapide (environ une journée de travail par échantillon) si des couches de l'ordre de 5 nm sont souhaitées. Néanmoins, lorsque des revêtements épais sont souhaités (épaisseur supérieure à 10 nm), alors des ondulations se produisent à la surface. Pour l'instant nous ne connaissons pas l'origine de celle-ci, mais il est possible qu'il s'agisse d'un phénomène d'instabilité de Rayleigh (due à une grande différence de tension de surface). Il serait souhaitable d'étudier ce phénomène, et de pouvoir mettre au point une méthode qui permette de synthétiser des couches de polymères d'épaisseur variable et aussi large que souhaité.

ANNEXE A

SUPPORTING INFORMATION FOR:

Probing the carbon nanotube-surfactant interaction for the preparation of composites

Weiheng Zhong, Jerome P. Claverie*

NanoQAM, Quebec Center for Functional Materials, Department of Chemistry, University of Quebec in Montreal, Succ Centre Ville, PO Box 8888, Montreal, QC, H3C3P8, Canada. Fax: 514 9874054 E-mail: claverie.jerome@uqam.ca

* claverie.jerome@uqam.ca

Carbon

Volume 51, January 2013, pages 72-84

Table A.1 Conditions for Each Isotherm

Experiments with SDS

MWCNT - 21°C in water

MWCNT (mg)	Ctotal (M)	Cfree (M)	Gamma (mol/m2)
20,1	2,74E-04	5,27E-05	4,13162E-07
20,1	2,74E-04	5,18E-05	4,17639E-07
20,1	2,74E-04	5,32E-05	4,10178E-07
19,8	4,95E-04	1,17E-04	1,21516E-06
19,8	4,95E-04	1,16E-04	1,22432E-06
19,8	4,95E-04	1,12E-04	1,24265E-06
19,8	4,95E-04	1,01E-04	1,30373E-06
19,8	4,95E-04	1,34E-04	1,12353E-06
19,6	7,62E-04	2,94E-04	1,63153E-06
19,6	7,62E-04	3,07E-04	1,55799E-06
19,5	1,01E-03	5,20E-04	1,66658E-06
19,5	1,01E-03	5,14E-04	1,69877E-06
19,5	1,01E-03	5,12E-04	1,70951E-06
19,5	1,01E-03	5,02E-04	1,76316E-06
20	1,24E-03	7,10E-04	1,82368E-06
20	1,24E-03	7,06E-04	1,84639E-06
20	1,24E-03	7,15E-04	1,79946E-06
20	1,24E-03	7,11E-04	1,81687E-06
19,7	1,52E-03	9,60E-04	1,93702E-06

MWCNT - 40°C in water

MWCNT (mg)	Ctotal (M)	Cfree (M)	Gamma (mol/m2)
19,8	2,58E-04	5,27E-05	3,29008E-07
19,8	2,58E-04	5,27E-05	3,29008E-07
19,8	2,58E-04	5,15E-05	3,35022E-07
20,6	5,03E-04	1,75E-04	8,89074E-07
20,6	5,03E-04	1,75E-04	8,89074E-07
20,6	5,03E-04	1,73E-04	8,97782E-07
20,6	5,03E-04	1,76E-04	8,82543E-07
19,9	7,53E-04	3,35E-04	1,33589E-06
19,9	7,53E-04	3,38E-04	1,31786E-06
19,9	7,53E-04	3,45E-04	1,28182E-06
19,9	7,53E-04	3,43E-04	1,29308E-06
20,1	9,94E-04	5,13E-04	1,64143E-06
20,1	9,94E-04	5,20E-04	1,60501E-06
20,1	9,94E-04	5,05E-04	1,68391E-06
20,1	9,94E-04	5,31E-04	1,54355E-06
20	1,23E-03	7,32E-04	1,69843E-06
20	1,23E-03	7,24E-04	1,74472E-06
20	1,23E-03	7,13E-04	1,80027E-06
20	1,23E-03	7,09E-04	1,82573E-06
20,4	1,48E-03	9,34E-04	1,85149E-06
20,4	1,48E-03	9,43E-04	1,80678E-06
20,4	1,48E-03	9,25E-04	1,90291E-06

MWCNT - 60°C in water

MWCNT (mg)	Ctotal (M)	Cfree (M)	Gamma (mol/m2)
19,9	2,70E-04	1,04E-04	1,23325E-07
19,9	2,70E-04	1,05E-04	1,1542E-07
19,9	2,70E-04	1,01E-04	1,39136E-07
19,9	2,70E-04	1,01E-04	1,39136E-07
19,8	5,19E-04	2,77E-04	4,86616E-07
19,8	5,19E-04	3,13E-04	2,92211E-07
19,8	5,19E-04	3,12E-04	2,95028E-07
19,8	5,19E-04	3,14E-04	2,83759E-07
19,9	7,48E-04	4,86E-04	5,15655E-07
19,9	7,48E-04	4,85E-04	5,23567E-07
20,2	9,87E-04	6,96E-04	6,12132E-07
20,2	9,87E-04	6,92E-04	6,36721E-07
20,2	9,87E-04	6,96E-04	6,12132E-07
20,2	9,87E-04	6,98E-04	5,99837E-07
19,9	1,27E-03	9,52E-04	6,68034E-07
19,9	1,27E-03	9,50E-04	6,78627E-07
19,9	1,27E-03	9,52E-04	6,68034E-07
19,9	1,27E-03	9,51E-04	6,73331E-07
20,8	1,50E-03	1,16E-03	6,85635E-07
20,8	1,50E-03	1,15E-03	7,4687E-07
20,8	1,50E-03	1,16E-03	7,22376E-07

SWCNT 21°C

SWCNT (mg)	Ctotal (M)	Cfree (M)	Gamma (mol/m2)
19,1	2,54E-04	6,94E-06	5,84583E-07
19,1	2,54E-04	7,43E-06	5,81824E-07
20,1	4,99E-04	1,26E-04	1,16558E-06
20,1	4,99E-04	1,24E-04	1,17923E-06
20,1	4,99E-04	1,26E-04	1,16558E-06
20,1	4,99E-04	1,29E-04	1,15193E-06
20,4	7,82E-04	1,75E-04	2,31235E-06
20,4	7,82E-04	1,61E-04	2,38641E-06
20,4	7,82E-04	1,89E-04	2,23829E-06
20,6	9,95E-04	2,74E-04	2,8317E-06
20,6	9,95E-04	2,62E-04	2,8916E-06
20,6	9,95E-04	2,60E-04	2,90159E-06
20,6	9,95E-04	2,79E-04	2,8055E-06
20,2	1,24E-03	3,96E-04	3,48744E-06
20,2	1,24E-03	4,07E-04	3,42824E-06
20,2	1,24E-03	3,97E-04	3,4825E-06
20,2	1,24E-03	4,17E-04	3,37274E-06
20,1	1,50E-03	5,55E-04	3,95253E-06
20,1	1,50E-03	5,55E-04	3,95253E-06
20,1	1,50E-03	5,64E-04	3,90769E-06
20,1	1,50E-03	5,79E-04	3,82921E-06
19,2	1,75E-03	6,80E-04	4,73197E-06
19,2	1,75E-03	6,30E-04	5,00753E-06
19,2	1,75E-03	6,70E-04	4,78364E-06
20,3	1,99E-03	8,24E-04	4,93369E-06
20,3	1,99E-03	8,54E-04	4,77839E-06
20,3	1,99E-03	8,13E-04	4,99121E-06
20,3	1,99E-03	8,12E-04	4,9984E-06
21	2,22E-03	8,92E-04	5,59913E-06
21	2,22E-03	9,38E-04	5,36232E-06
21	2,22E-03	9,67E-04	5,21573E-06
21	2,22E-03	9,74E-04	5,18049E-06
20,1	2,49E-03	1,21E-03	5,43606E-06
20,1	2,49E-03	1,21E-03	5,45351E-06
20,1	2,49E-03	1,21E-03	5,47679E-06
20,1	2,49E-03	1,21E-03	5,47533E-06

MWCNT 21°C - NaCl 50 mM

MWCNT (mg)	Ctotal (M)	Cfree (M)	Gamma (mol/m2)
20,3	2,53E-04	6,19E-05	2,54056E-07
20,3	2,53E-04	6,03E-05	2,62328E-07
20,3	2,53E-04	6,07E-05	2,6026E-07
19,8	4,99E-04	4,64E-05	1,60766E-06
20,4	7,43E-04	9,87E-05	2,50464E-06
20,4	7,43E-04	1,05E-04	2,47026E-06
20,4	7,43E-04	1,04E-04	2,47886E-06
19,8	9,95E-04	2,37E-04	3,10453E-06
19,8	9,95E-04	2,44E-04	3,06867E-06
19,8	9,95E-04	2,25E-04	3,16827E-06
19,8	9,95E-04	2,33E-04	3,12246E-06
19,9	1,26E-03	3,12E-04	4,03327E-06
19,9	1,26E-03	2,99E-04	4,10136E-06
19,9	1,26E-03	2,80E-04	4,20578E-06
19,9	1,26E-03	2,75E-04	4,23074E-06
19,8	1,52E-03	4,47E-04	4,64559E-06
19,8	1,52E-03	4,40E-04	4,68497E-06
19,8	1,52E-03	4,53E-04	4,61277E-06
19,8	1,52E-03	4,13E-04	4,82773E-06
20,2	1,77E-03	8,04E-04	3,94972E-06
20,2	1,77E-03	7,89E-04	4,02796E-06
20,2	1,77E-03	7,68E-04	4,13881E-06
20,2	1,77E-03	7,97E-04	3,98884E-06
20,6	1,99E-03	9,05E-04	4,41881E-06
20,6	1,99E-03	8,76E-04	4,56951E-06
20,6	1,99E-03	9,18E-04	4,35184E-06
20,6	1,99E-03	9,61E-04	4,13249E-06
20,3	2,24E-03	1,10E-03	4,71803E-06
20,3	2,24E-03	1,15E-03	4,47485E-06
20,3	2,24E-03	1,19E-03	4,25282E-06
20,3	2,24E-03	1,27E-03	3,84047E-06
20,7	2,51E-03	1,28E-03	5,0301E-06
20,7	2,51E-03	1,40E-03	4,46241E-06
20,7	2,51E-03	1,31E-03	4,89321E-06
20,7	2,51E-03	1,38E-03	4,54092E-06
20,9	2,78E-03	1,57E-03	4,82678E-06
20,9	2,78E-03	1,67E-03	4,29511E-06

20,9	2,78E-03	1,66E-03	4,34293E-06
20,9	2,78E-03	1,66E-03	4,34574E-06

MWCNT 21°C - unwashed

MWCNT (mg)	Ctotal (M)	Cfree (M)	Gamma (mol/m2)
19,8	2,49E-04	1,96E-05	1,18826E-06
19,8	2,49E-04	2,11E-05	1,17982E-06
19,8	2,49E-04	2,05E-05	1,18319E-06
20,2	5,07E-04	1,56E-04	1,70928E-06
20,2	5,07E-04	1,58E-04	1,70214E-06
20,2	5,07E-04	1,57E-04	1,70654E-06
20,4	7,42E-04	2,95E-04	2,13914E-06
20,4	7,42E-04	2,98E-04	2,12317E-06
20,4	7,42E-04	2,91E-04	2,16283E-06
20,1	1,29E-03	6,90E-04	2,87092E-06
20,1	1,29E-03	6,87E-04	2,88819E-06
20,1	1,29E-03	6,90E-04	2,8715E-06
19,9	1,50E-03	1,11E-03	1,45836E-06
19,9	1,50E-03	1,10E-03	1,50707E-06
19,9	1,50E-03	1,10E-03	1,51099E-06
19,7	1,52E-03	1,25E-03	7,37554E-07
19,7	1,52E-03	1,23E-03	8,62978E-07
19,7	1,52E-03	1,24E-03	8,09871E-07
20,5	2,00E-03	1,69E-03	6,78872E-07
20,5	2,00E-03	1,70E-03	6,39776E-07
20,5	2,00E-03	1,69E-03	6,75071E-07
19,8	3,82E-04	9,13E-05	1,4767E-06
19,8	3,82E-04	8,96E-05	1,48628E-06
19,8	3,82E-04	9,02E-05	1,4829E-06
19,8	6,41E-04	3,05E-04	1,62203E-06
19,8	6,41E-04	3,00E-04	1,64991E-06
19,8	6,41E-04	3,04E-04	1,62886E-06
20,1	1,14E-03	5,04E-04	3,03323E-06
20,1	1,14E-03	4,70E-04	3,22476E-06
20,1	1,14E-03	4,71E-04	3,22086E-06
20,3	1,35E-03	6,82E-04	3,05494E-06
20,3	1,35E-03	6,86E-04	3,02959E-06
20,3	1,35E-03	6,76E-04	3,088E-06
20,5	1,57E-03	9,81E-04	2,53806E-06
20,5	1,57E-03	9,68E-04	2,61445E-06
20,5	1,57E-03	9,70E-04	2,5995E-06
19,9	1,73E-03	1,18E-03	2,37784E-06
19,9	1,73E-03	1,16E-03	2,48251E-06

MWCNT 21°C SDBS

MWCNT (mg)	Ctotal (M)	Cfree (M)	Gamma (mol/m2)
20,2	2,58E-04	2,32E-05	4,65854E-07
20,2	2,58E-04	7,08E-05	9,39064E-07
20,2	2,58E-04	7,13E-05	9,36674E-07
20,2	2,58E-04	6,82E-05	9,52138E-07
19,8	5,07E-04	1,46E-04	1,77254E-06
19,8	5,07E-04	1,44E-04	1,85778E-06
19,8	5,07E-04	1,53E-04	1,81457E-06
19,7	7,50E-04	4,03E-04	1,62794E-06
19,7	7,50E-04	4,04E-04	1,82731E-06
19,7	7,50E-04	3,99E-04	1,85463E-06
19,8	1,02E-03	5,39E-04	2,21073E-06
19,8	1,02E-03	5,20E-04	2,57538E-06
19,8	1,02E-03	5,28E-04	2,53641E-06
19,6	1,28E-03	7,93E-04	2,15134E-06
19,6	1,28E-03	7,95E-04	2,54459E-06
19,6	1,28E-03	7,95E-04	2,54869E-06
20,5	1,53E-03	9,59E-04	2,37881E-06
20,5	1,53E-03	9,53E-04	2,86929E-06
20,5	1,53E-03	9,19E-04	3,03923E-06
19,9	2,05E-03	1,32E-03	3,07973E-06
19,9	2,05E-03	1,33E-03	3,69134E-06
19,9	2,05E-03	1,33E-03	3,7281E-06
19,5	2,57E-03	1,69E-03	3,66214E-06
19,5	2,57E-03	1,68E-03	4,60384E-06
19,5	2,57E-03	1,71E-03	4,48079E-06

MWCNT 21°C - Triton X100

MWCNT (mg)	Ctotal (M)	Cfree (M)	Gamma (mol/m2)
19,9	1,14E-04	1,40E-06	1,12858E-07
19,9	1,14E-04	1,25E-06	1,13691E-07
19,9	1,14E-04	1,58E-06	1,11859E-07
20,3	3,26E-04	2,52E-05	1,04015E-06
20,3	3,26E-04	2,49E-05	1,04179E-06
20,3	3,26E-04	2,50E-05	1,04146E-06
19,9	4,36E-04	5,75E-05	1,44098E-06
19,9	4,36E-04	5,58E-05	1,45019E-06
19,9	4,36E-04	5,60E-05	1,44924E-06
20,2	5,43E-04	9,78E-05	1,73864E-06
20,2	5,43E-04	9,75E-05	1,74002E-06
20,2	5,43E-04	9,75E-05	1,74035E-06
19,7	6,57E-04	1,33E-04	2,16627E-06
19,7	6,57E-04	1,32E-04	2,16887E-06
19,7	6,57E-04	1,33E-04	2,16627E-06
19,9	7,52E-04	1,73E-04	2,42471E-06
19,9	7,52E-04	1,75E-04	2,41117E-06
19,9	7,52E-04	1,76E-04	2,40802E-06
20,1	8,55E-04	2,03E-04	2,77202E-06
20,1	8,55E-04	2,04E-04	2,76889E-06
20,1	8,55E-04	2,03E-04	2,77297E-06
20,2	9,81E-04	2,35E-04	3,17083E-06
20,2	9,81E-04	2,35E-04	3,16836E-06
20,2	9,81E-04	2,33E-04	3,17868E-06

MWCNT – 21°C - BzT

MWCNT (mg)	Ctotal (M)	Cfree (M)	Gamma (mol/m2)
19,9	9,94E-05	2,96E-05	1,55782E-07
19,9	9,94E-05	2,80E-05	1,6473E-07
19,9	9,94E-05	2,80E-05	1,6445E-07
19,9	9,94E-05	2,80E-05	1,6473E-07
20,3	2,30E-04	5,51E-05	1,86545E-07
20,3	2,30E-04	5,43E-05	1,90635E-07
20,3	2,30E-04	5,50E-05	1,8709E-07
20,3	2,30E-04	5,40E-05	1,92271E-07
19,8	2,47E-04	5,96E-05	2,65132E-07
19,8	2,47E-04	6,14E-05	2,5466E-07
19,8	2,47E-04	6,26E-05	2,47868E-07
19,8	2,47E-04	6,24E-05	2,49E-07
19,7	3,17E-04	8,71E-05	4,73842E-07
19,7	3,17E-04	8,64E-05	4,77871E-07
19,7	3,17E-04	8,84E-05	4,66382E-07
19,7	3,17E-04	8,88E-05	4,63994E-07
19,8	3,71E-04	1,25E-04	5,75868E-07
19,8	3,71E-04	1,20E-04	6,01229E-07
19,8	3,71E-04	1,24E-04	5,78923E-07
19,8	3,71E-04	1,20E-04	6,01993E-07
20,3	4,82E-04	2,08E-04	6,07843E-07
20,3	4,82E-04	2,07E-04	6,11578E-07
20,3	4,82E-04	2,12E-04	5,83276E-07
20,3	4,82E-04	2,02E-04	6,42035E-07
19,8	5,79E-04	3,01E-04	5,95295E-07
19,8	5,79E-04	3,04E-04	5,78938E-07
19,8	5,79E-04	3,02E-04	5,89253E-07
19,8	5,79E-04	2,99E-04	6,10619E-07
19,9	6,76E-04	3,61E-04	7,432E-07
19,9	6,76E-04	3,60E-04	7,52243E-07
19,9	6,76E-04	3,59E-04	7,53993E-07
20,2	7,72E-04	4,54E-04	7,10857E-07
20,2	7,72E-04	4,50E-04	7,34881E-07
20,2	7,72E-04	4,53E-04	7,15633E-07
20,2	7,72E-04	4,19E-04	9,02901E-07
20,4	8,57E-04	4,60E-04	1,09997E-06
20,4	8,57E-04	4,62E-04	1,08564E-06

20,3	9,42E-04	5,25E-04	1,18747E-06
20,3	9,42E-04	5,22E-04	1,20024E-06
20,0	1,14E-03	6,77E-04	1,37266E-06
20,0	1,14E-03	6,79E-04	1,35909E-06
20,0	1,14E-03	6,83E-04	1,33697E-06
20,0	1,14E-03	6,72E-04	1,40171E-06
19,6	1,33E-03	7,76E-04	1,79501E-06
19,6	1,33E-03	7,77E-04	1,78827E-06

RAMAN SPECTRA (RBM BANDS)

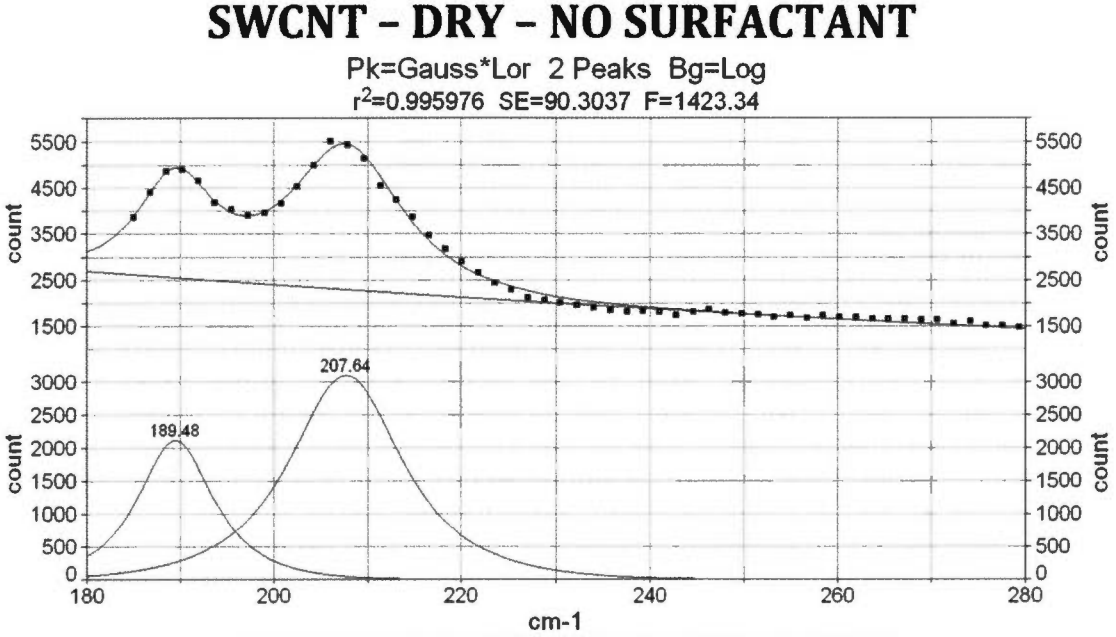

Peak	Wavenumber (cm^{-1})	FWHM (cm^{-1})	% Area
1	189.48	9.67	27.63
2	207.64	14.14	72.37

Figure A.1 Raman spectrum of SWCNT

SWCNT IN WATER NO SURFACTANT

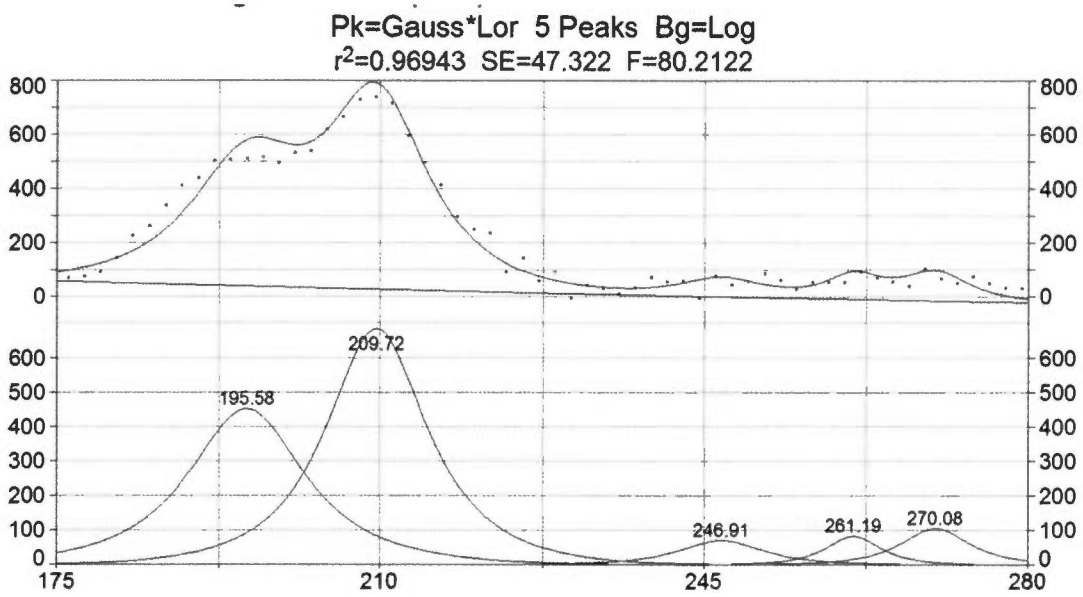

Peak	Wavenumber (cm^{-1})	FWHM (cm^{-1})	% Area
1	195.58	14.89	37.46
2	209.72	12.82	49.96
3	246.91	10.75	4.31
4	261.19	7.01	3.30
5	270.08	8.74	4.97

Figure A.2 Raman spectrum of SWCNT

SWCNT – DISPERSED IN SDS/WATER (0.5mM)
T = 21°C

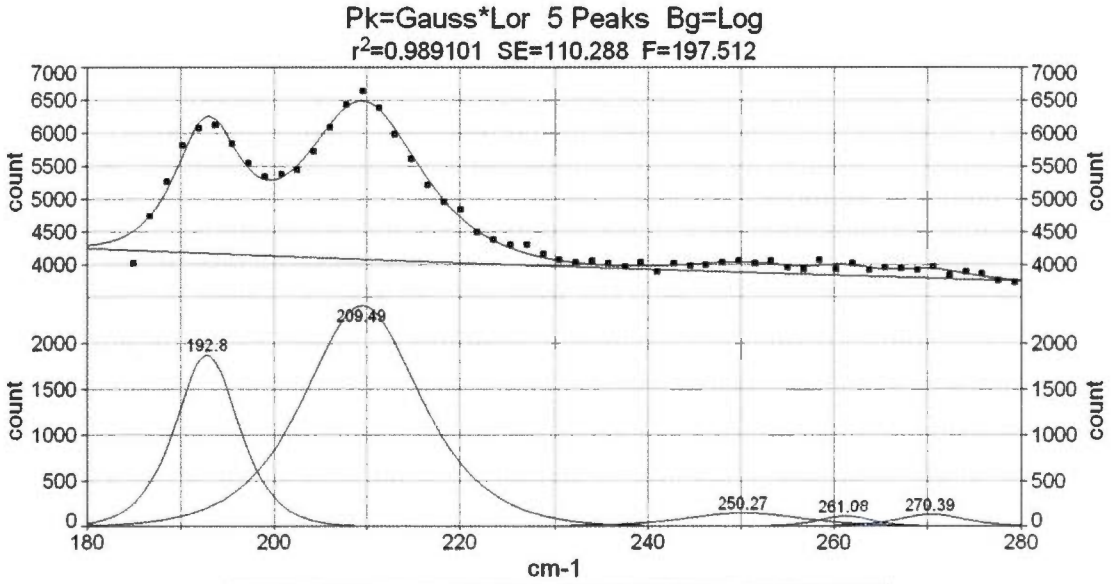

Peak	Wavenumber (cm^{-1})	FWHM (cm^{-1})	% Area
1	192.78	8.00	26.75
2	209.49	14.71	65.54
3	250.26	14.88	4.19
4	261.08	6.81	1.44
5	270.39	8.61	2.08

Figure A.3 Raman spectrum of SWCNT

SWCNT – DISPERSED IN SDS/WATER (1.5mM)
T = 21°C

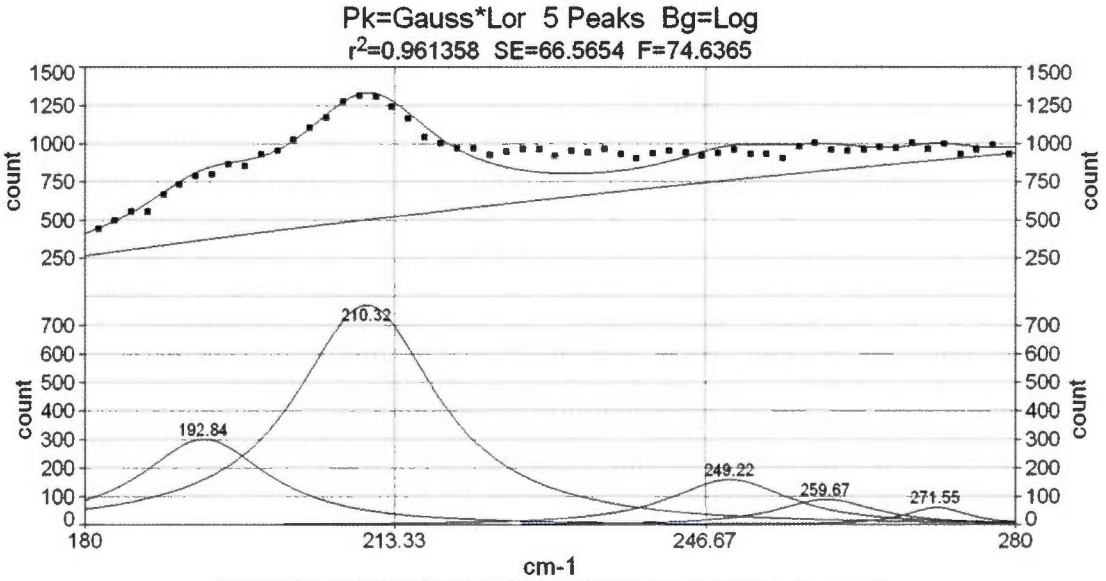

Peak	Wavenumber (cm^{-1})	FWHM (cm^{-1})	% Area
1	192.84	16.66	21.21
2	210.32	18.27	60.68
3	249.22	15.73	12.80
4	259.67	13.54	5.13
5	271.55	8.46	2.19

Figure A.4 Raman spectrum of SWCNT

SWCNT – DISPERSED IN SDS/WATER (3.0mM)
T = 21°C

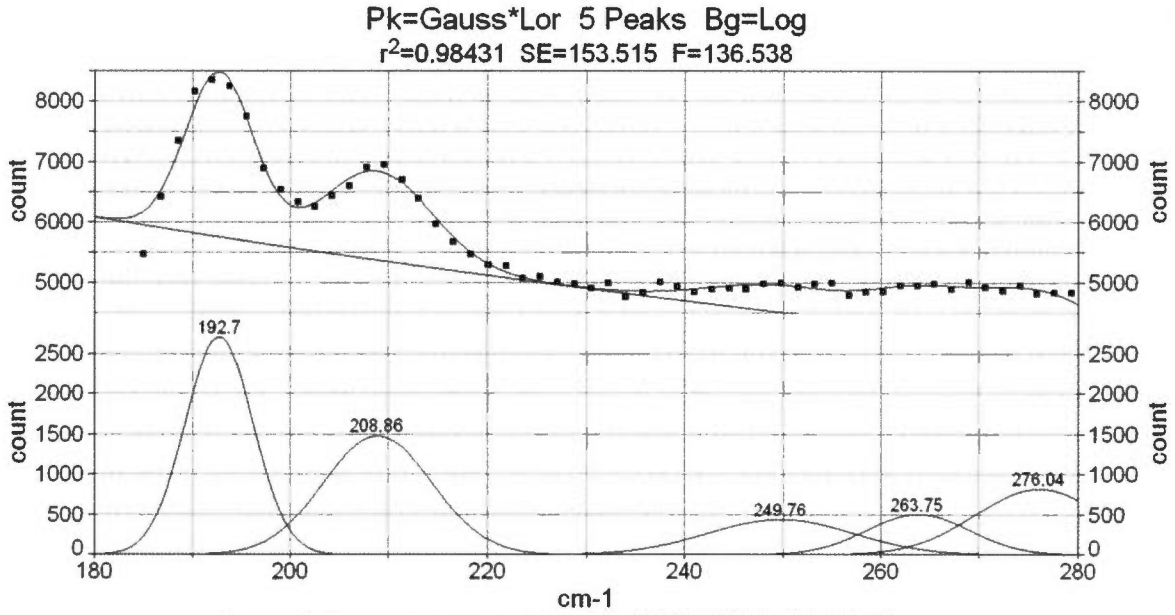

Peak	Wavenumber (cm^{-1})	FWHM (cm^{-1})	% Area
1	192.70	8.20	34.36
2	208.86	12.96	30.11
3	249.76	17.48	12.06
4	263.75	12.38	9.77
5	276.04	15.31	13.70

Figure A.5 Raman spectrum of SWCNT

Tg of THE POLYMER DISPERSION MEASURED BY DIFFERENTIAL SCANNING CALORIMETRY

Differential scanning calorimetry measurements (DSC) of solid samples were performed on a DSC823e (TOPEM modulation) equipped with an FRS5 sample cell, a sample robot, a Julabo FT400 intracooler and an HRS7 sensor from Mettler Toledo. Samples were heated from -20°C to 100°C at rates of 10, 20, 30 and 40°C/min and data were analyzed with STAR software. All reported values are for samples which have first been cooled from 100°C at a rate of 10°C/min. Due to the compositional drift which occurs during polymerization, the Tg transition is very broad.

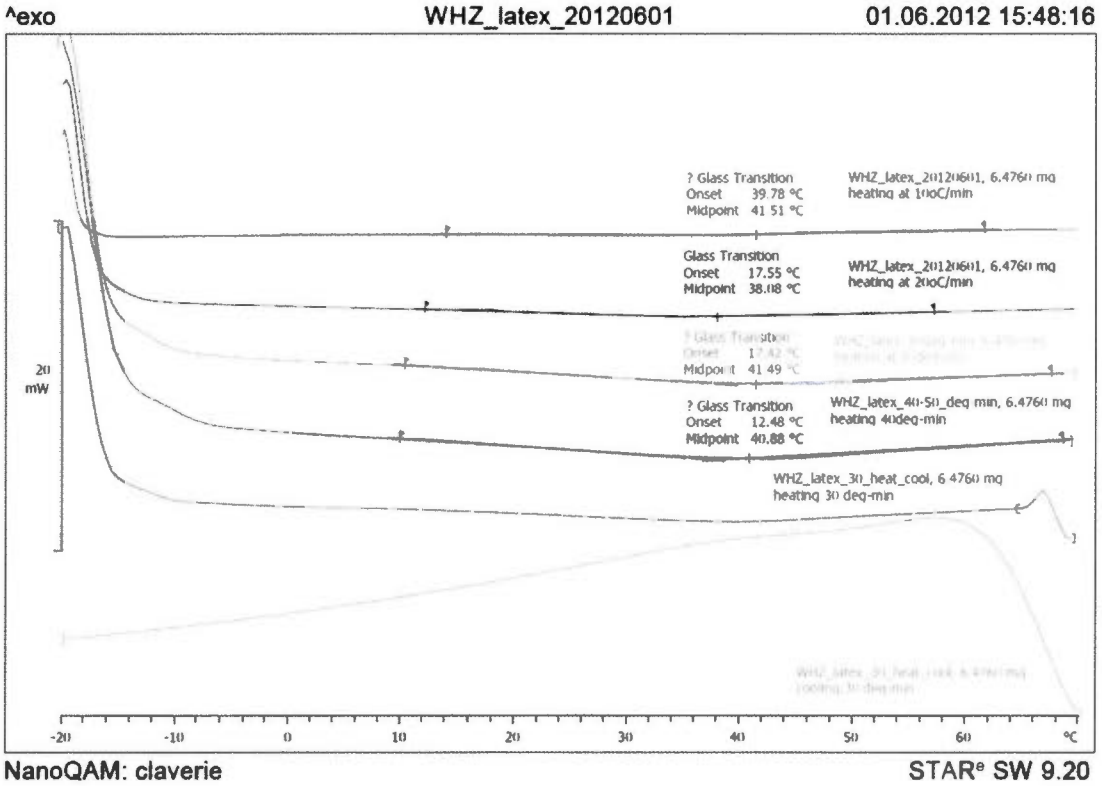

Rate °/min	Onset of Tg °C	Midpoint of Tg °C
10	21.5	41.5
20	17.5	38.0
30	17.4	41.5
40	12.5	41.0

Figure A.6 Tg of the polymer dispersion measured by DSC

Absorption Spectrum of a MWCNT Dispersion (1 g/L) in water containing SDS (0.5 g/L)

Picture of the 1mm cuvette

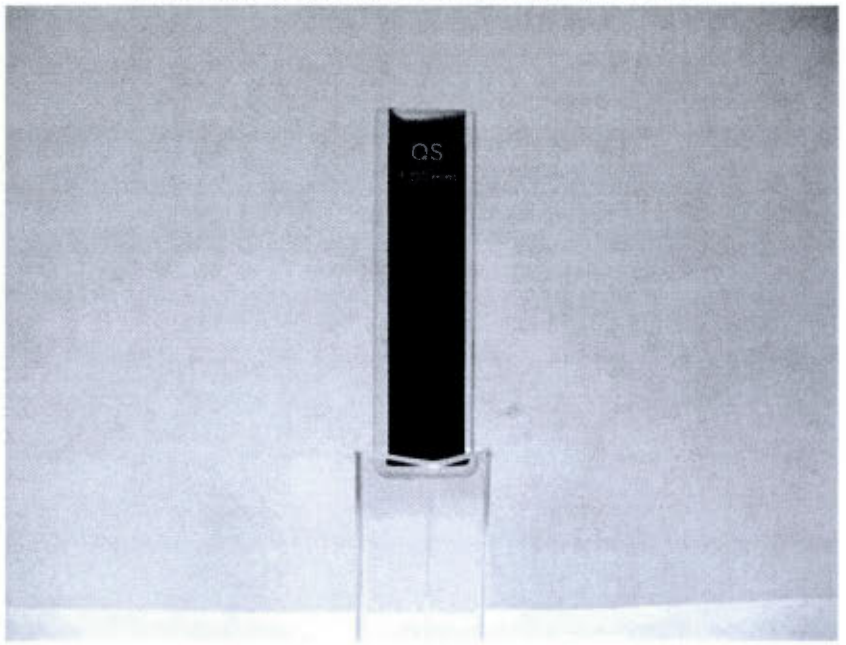

Absorption Spectrum:

Zero values are due to instrument saturation

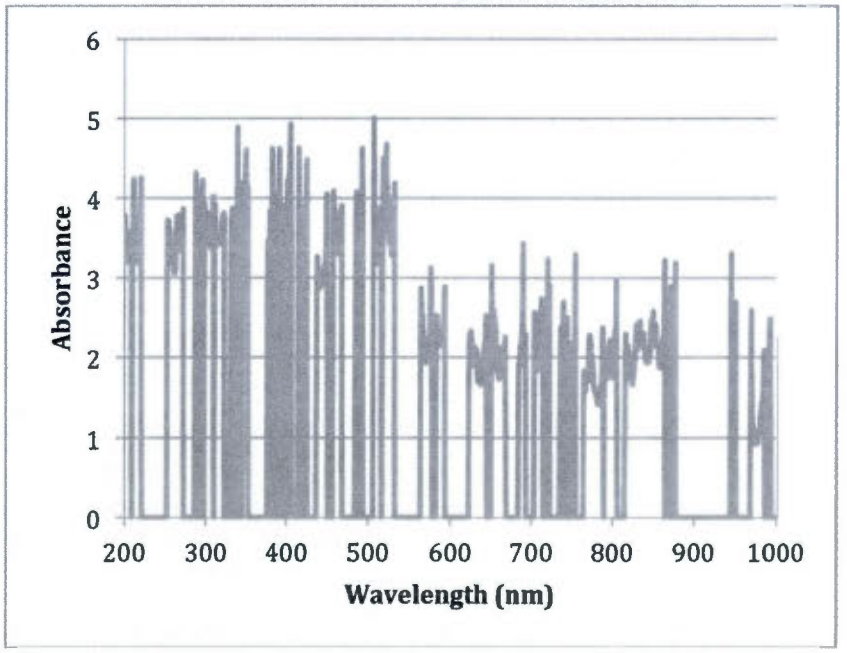

Figure A.7 Absorption Spectrum of a MWCNT Dispersion in water containing SDS

Dispersion of MWCNTs (1 g/L) in water with various concentration of SDS

Concentration of SDS (g/L) from upper left to bottom right: 0.01; 0.04; 0.06; 0.08; 0.10, 0.20; 0,30; 0.40; 0.50; 0.60

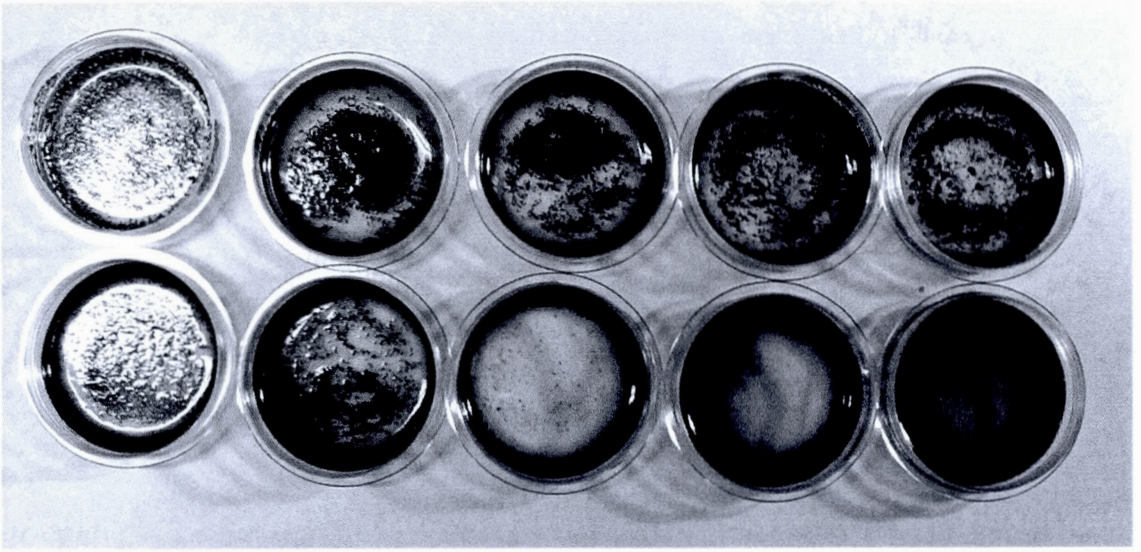

Figure A.8 Dispersion of MWCNTs in water with various concentrations of SDS

Dispersion of MWCNTs (1 g/L) in water with various concentration of SDBS

Concentration of SDBS (g/L) from left to right: 0.10; 0.20; 0.30; 0,.0; 0.50; 0.60

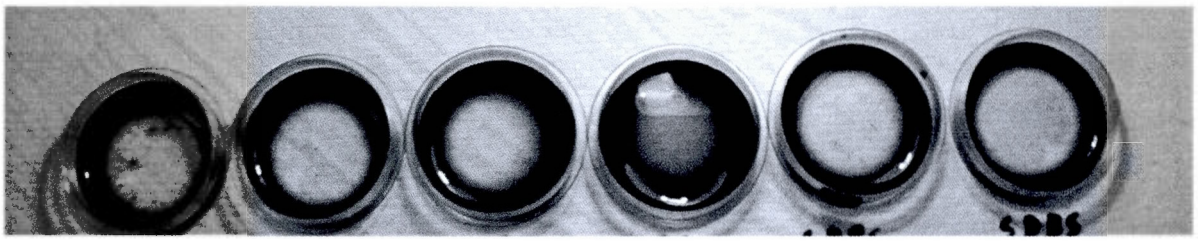

Figure A.9 Dispersion of MWCNTs in water with various concentrations of SBDS

Dispersion of MWCNTs (1 g/L) in water with various concentration of BZT

Concentration of BZT (g/L) from left to right: 0.10; 0.20; 0.30; 0,.0; 0.50; 0.60

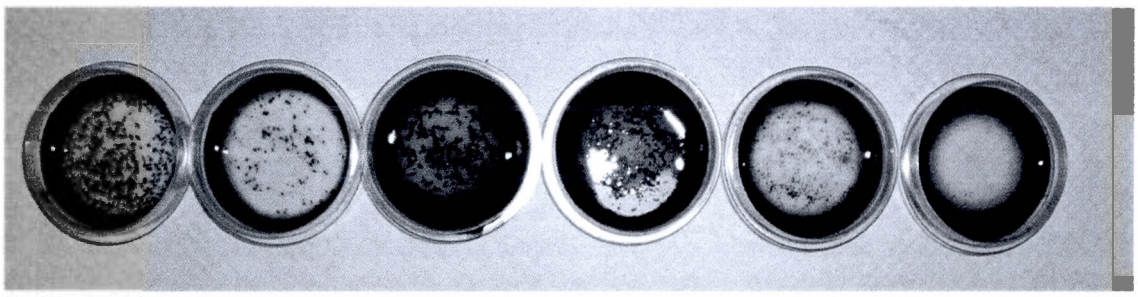

Figure A.10 Dispersion of MWCNTs in water with various concentrations of BZT

ANNEXE B

SUPPORTING INFORMATION FOR:

A versatile encapsulation method of non-covalently modified carbon nanotubes by RAFT polymerization

Weiheng Zhong, Jules Nguendia Zeuna, Jerome P. Claverie*

NanoQAM, Quebec Center for Functional Materials, Department of Chemistry, University of Quebec in Montreal, Succ Centre Ville, PO Box 8888, Montreal, QC, H3C3P8, Canada. Fax: 514 9874054 E-mail: claverie.jerome@uqam.ca

* claverie.jerome@uqam.ca

Journal of Polymer Science Part A: Polymer Chemistry

Volume 50, Issue 21, November 2012, pages 4403–4407

Experimental Section

Materials

Multiwall carbon nanotubes (MWNT, Baytubes® C 150 P) were graciously supplied by Bayer Material Science whereas single wall carbon nanotubes (SWNT, C-SWCNT) were purchased from Raymor Nanotech. Nanopure water (σ = 18.2 MΩ.cm) was obtained from Milli-Q Plus system. Sodium dodecyl sulfate (SDS, ACS grade, Sigma-Aldrich) was purified by recrystallization in order to remove dodecanol impurity. In short, 30 g of SDS was dissolved in 150 mL solution of benzene and ethanol (50:50 v:v) under reflux. The solution was then cooled to room temperature, and SDS crystals were then collected by vacuum filtration and dried in vacuum overnight at 70°C. The procedure was repeated three times. Styrene (S), n-butyl acrylate (BA) and methyl methacrylate (MMA) were filtered on basic alumina before use in order to remove the inhibitor. Acrylic acid (AA) was distilled under reduced pressure before use. The initiator for the whole study was 4,4-azobis(4-cyanovaleric acid) (ABV, from Sigma-Aldrich). Sonication was performed with a Branson ultrasonic sonifier (450W nominal power) equipped with a 19mm (3/4") diameter solid horn.

CNT purification

The purification procedure was identical for MWNT and SWNT, and was adapted from Musumeci et al.[1] Nanotubes (200 mg) were suspended in 100 mL of an aqueous solution of HCl, 1N and dispersed by sonication (for 5 minutes, amplitude 20%). The suspension was then centrifuged at 3500 rpm for 10 minutes at room temperature and the nanotubes were separated from the supernatant. This procedure was repeated 5 times. The procedure was then repeated using nanopure water instead of the acidic solution, until the pH of the supernatant was neutral. The nanotubes were then dried overnight in an air-convection oven at 70°C. The role of the purification was to remove metallic impurities which could greatly change the capacity of a dispersant to stabilize the CNT dispersion.[2]

Transmission Electron Microscopy (TEM)

20 mL of encapsulated CNT sample was diluted with 2 mL of ultrapure water and a 20 mL drop of the diluted solution was deposited on a Cu / carbon grid (mesh 200). For the pictures of samples of CNT coated with PAA, PABA, PSAA prior to polymerization, Lacey-formvar grids were used (mesh 200). The grid was dried overnight in air and analyzed with a Jeol JEM-2100F microscope equipped with a field emission gun running at 200 kV.

Synthesis of the dispersants

Dispersants PABA and PAA were respectively synthesized and characterized using the reports of Hawkett[3] and Claverie.[4] For PSAA, the synthesis was adapted from Beattie et al.[5] In a three-neck 50 mL round bottom flask equipped with a cold-water reflux condenser and a nitrogen entry were added 1.38 g of RAFT agent 2 butylsulfanyl thiocarbonylsulfanylpropionic acid[3] (6 mmol, 1eq), 4.57g of AA (63 mmol, 10 eq), 3.28g of styrene (34 mmol, 5eq) and 0.02g of ABV (6 mmol, 0.1 eq) in 23 mL of dimethylacetamide (DMAc). The solution was purged with nitrogen for 30 minutes, and was then stirred and heated to a temperature of 60°C for 8 hours under a nitrogen blanket. Then, 80 % of solvent was removed by rotary evaporator and a yellow viscous liquid was obtained. This viscous solution was slowly added to 200 mL of hexane under vigorous stirring. The precipitate was collected and the polymer was dried in vacuum. Yield = 5.49g – Styrene conversion = 63%, acrylic acid conversion = 34%.

^{1}H NMR (300 MHz, Acetone-d_6, δ): 7.18 (b, 5H, Ar H), 5.28 (b, 1H, -S-**CH**Ph), 4.84 (b, 1H, -SC**H**CO_2H), 4.41 (b, 1H, -S-C**H**CO_2H), 3.36 (b, 2H, -S-CH_2), 2.7- 0.95 (b), 0,87 (t, 3H, CH_3CH_2).

^{13}C NMR (75.43 MHz, Acetone-d_6, δ): 138-136 (b, Ar), 46 (b, CH_2 PS), 44 (b, CH, PS), 42 (b, CH AA), 35 (b, CH_2 AA), 31 (CH), 27 (CH_2), 21 (CH_2), 14.8 – 14.1 (CH_3)

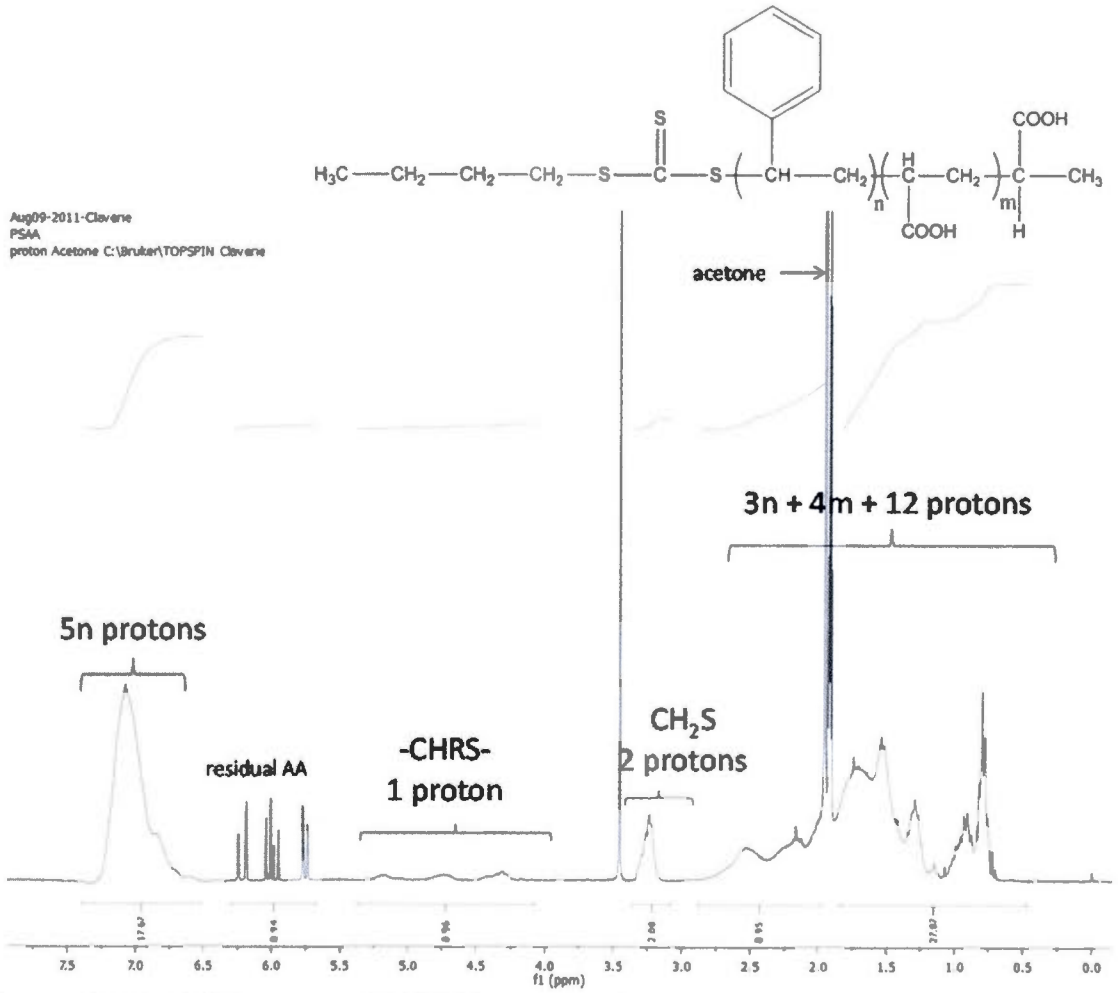

Figure B.1 RMN^{1}H spectra of RAFT dispersant PSAA

CNT encapsulation

For PABA and PSAA, a 1.25 g/L aqueous solution of RAFT dispersant was prepared by adding together 25 mg of RAFT dispersant, 50 mL of 0.5 N NaOH and 20 mL of ultrapure water. The sodium hydroxide was necessary to solubilise the dispersant in water (approximately 33% of the COOH groups are neutralized). For PAA, which is soluble under its acidic form in water, the RAFT dispersant was used as such. To 25 mL of an aqueous 1.25 g/L RAFT dispersion were added 50 mg of CNT and the mixture was sonicated for 5 minutes (incident power = 40%). A stable CNT dispersion was obtained to which 10 mL of an aqueous AVB solution (c = 0.202 mol/L) was added. The whole mixture was transferred into a round bottom flask and was purged with nitrogen for 30 minutes. The solution was heated at 80°C and an aqueous emulsion constituted of 210 mg of styrene and 50 mg of SDS was added at a rate of 5 mL/hour over 4 hours. The mixture was then heated at 80°C for an additional 2 hours to complete the polymerization.

Building of the adsorption isotherms

For PSAA and PABA, a 10 g/L stock solution was prepared by dissolving the dispersant (500 mg) in 50 mL water containing 10-3 mol of NaOH, so that approximately half of the COOH groups of PSAA were deprotonated (measured pH = 6.8). For PAA, a 2 g/L stock solution of PAA was prepared in water. In a vial, 10 mg of MWNT (resp. 5 mg of SWNT) and a given volume of the stock solution of dispersant were mixed together and the total volume was adjusted to 10 mL with water (carbonate buffer for PABA). The suspension was stirred using a small magnetic stir bar while being immersed in an ice bath (0°C) and was sonicated at 40% amplitude during 5 minutes. The role of the ice-bath is to prevent a large temperature increase during sonication. Magnetic stirring during sonication was necessary to allow the entire volume to be sonicated. Care was used to introduce the sonicator tip in such a way that it did not touch the magnetic stir bar. After the dispersion, the solution was left on an orbital shaker for 2 hours. Then, 3 mL of the solution was removed and filtered through a nylon filter 0.22 mm. We found that the hold-up of the dispersant on the filter was negligible. The absorption of the clear solutions were then quantified on a spectrophotometer (Ocean Optic spectrophotometer)

at 308 nm, which corresponds to the maximum of absorption of the trithiocarbonate unit. Certain preparations were diluted in order to respect the concentration range for which the Beer-Lambert law was linear.

Raman spectra

Raman spectra ranging from 100 cm^{-1} to 3000 cm^{-1} were acquired on a Renishaw RM 3000 confocal microscope equipped with a laser of wavelength 514 nm. A drop of the dispersion to analyze was dropped on an aluminum foil surface, and was covered with a cover glass. The intensity of the D band (1342 cm^{-1}) and the G band (1565 cm^{-1} and 1589 cm^{-1}) were used to monitor the possibility of covalent modification. For this purpose, all the peaks were deconvoluted using the software Peakfit from Systat.

GPC analysis of the polymers

A latex sample (3 mL) was dried in air and the solid was dissolved in THF (2 mL). The sample was filtered over a 0.2 mm syringe filter and the clear solution was then analyzed by GPC in THF equipped with two Polymer Labs Mixed B colunms and a RI detector. The instrument was calibrated with polystyrene standards.

Table 1 – Entry 1

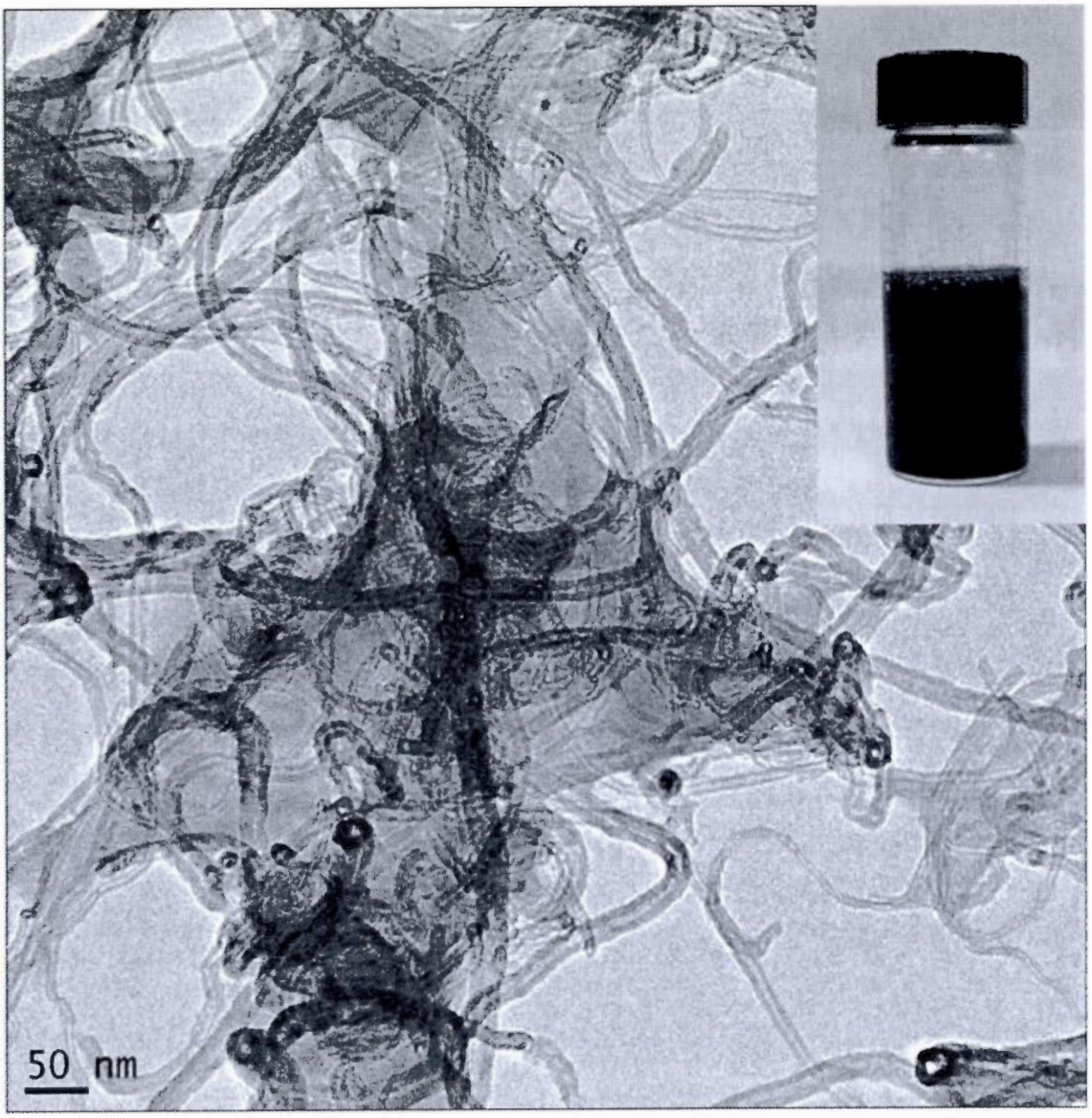

Figure B.2 TEM picture of CNT encapsulated in a polymer (entry 1)

Table 1 – Entry 1

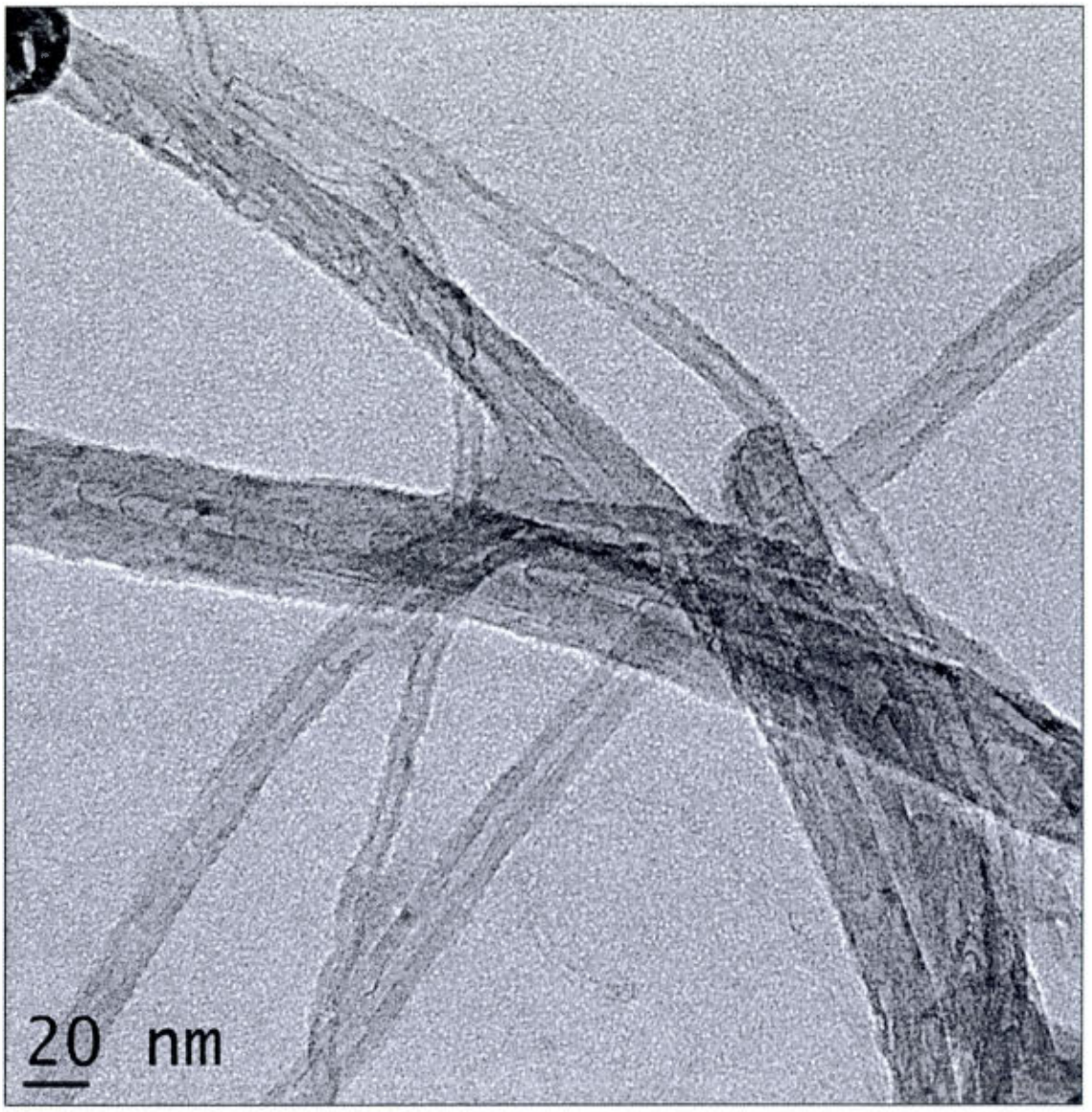

Figure B.3 TEM picture of CNT encapsulated in a polymer (entry 1)

Table 1 – Entry 1

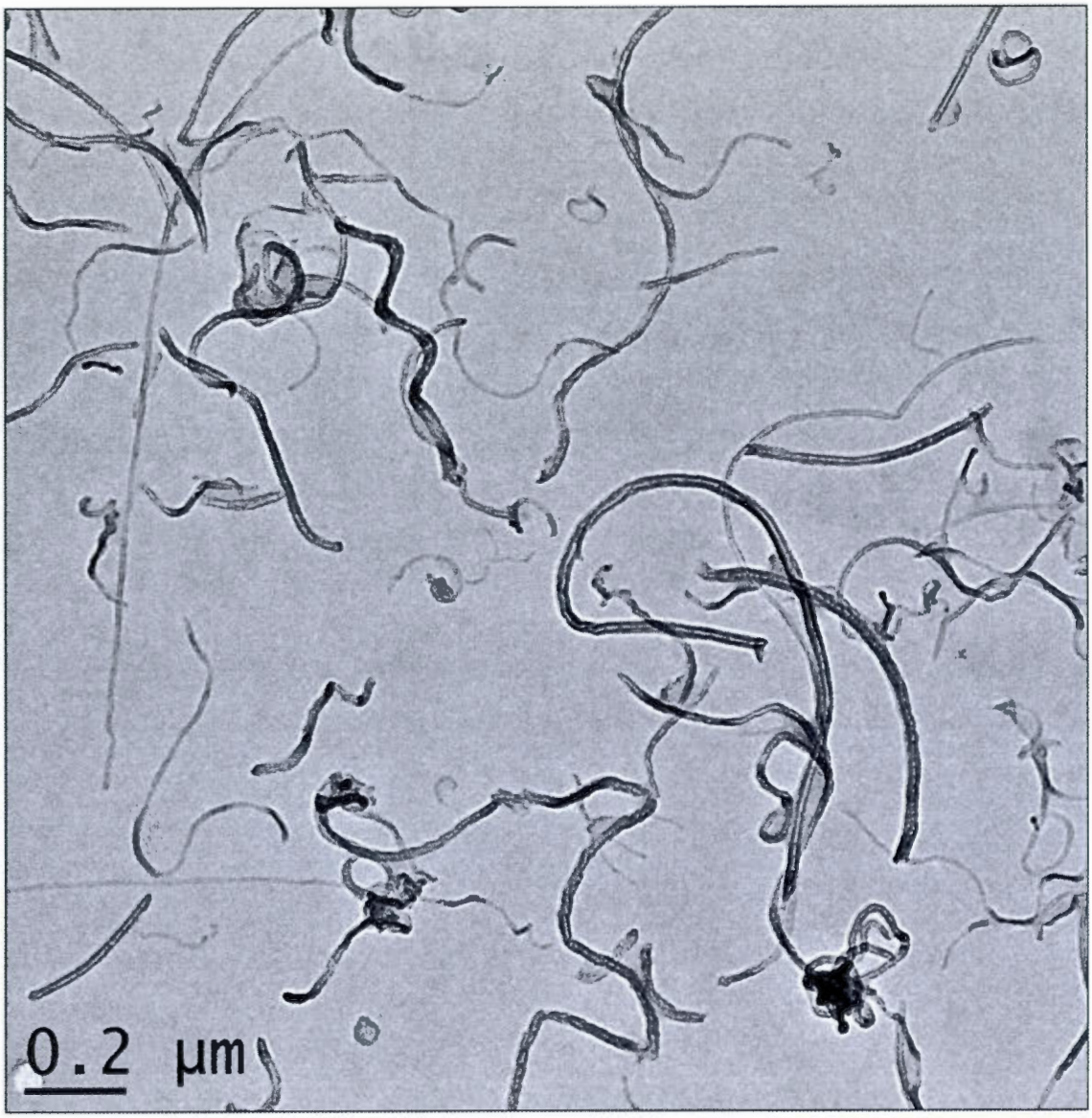

Figure B.3 TEM picture of CNT encapsulated in a polymer (entry 1)

Table 1 – Entry 2

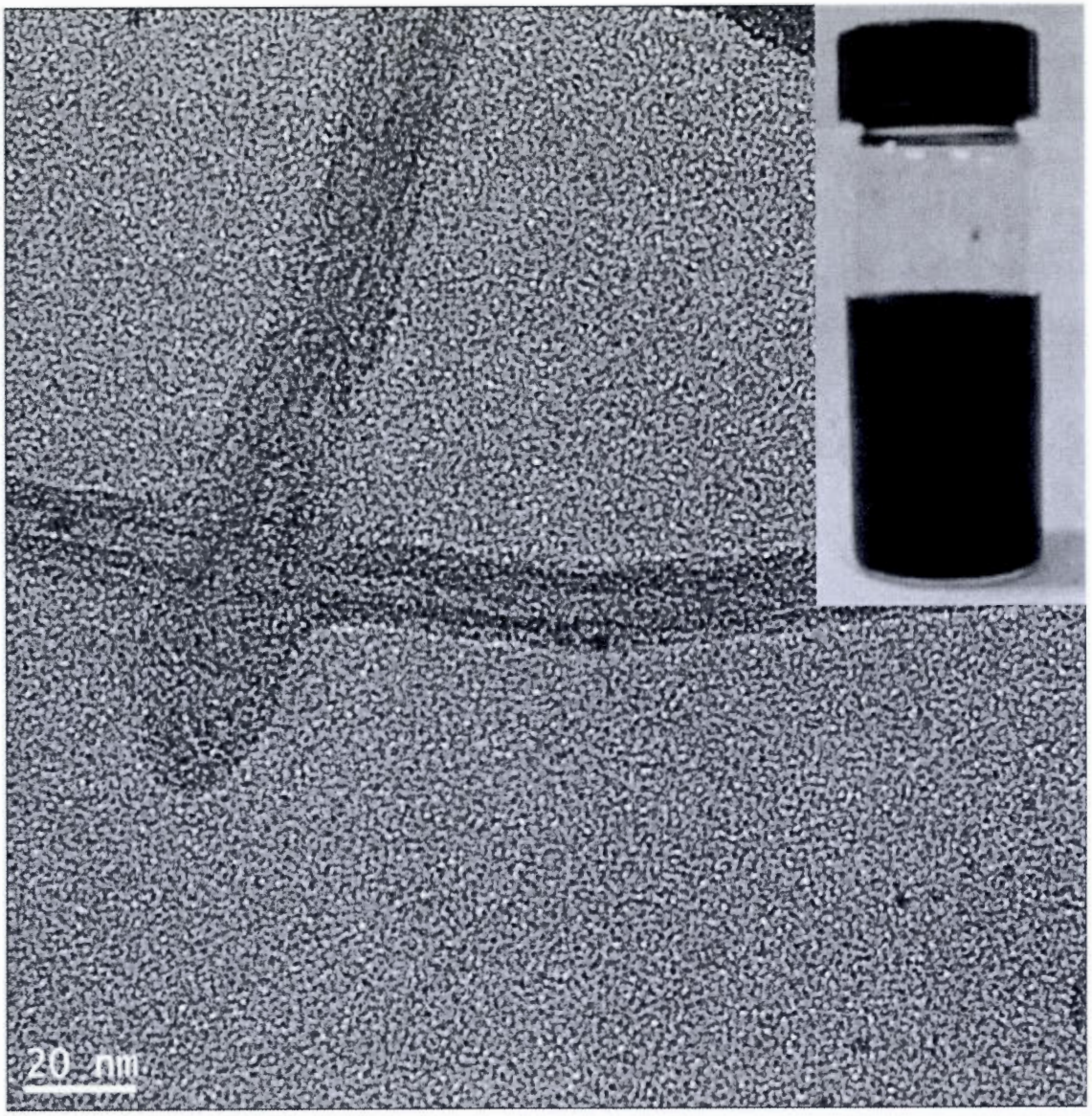

Figure B.4 TEM picture of CNT encapsulated in a polymer (entry 2)

Table 1 – Entry 2

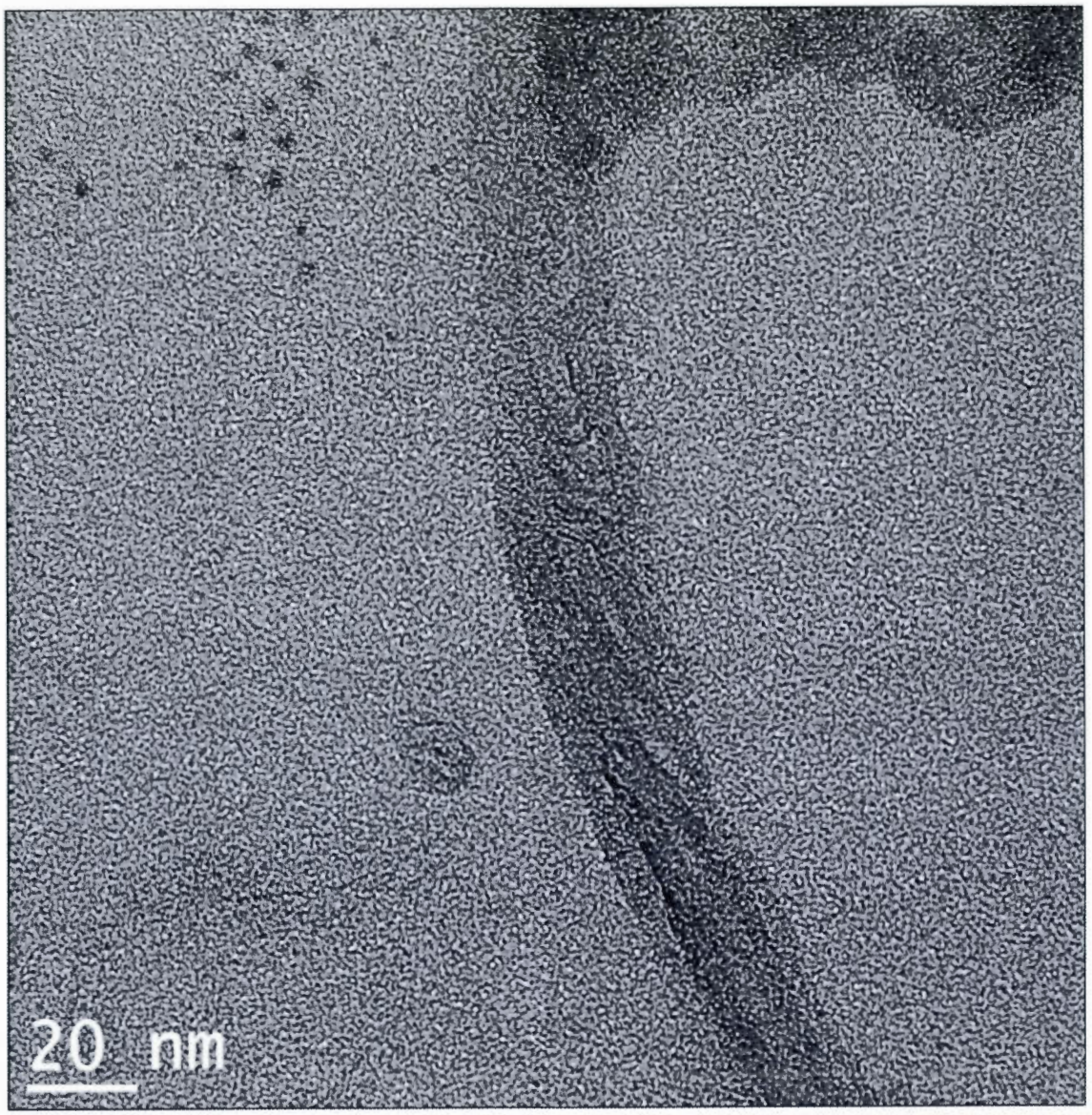

Figure B.5 TEM picture of CNT encapsulated in a polymer (entry 2)

Table 1 – Entry 3

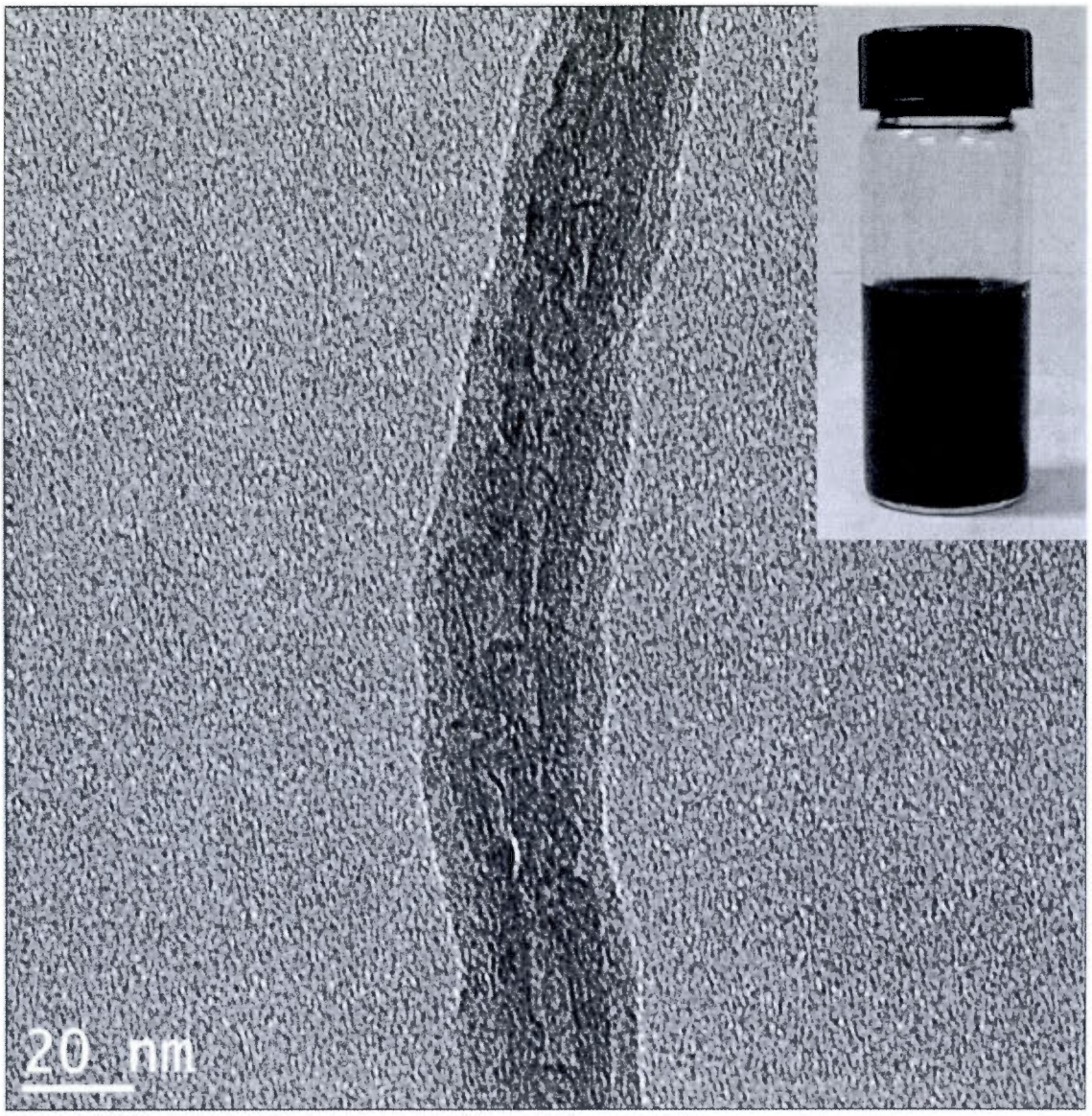

Figure B.6 TEM picture of CNT encapsulated in a polymer (entry 3)

Table 1 – Entry 3

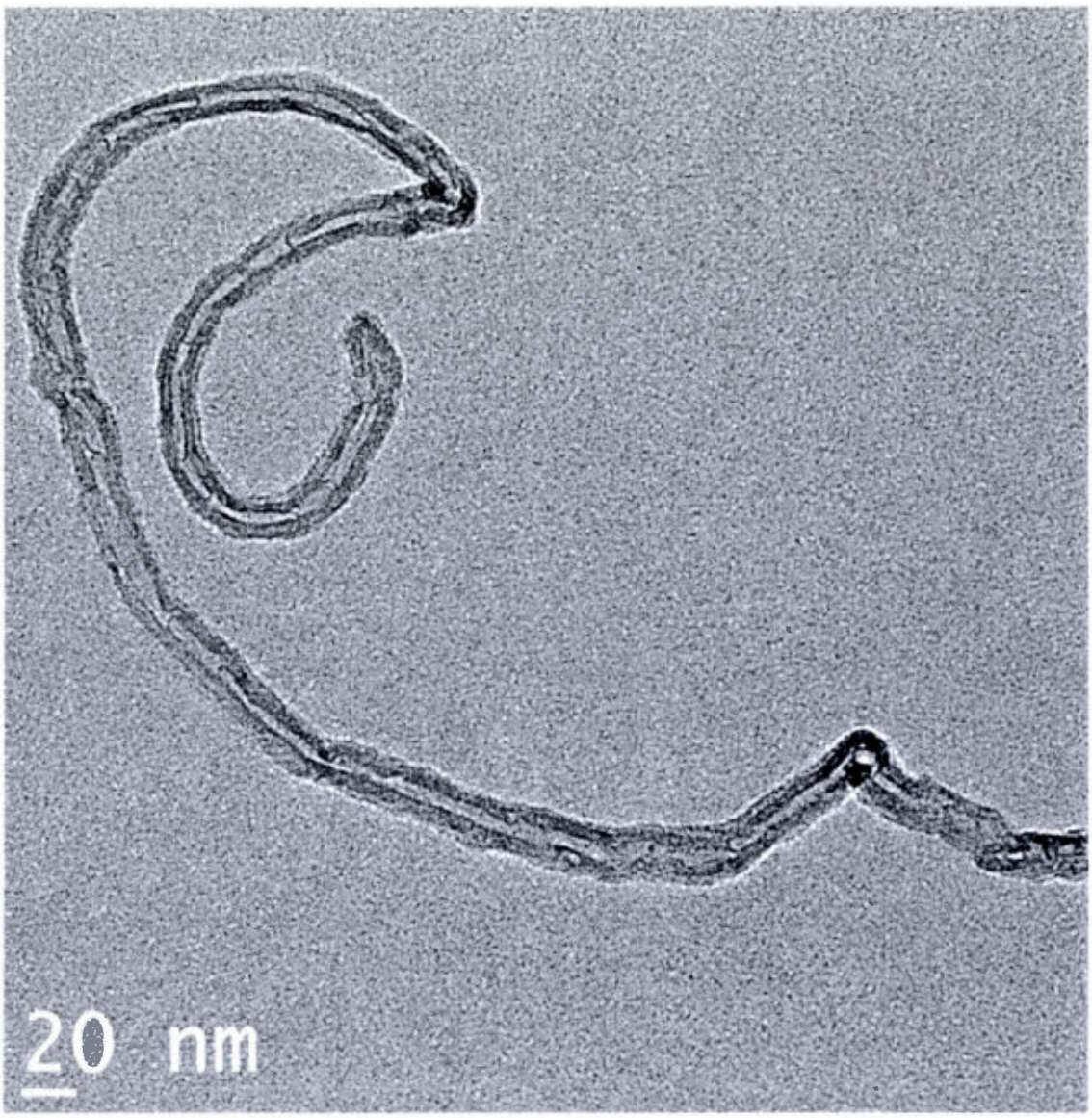

Figure B.7 TEM picture of CNT encapsulated in a polymer (entry 3)

Table 1 – Entry 5

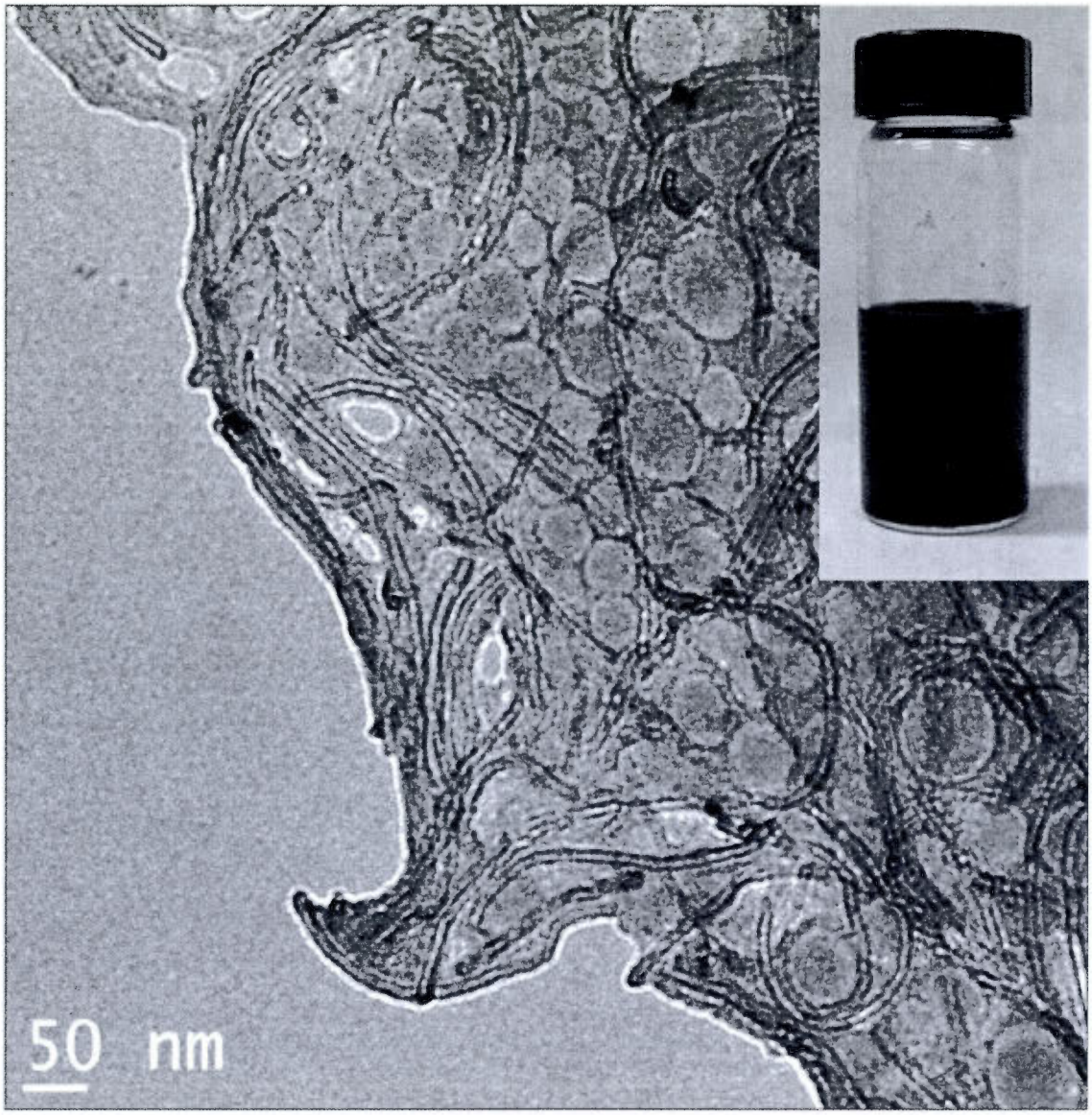

Figure B.9 TEM picture of CNT encapsulated in a polymer (entry 5)

Table 1 – Entry 5

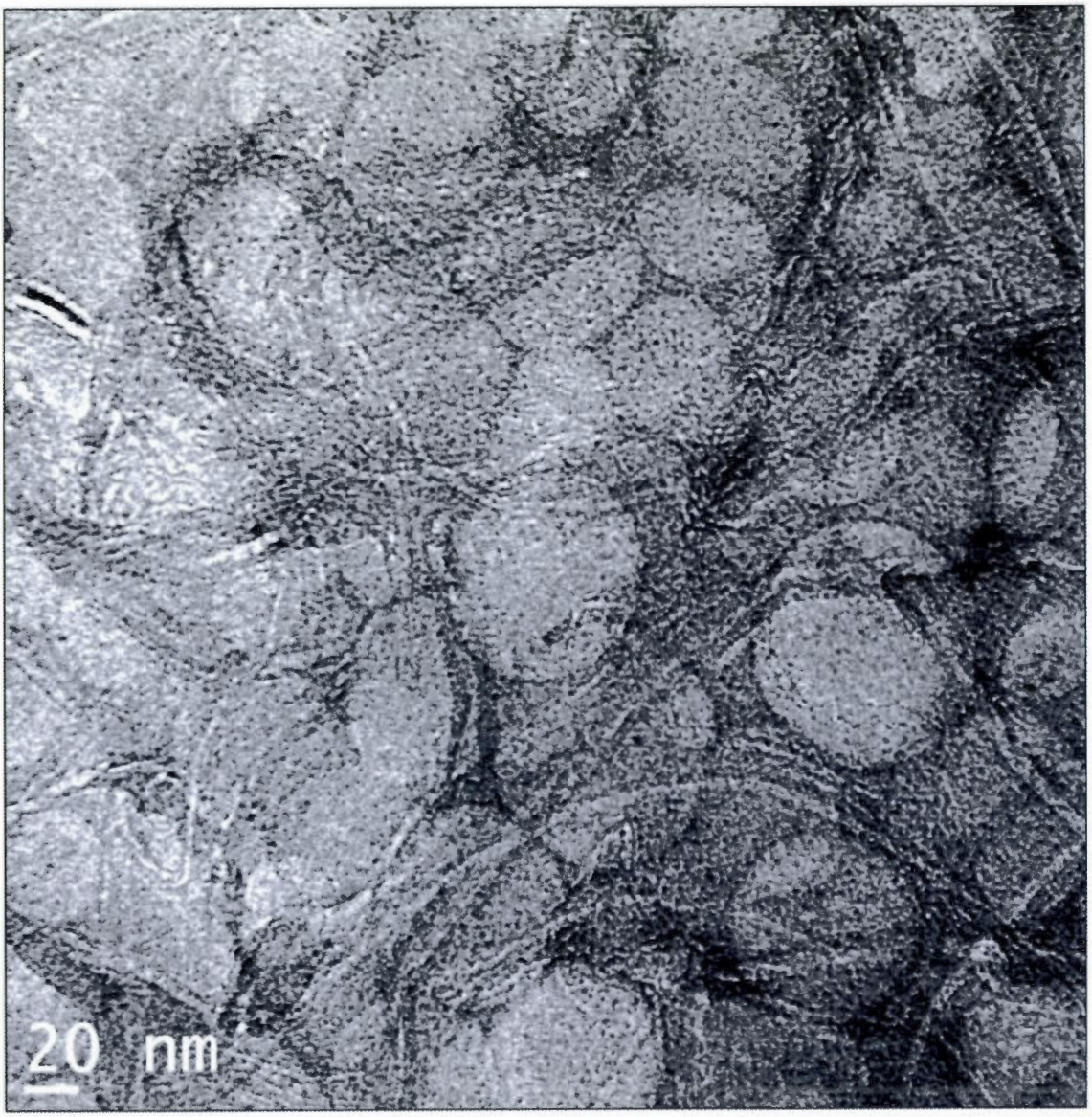

Figure B.10 TEM picture of CNT encapsulated in a polymer (entry 5)

Table 1 – Entry 6

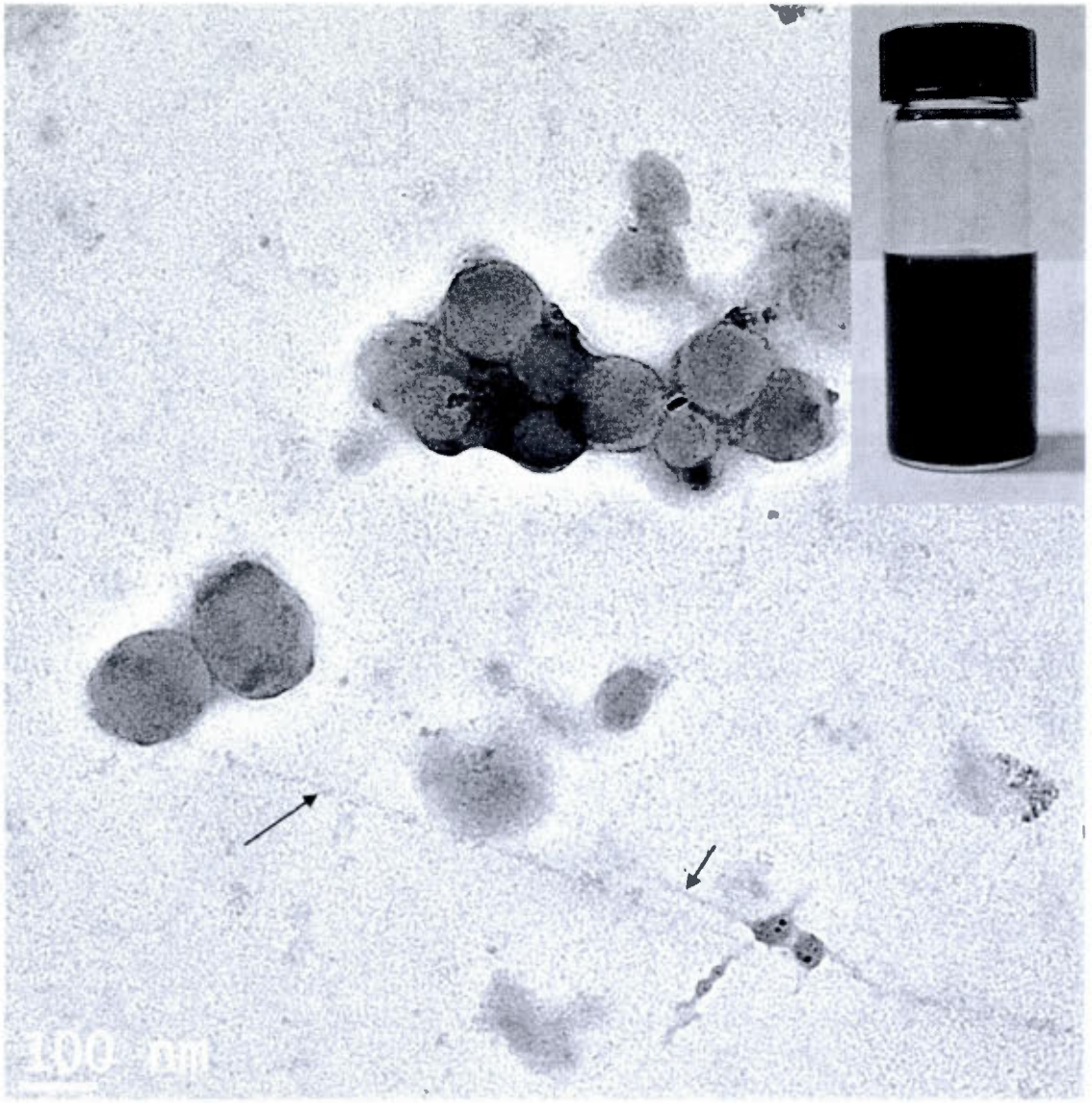

Figure B.11 TEM picture of CNT encapsulated in a polymer (entry 6): The SWNT are indicated by arrows. They offer very low contrast in comparison to polystyrene latex spheres.

Table 1 – Entry 6

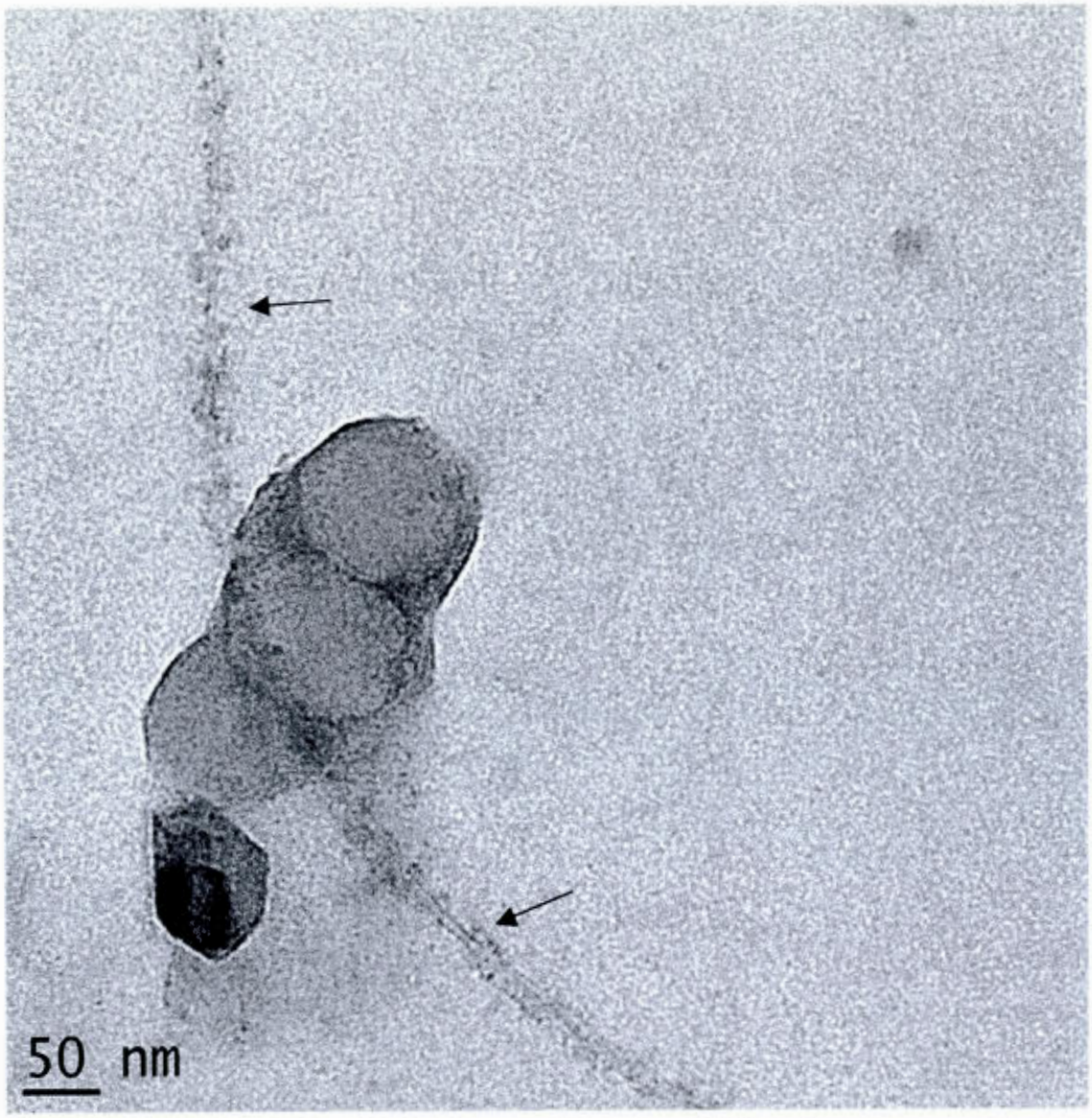

Figure B.12 TEM picture of CNT encapsulated in a polymer (entry 6): The SWNT are indicated by arrows. They offer very low contrast in comparison to polystyrene latex spheres.

Table 1 – Entry 6

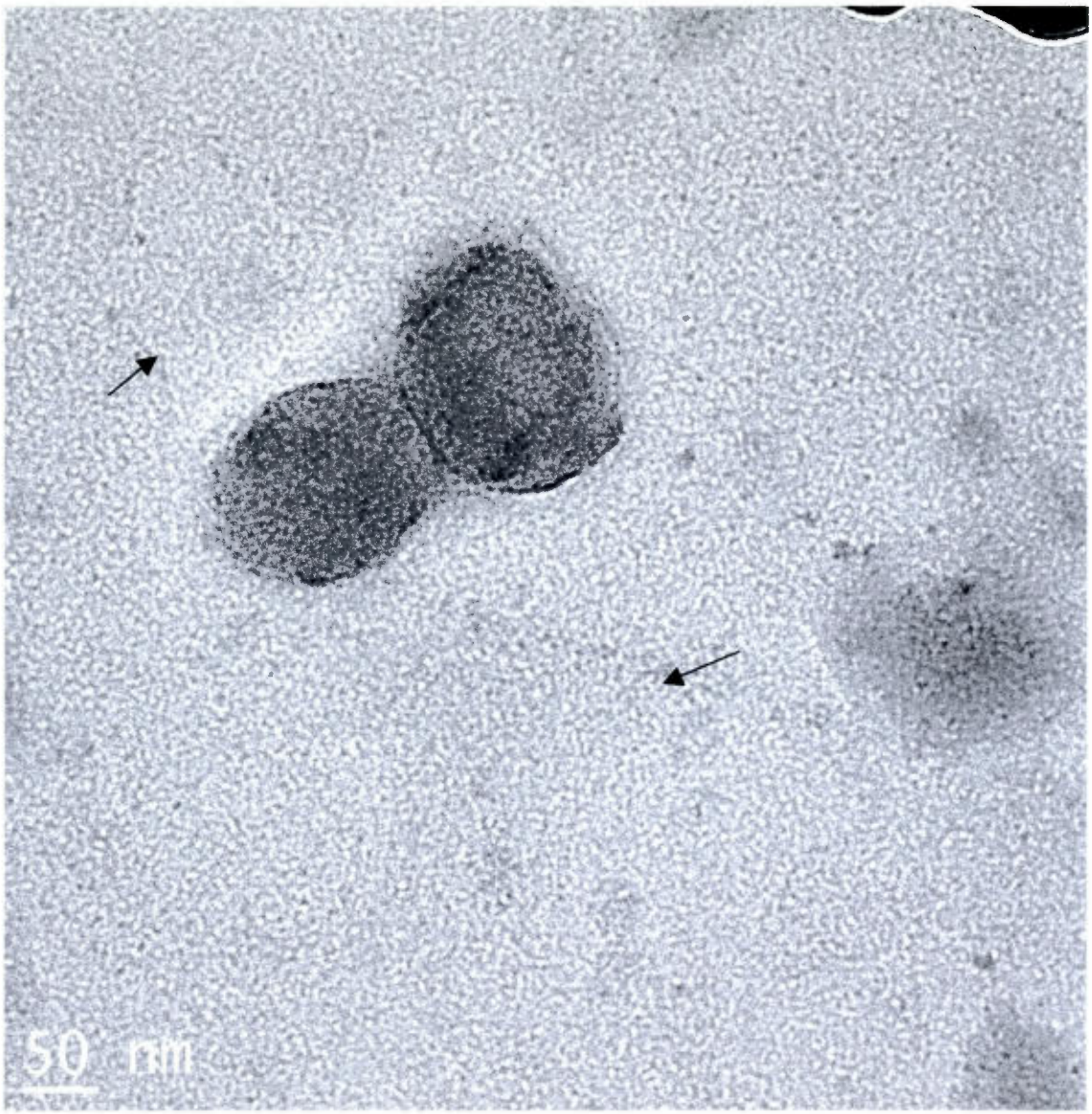

Figure B.13 TEM picture of CNT encapsulated in a polymer (entry 5): The SWNT are indicated by arrows. They offer very low contrast in comparison to polystyrene latex spheres.

Table 1 – Entry 7

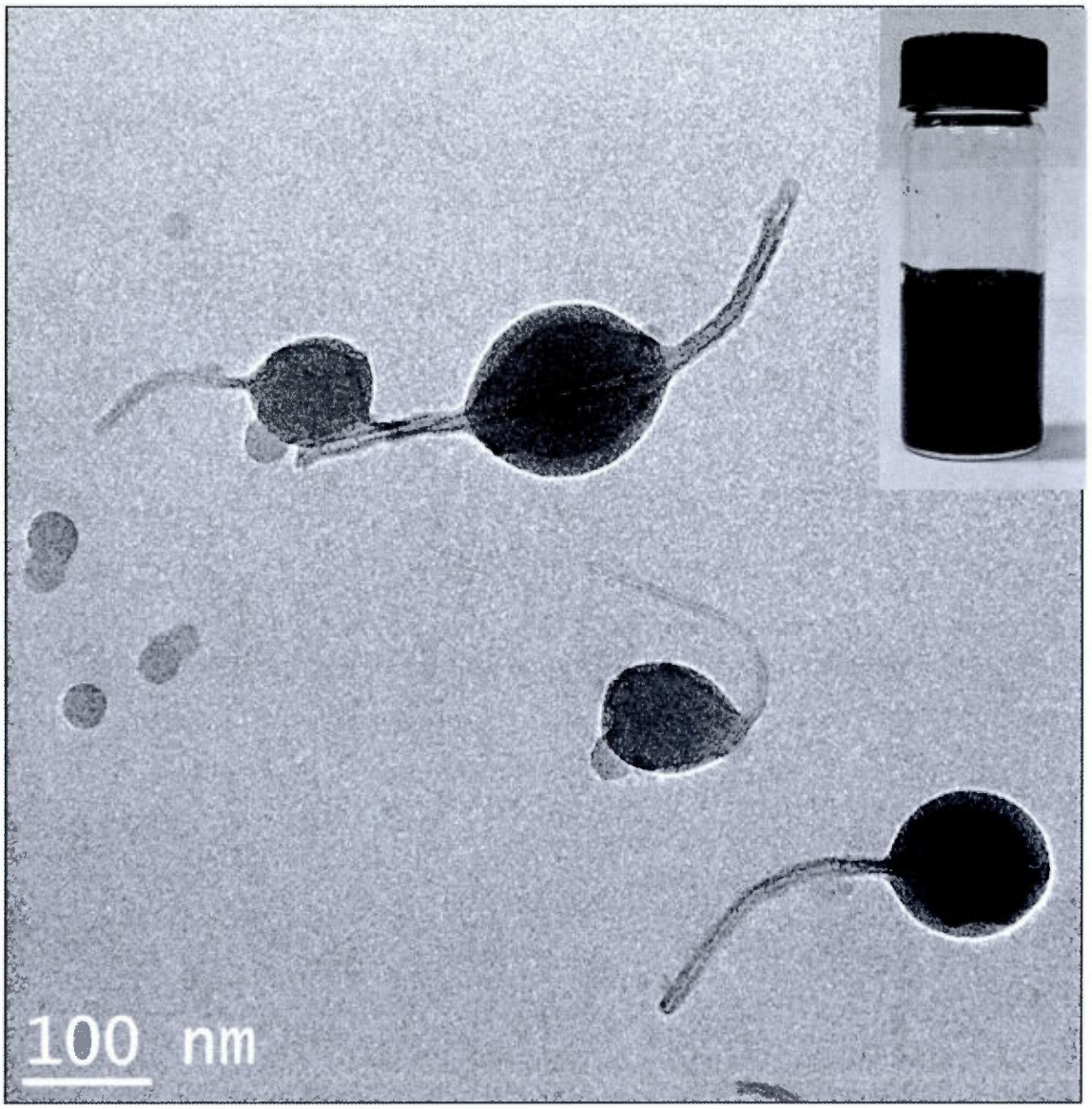

Figure B.14 TEM picture of CNT encapsulated in a polymer (entry 7)

Table 1 – Entry 7

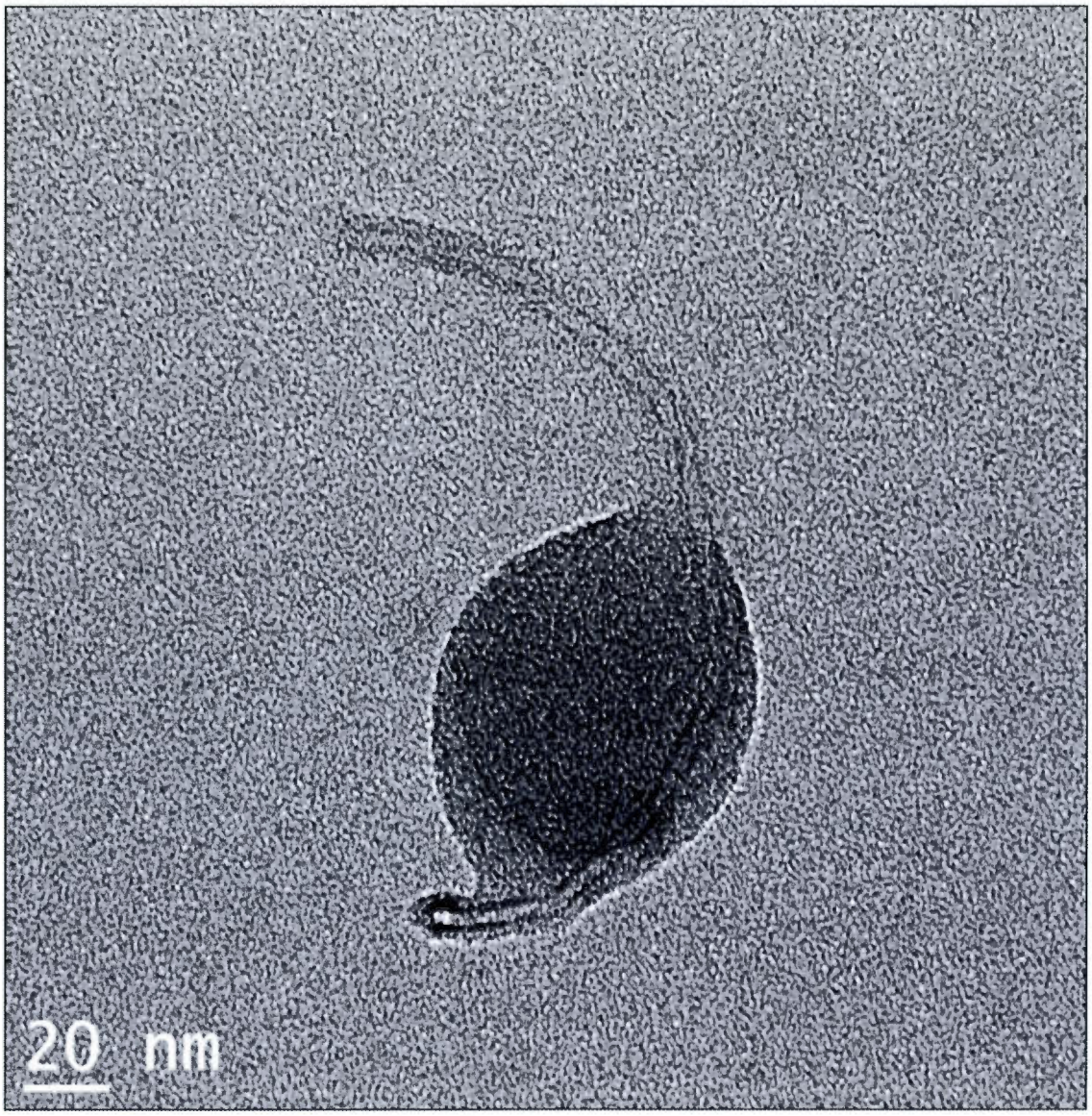

Figure B.15 TEM picture of CNT encapsulated in a polymer (entry 7)

Table 1 – Entry 8

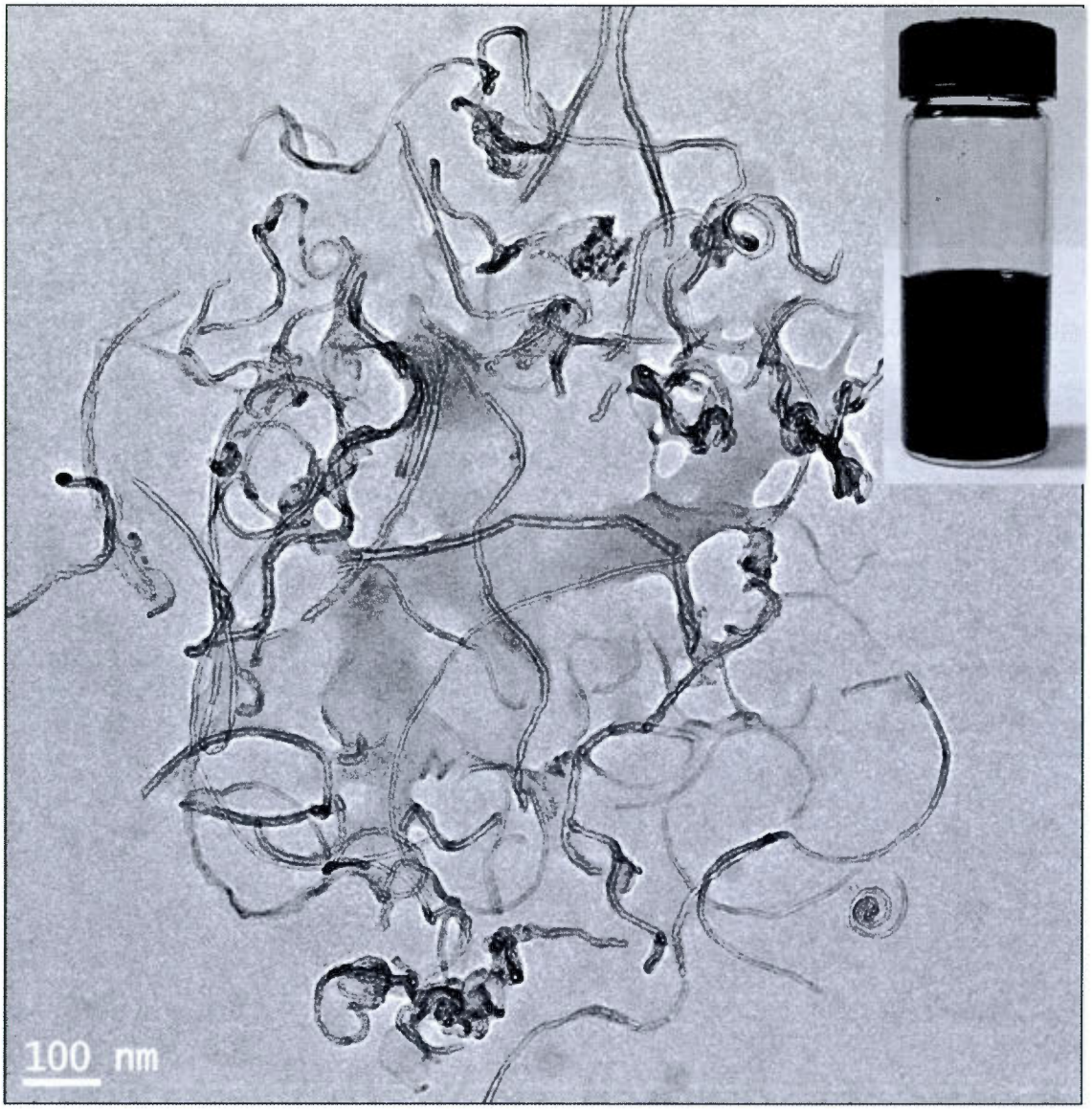

Figure B.16 TEM picture of CNT encapsulated in a polymer (entry 8)

Table 1 – Entry 8

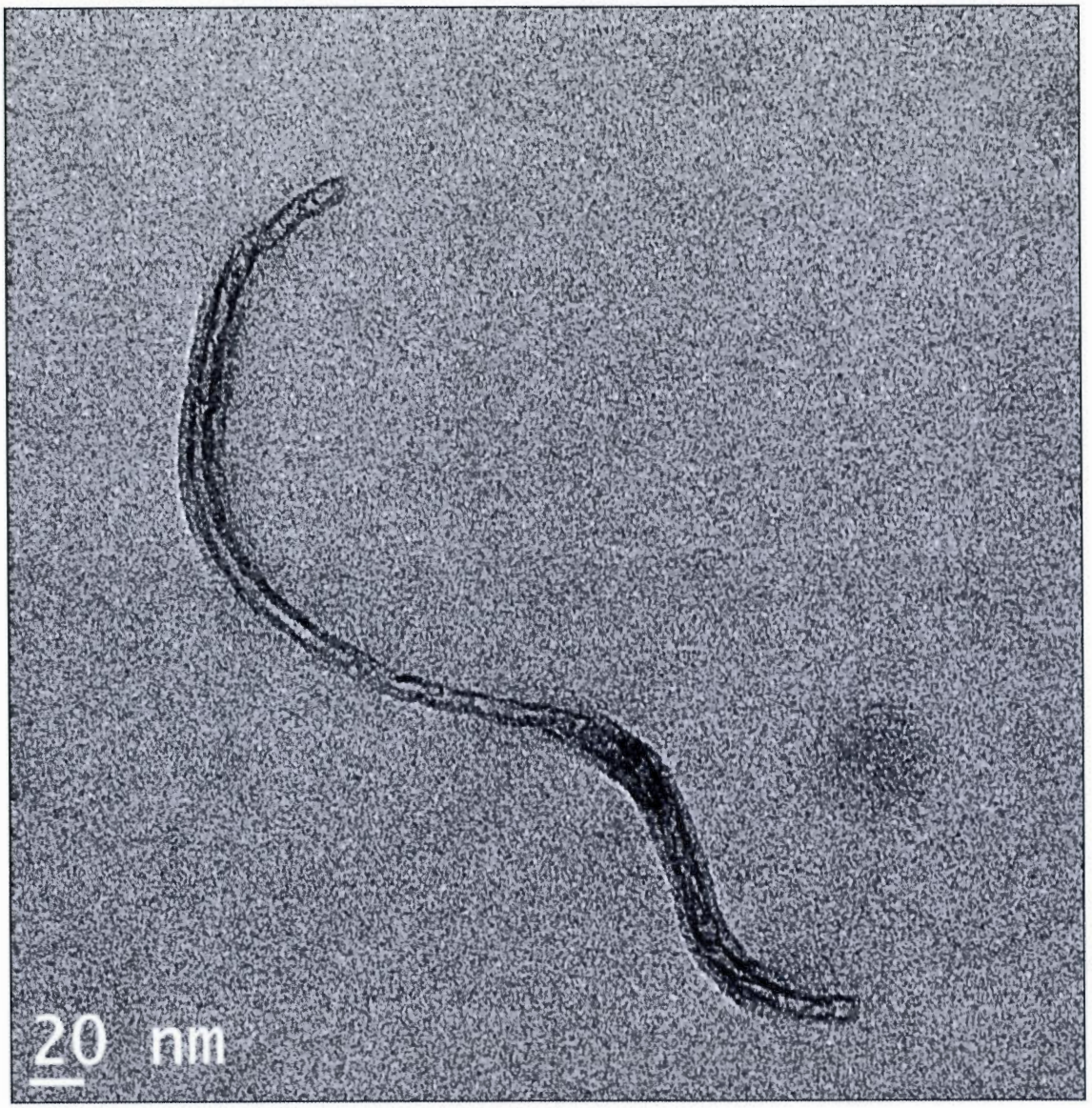

Figure B.17 TEM picture of CNT encapsulated in a polymer (entry 8)

Table 1 – Entry 8

Figure B.18 TEM picture of CNT encapsulated in a polymer (entry 8)

Table 1 – Entry 9

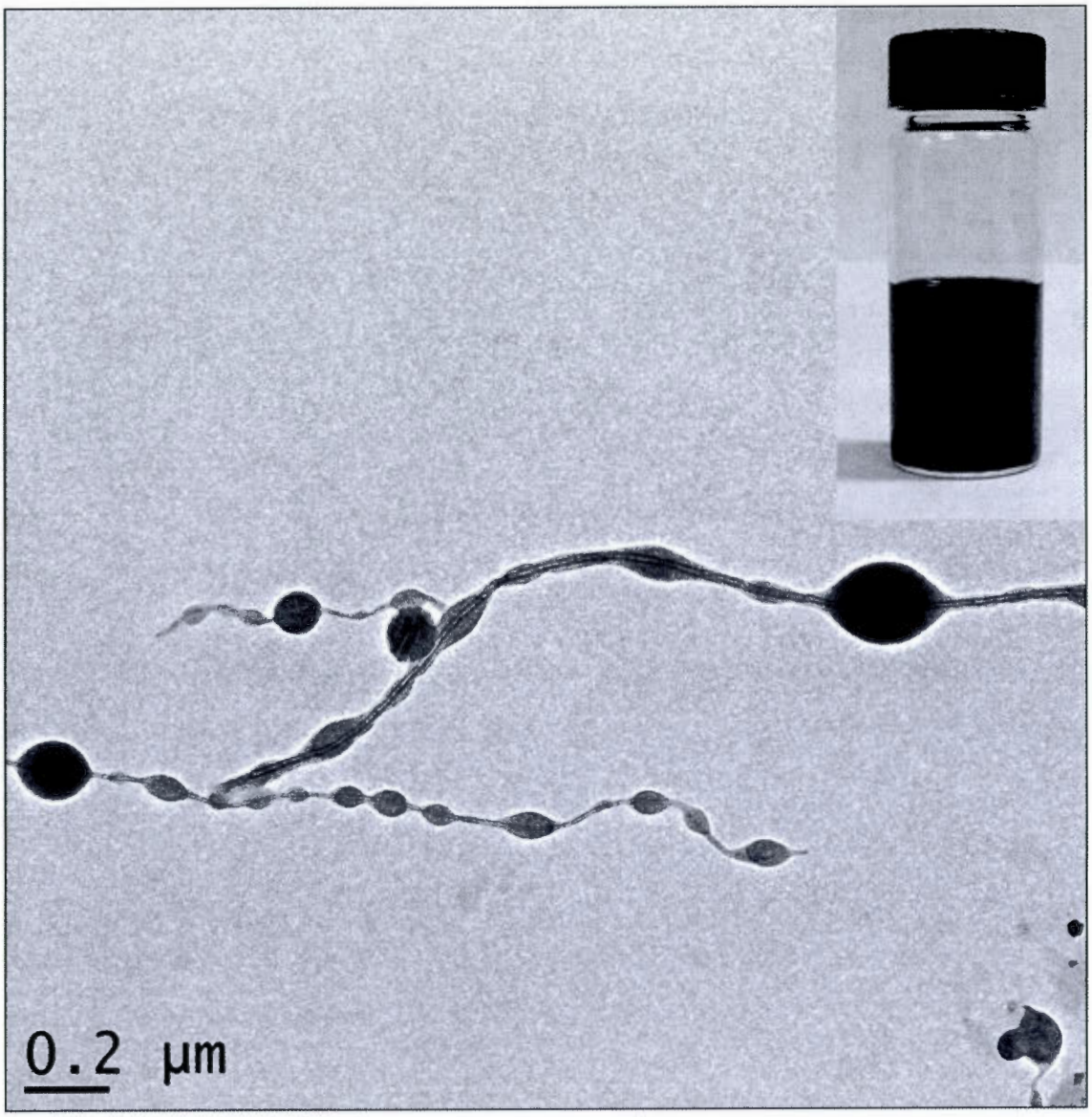

Figure B.19 TEM picture of CNT encapsulated in a polymer (entry 9)

Table 1 – Entry 9

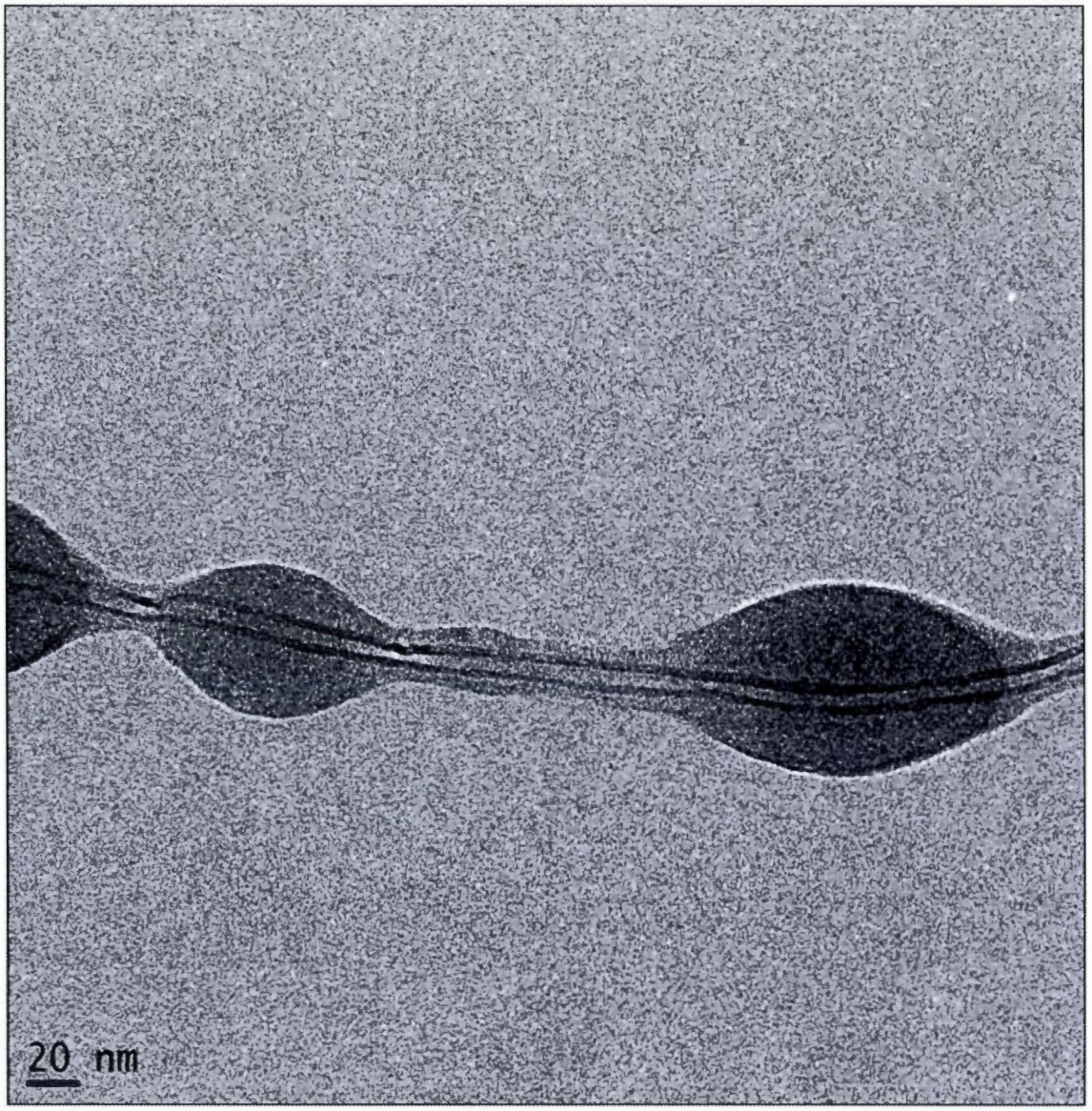

Figure B.20 TEM picture of CNT encapsulated in a polymer (entry 9)

Table 1 – Entry 9

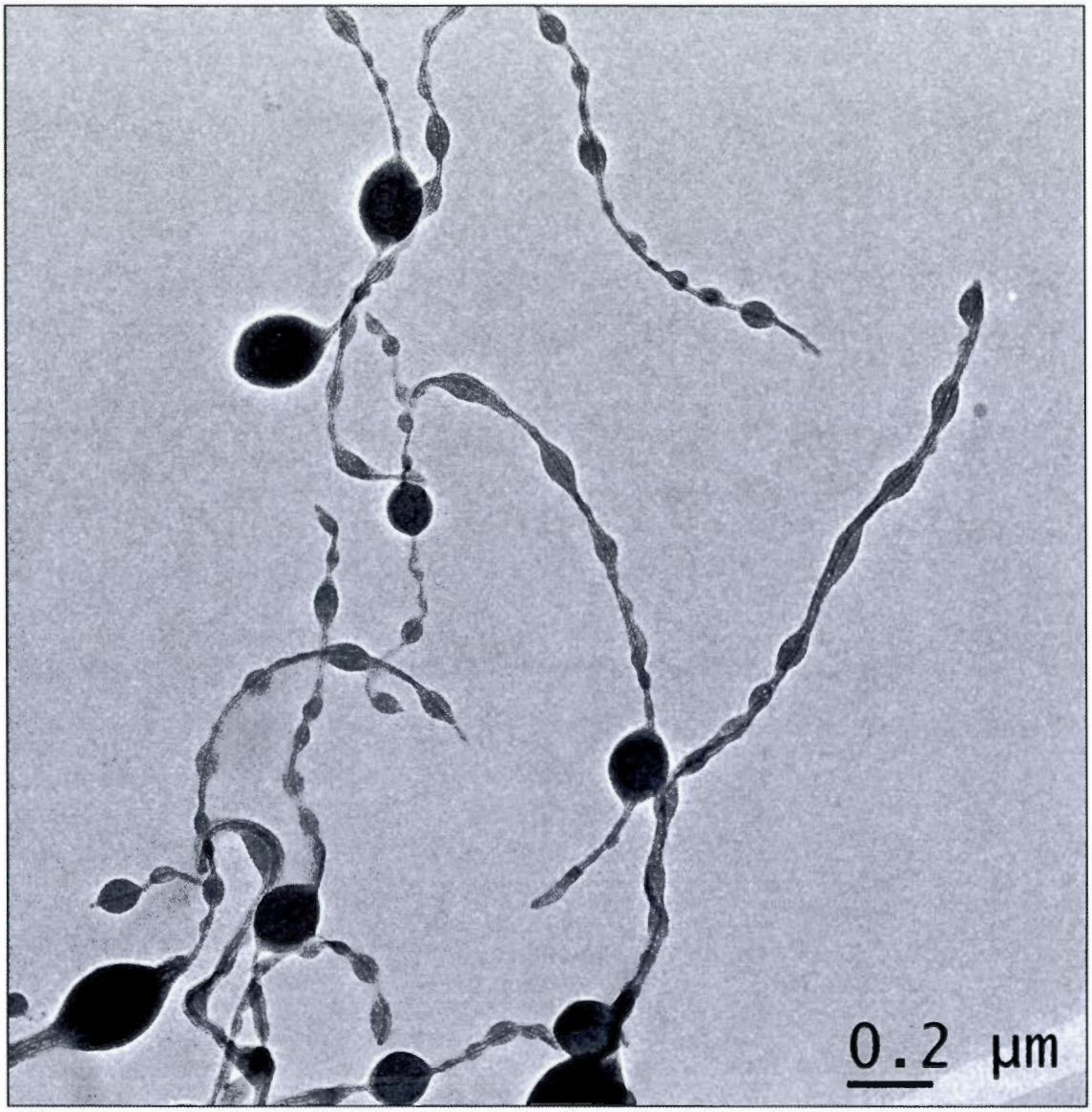

Figure B.21 TEM picture of CNT encapsulated in a polymer (entry 9)

Table 1 – Entry 9

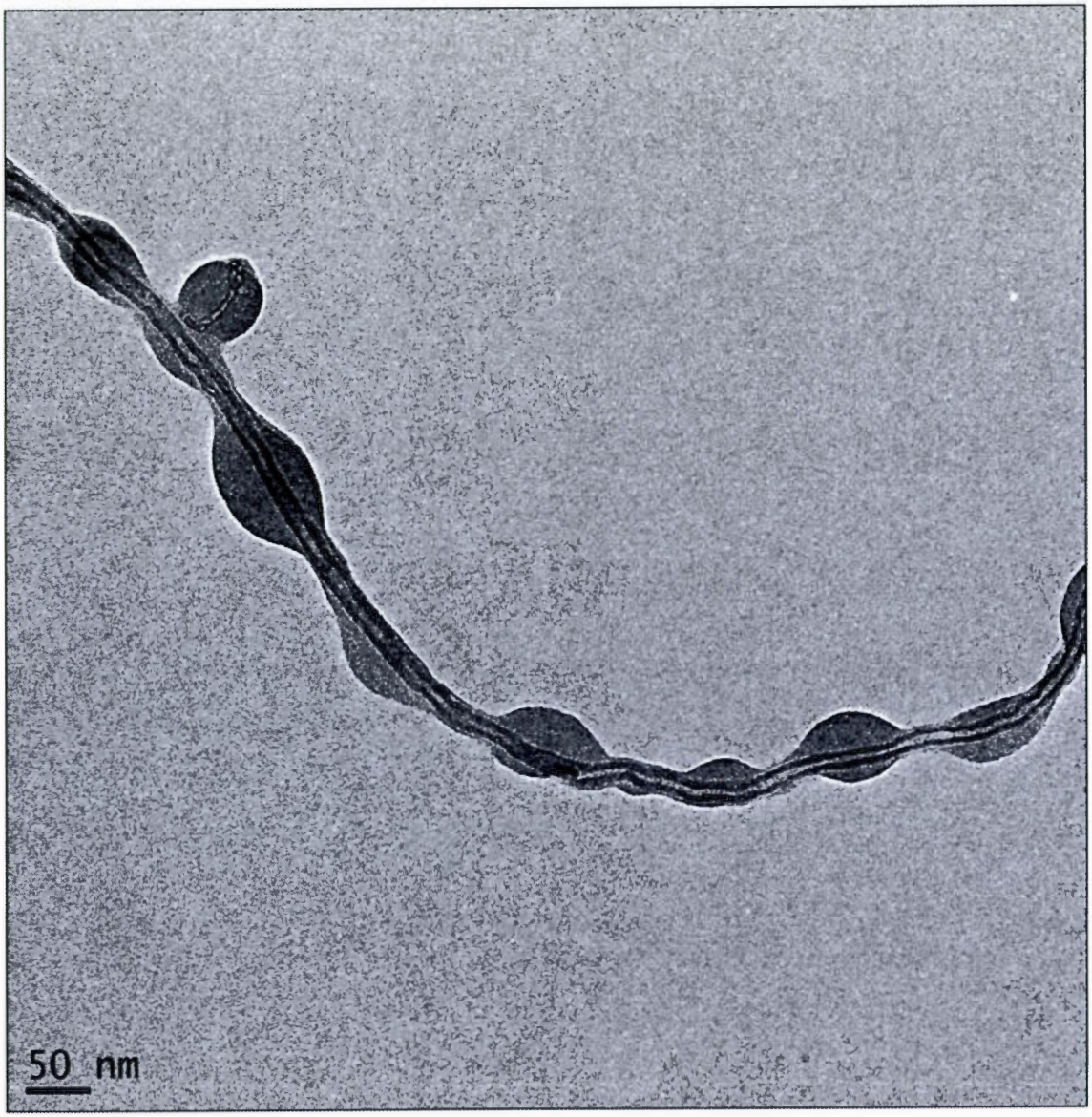

Figure B.22 TEM picture of CNT encapsulated in a polymer (entry 9)

Table 1 – Entry 10

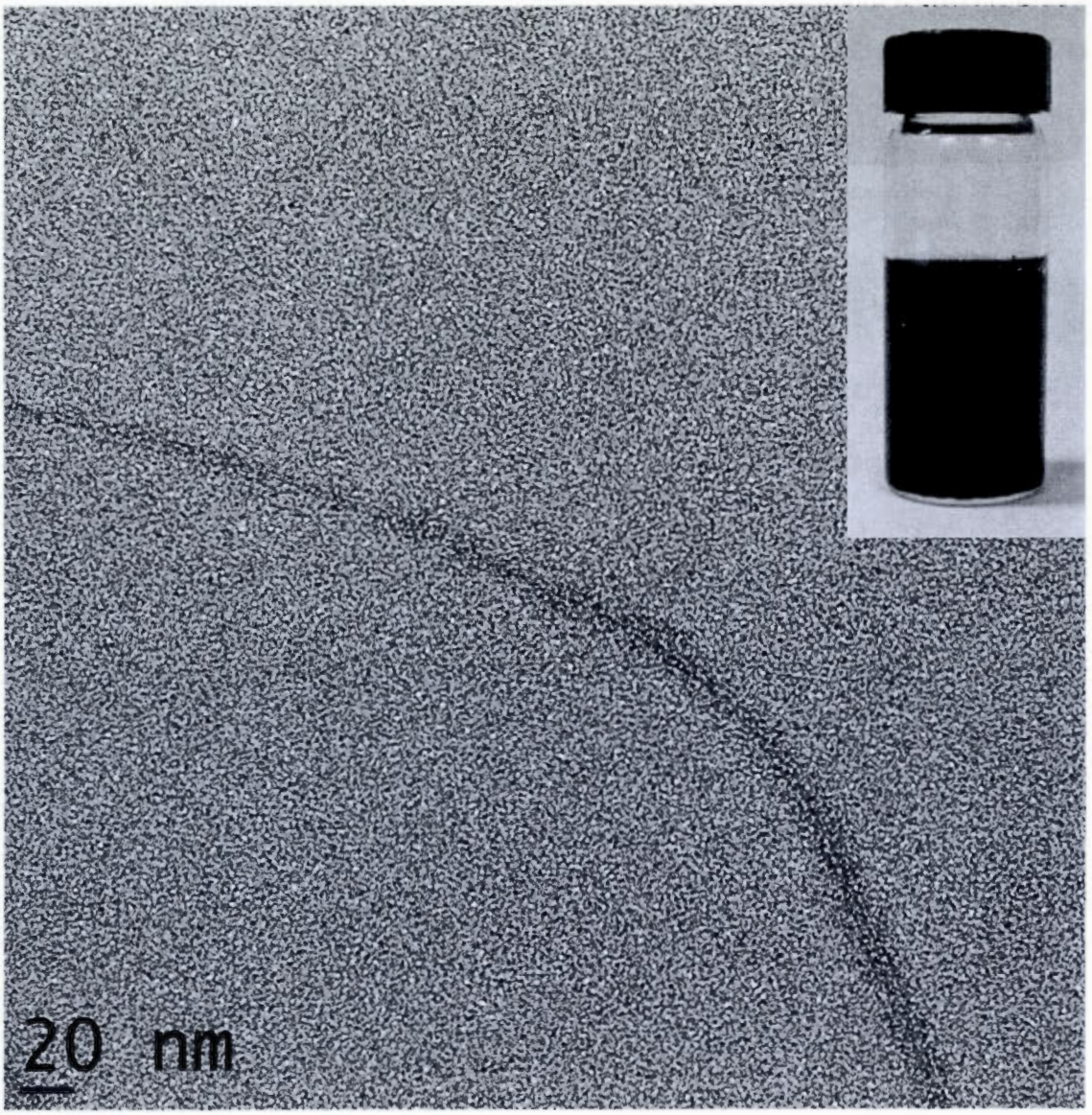

Figure B.23 TEM picture of CNT encapsulated in a polymer (entry 10)

Table 1 – Entry 11

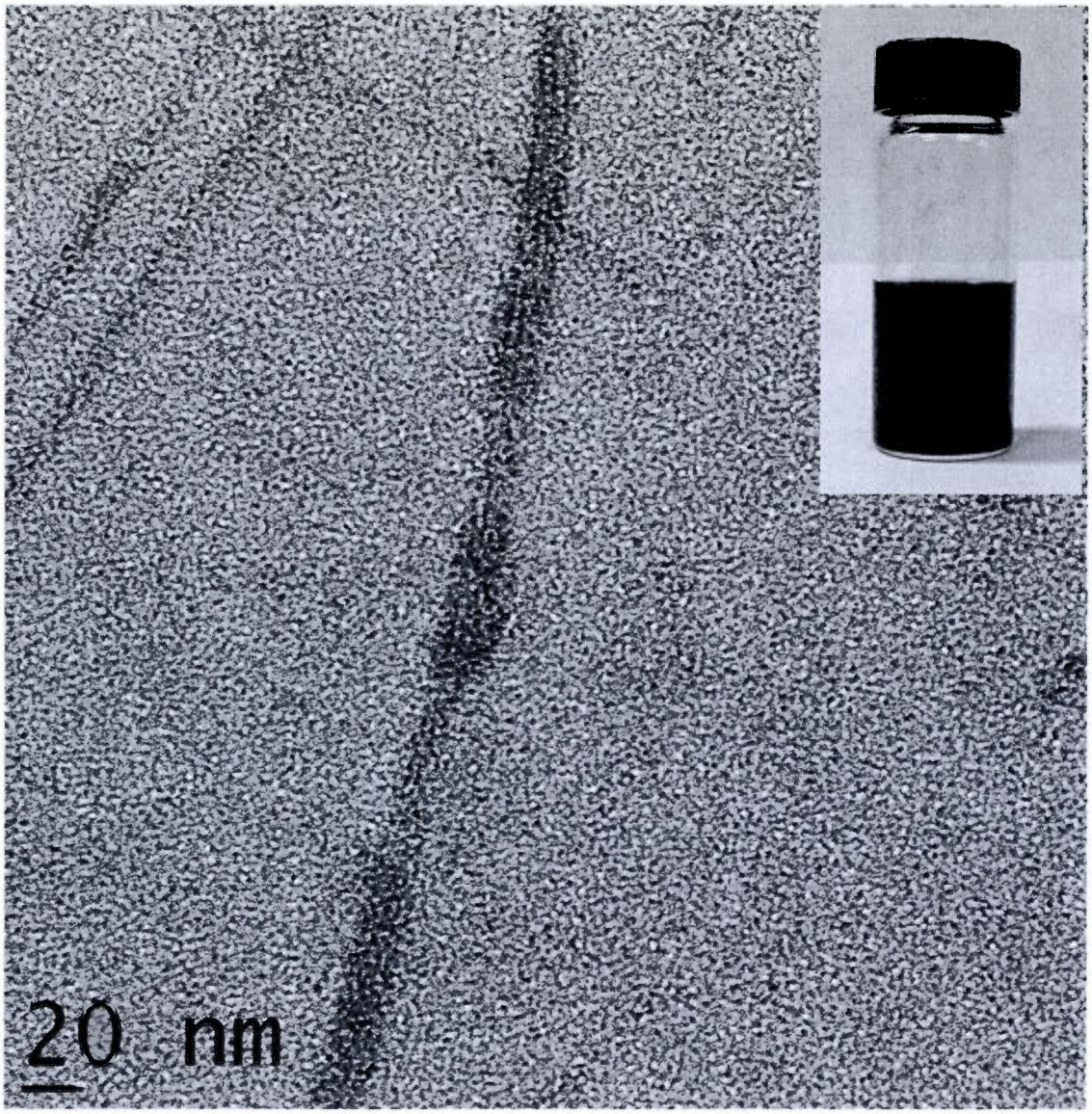

Figure B.24 TEM picture of CNT encapsulated in a polymer (entry 11)

Table 1 – Entry 11

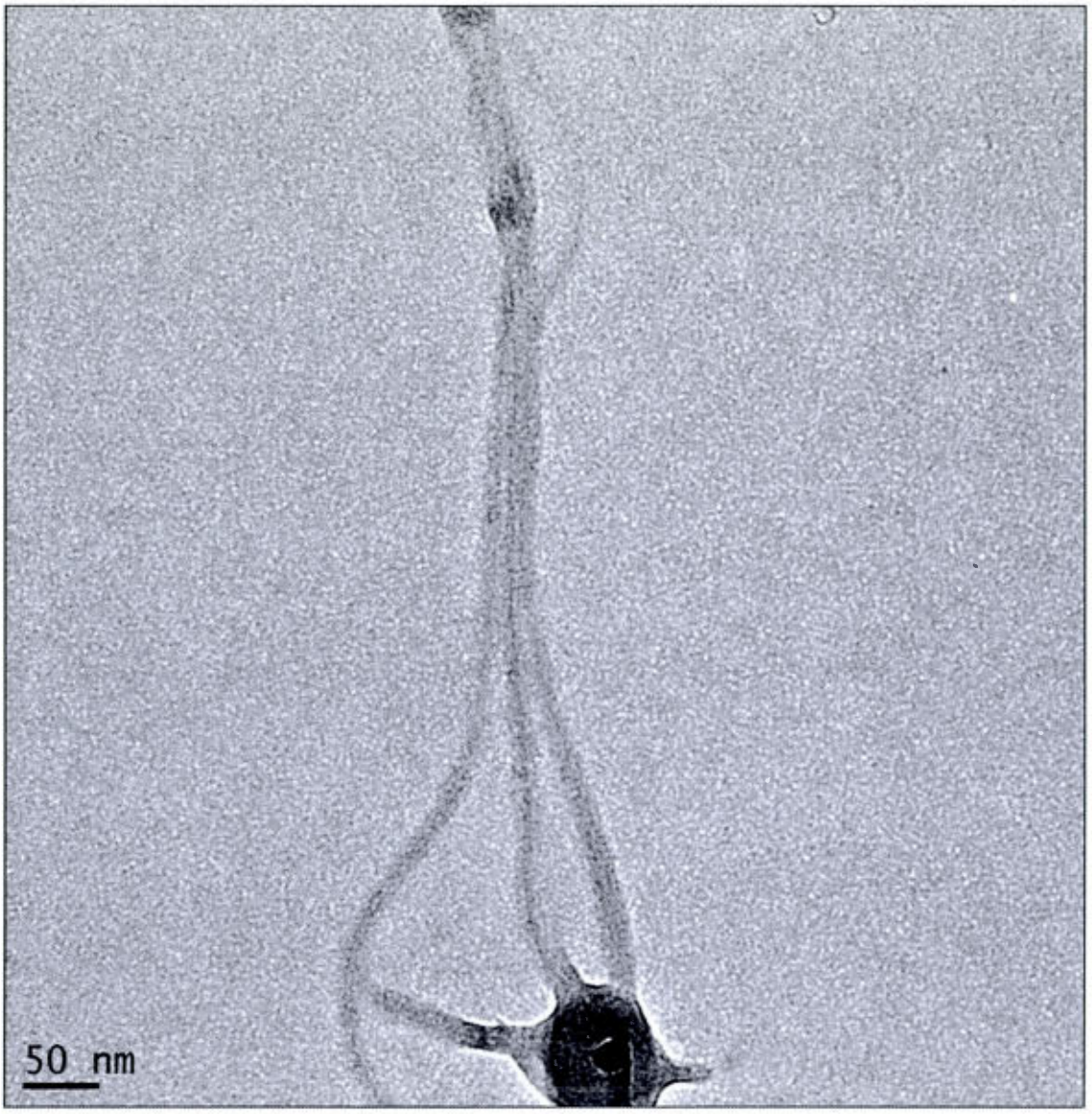

Figure B.25 TEM picture of CNT encapsulated in a polymer (entry 11)

Table 1 – Entry 12

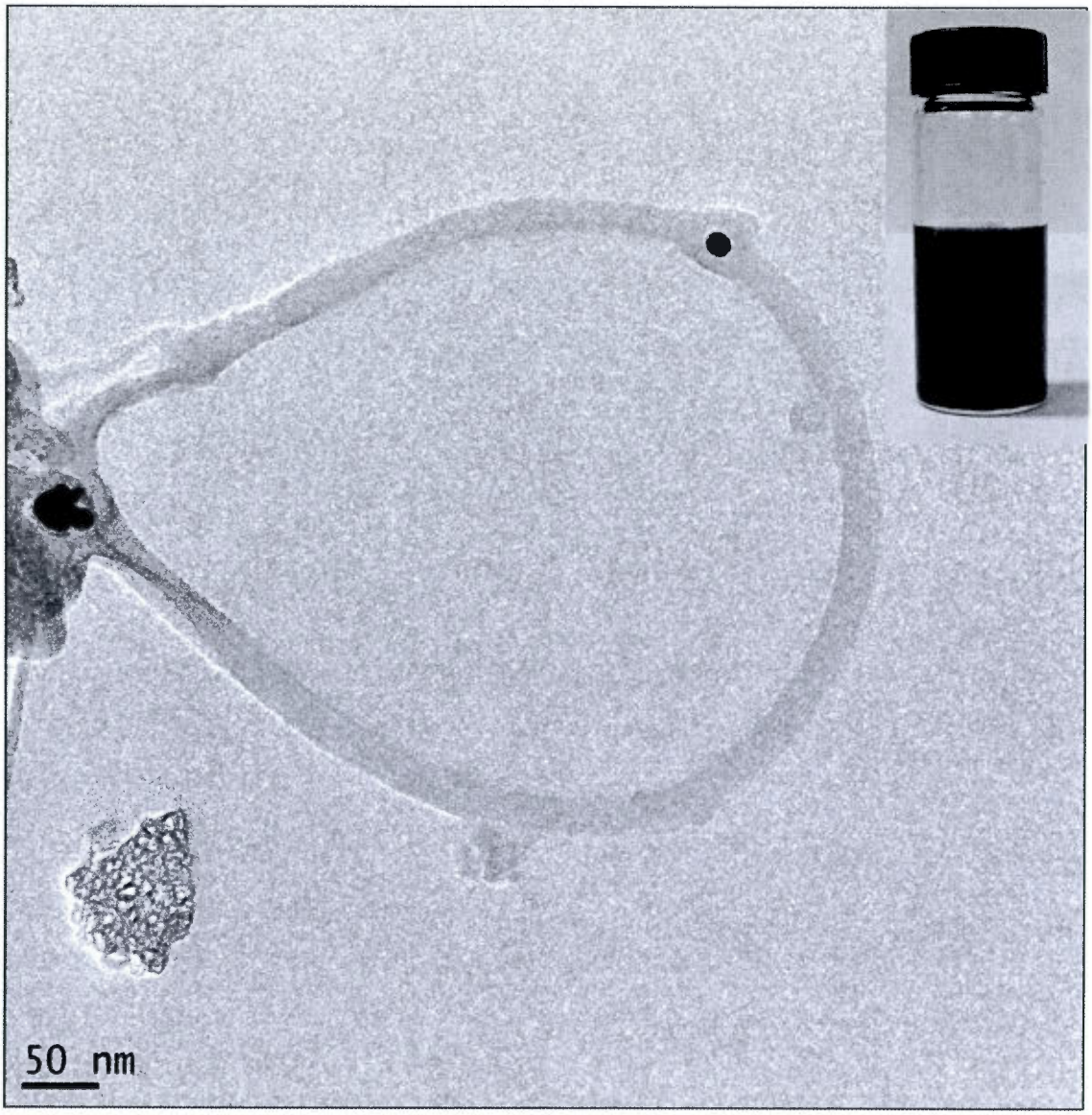

Figure B.26 TEM picture of CNT encapsulated in a polymer (entry 12)

Table 1 – Entry 12

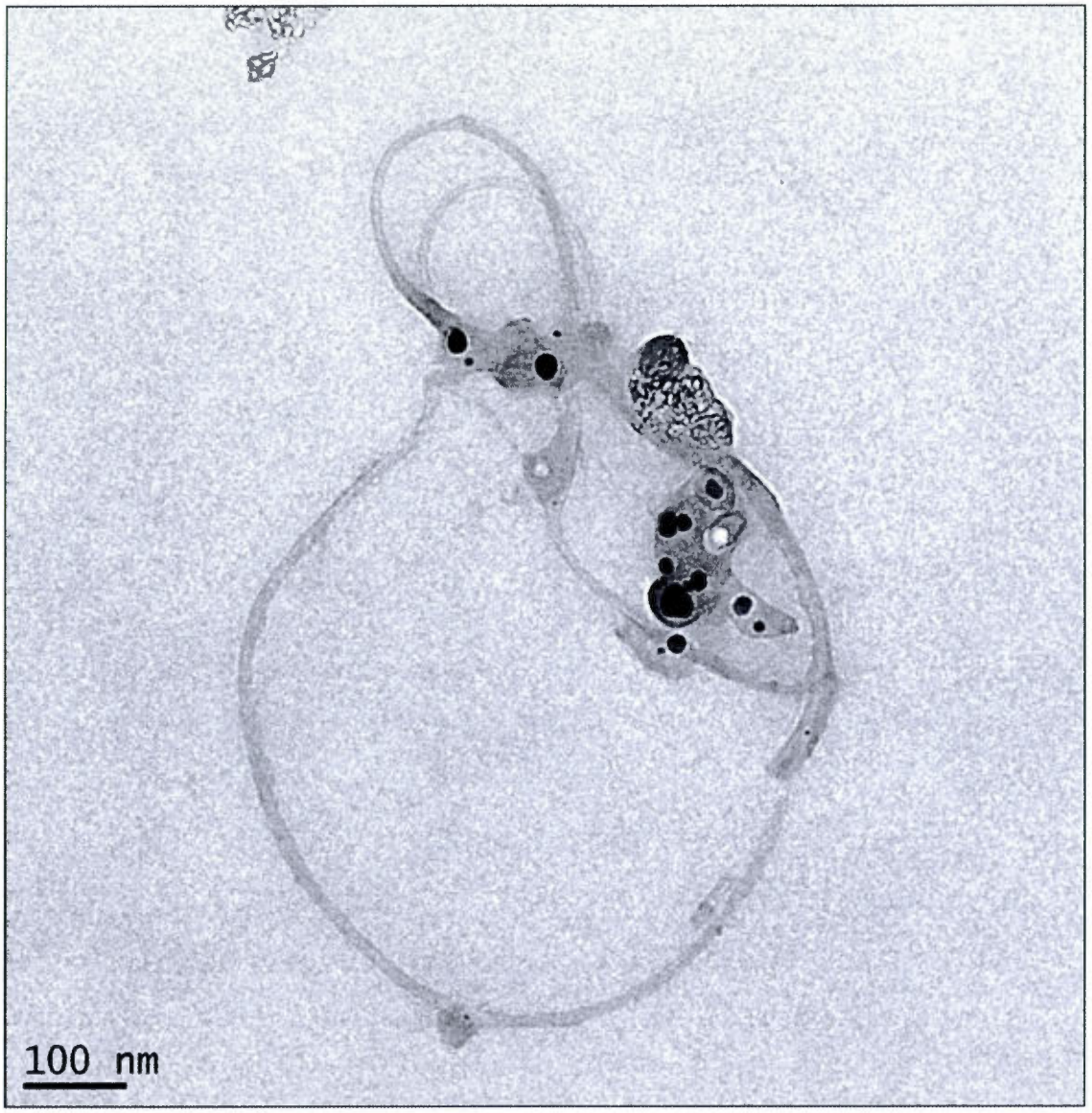

Figure B.27 TEM picture of CNT encapsulated in a polymer (entry 12)

Table 1 – Entry 12

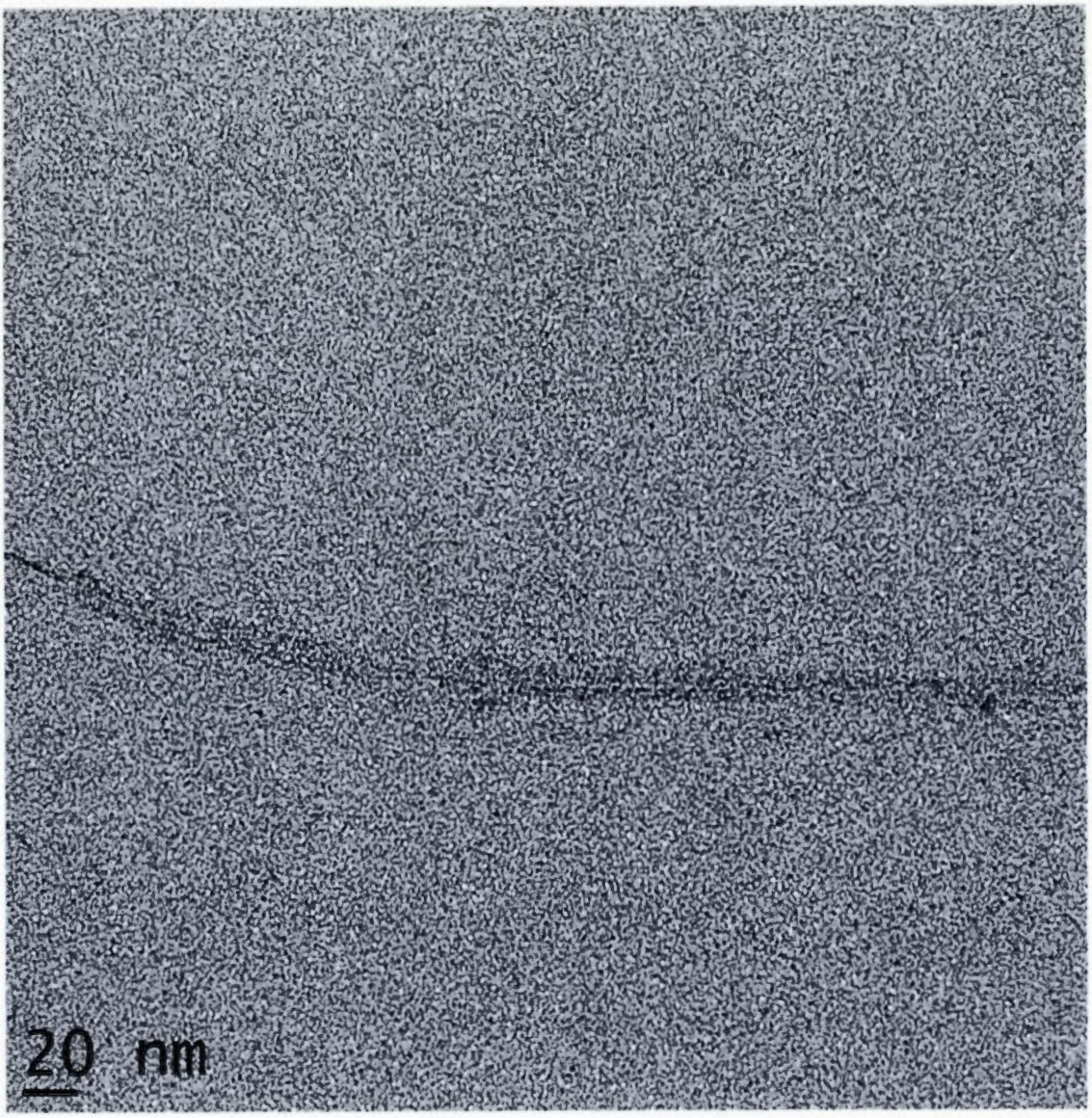

Figure B.28 TEM picture of CNT encapsulated in a polymer (entry 12)

Table 1 – Entry 12

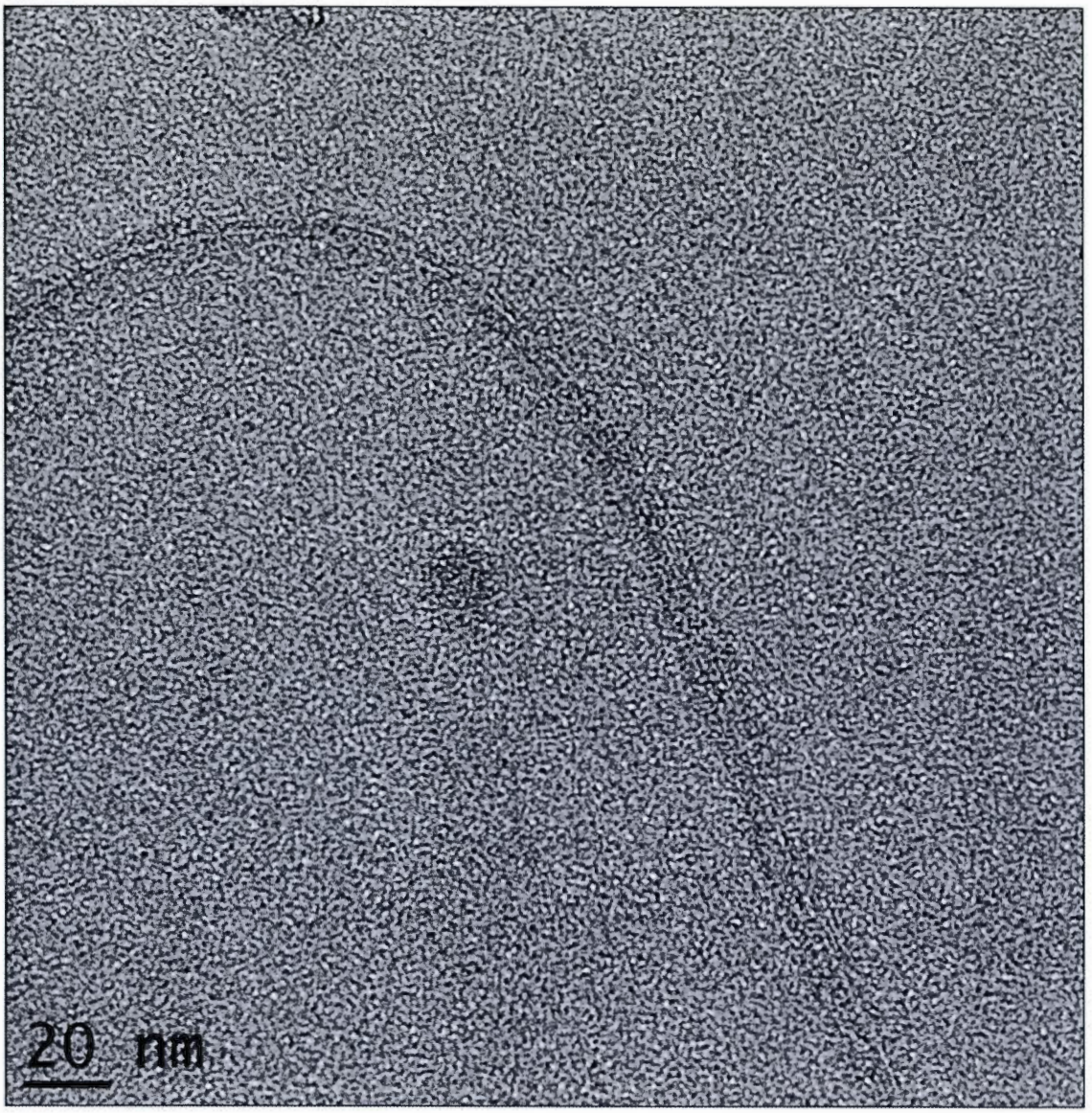

Figure B.29 TEM picture of CNT encapsulated in a polymer (entry 12)

Table 1 – Entry 4

Picture of the result of the (failed) encapsulation experiment.
Left : unshaked – Right : Hand shaken.

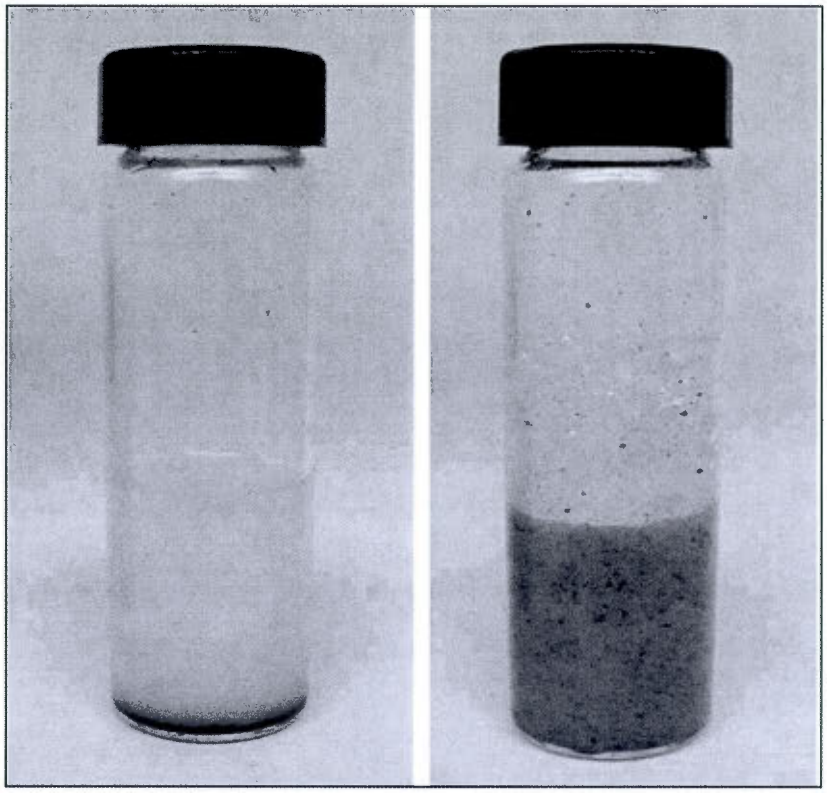

Figure B.30 Picture of the result of the (failed) encapsulation experiment

TEM of the MWNT prior encapsulation

Dispersant : PAA

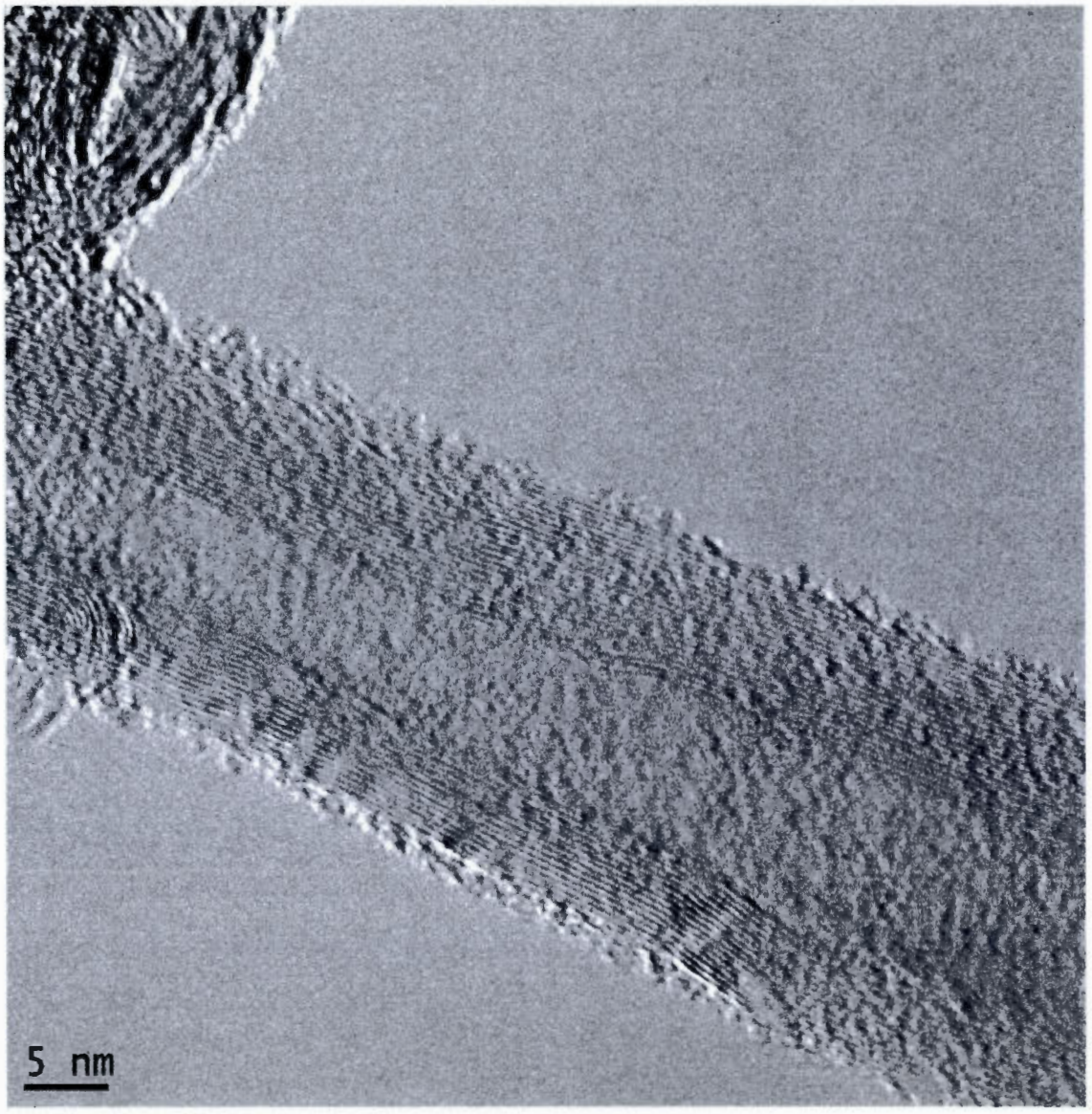

Figure B.31 TEM picture of MWNT prior encapsulation (PAA)

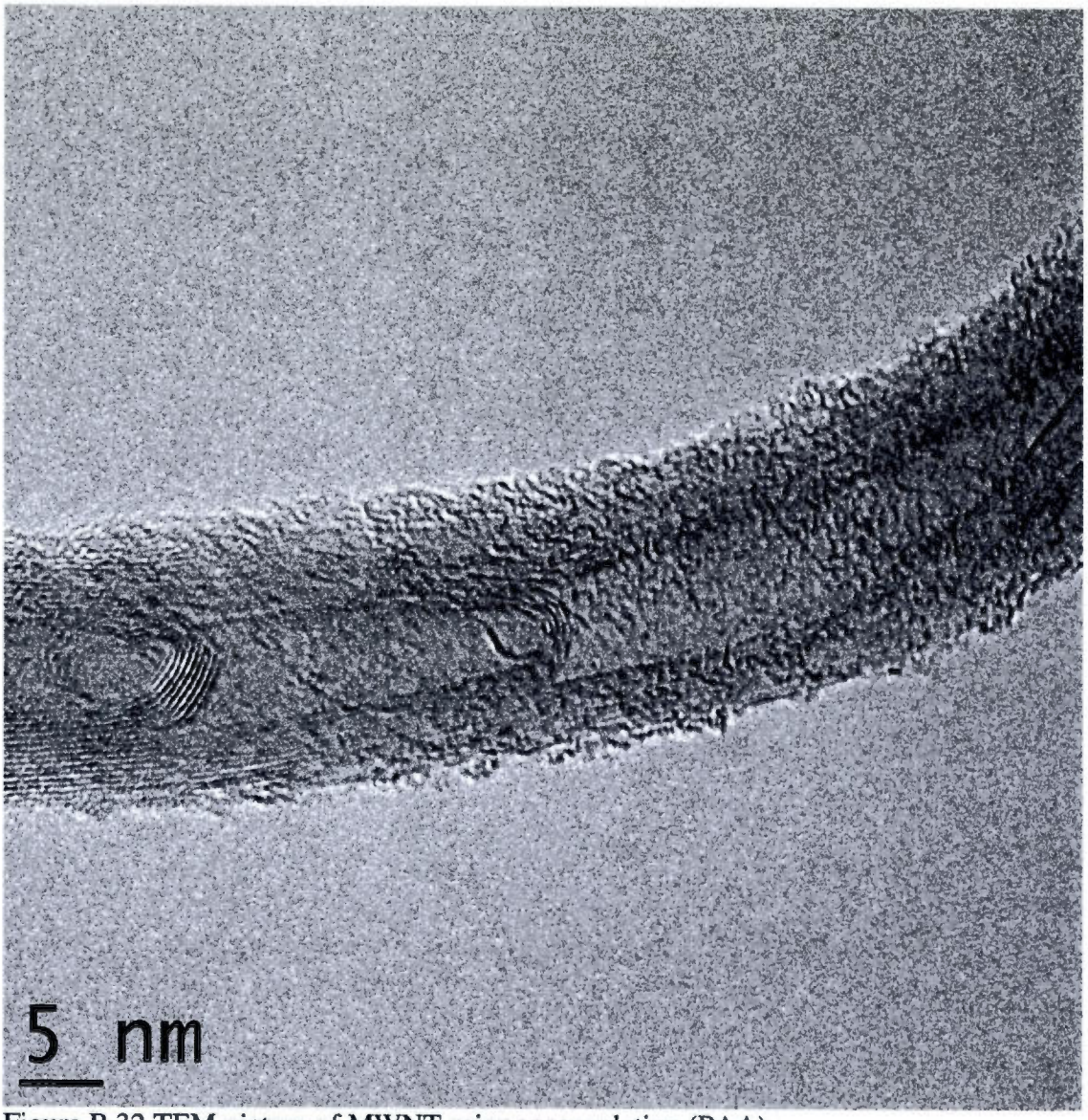

Figure B.32 TEM picture of MWNT prior encapsulation (PAA)

TEM of the MWNT prior encapsulation

Dispersant : PAABA

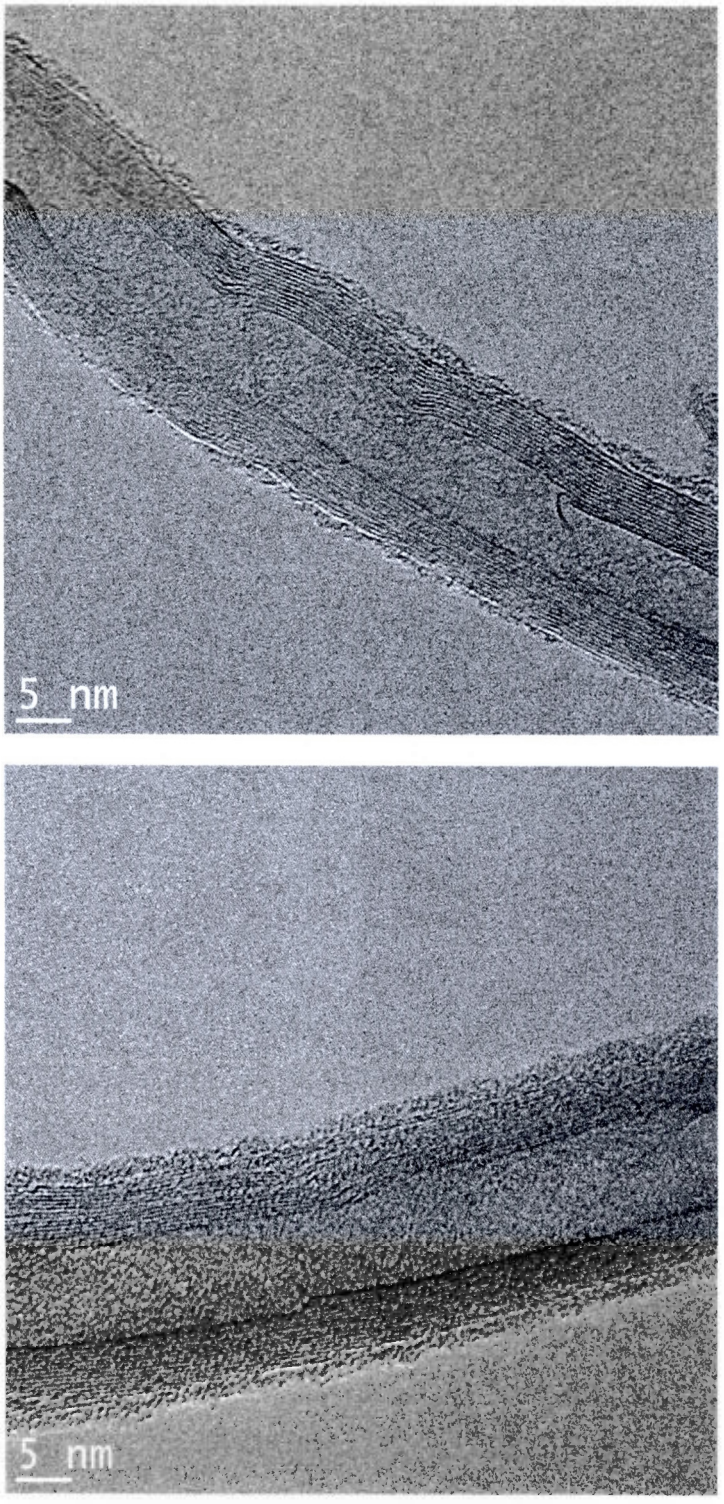

Figure B.33 TEM pictures of MWNT prior encapsulation (PAABA)

TEM of the MWNT prior encapsulation

Dispersant : PSAA

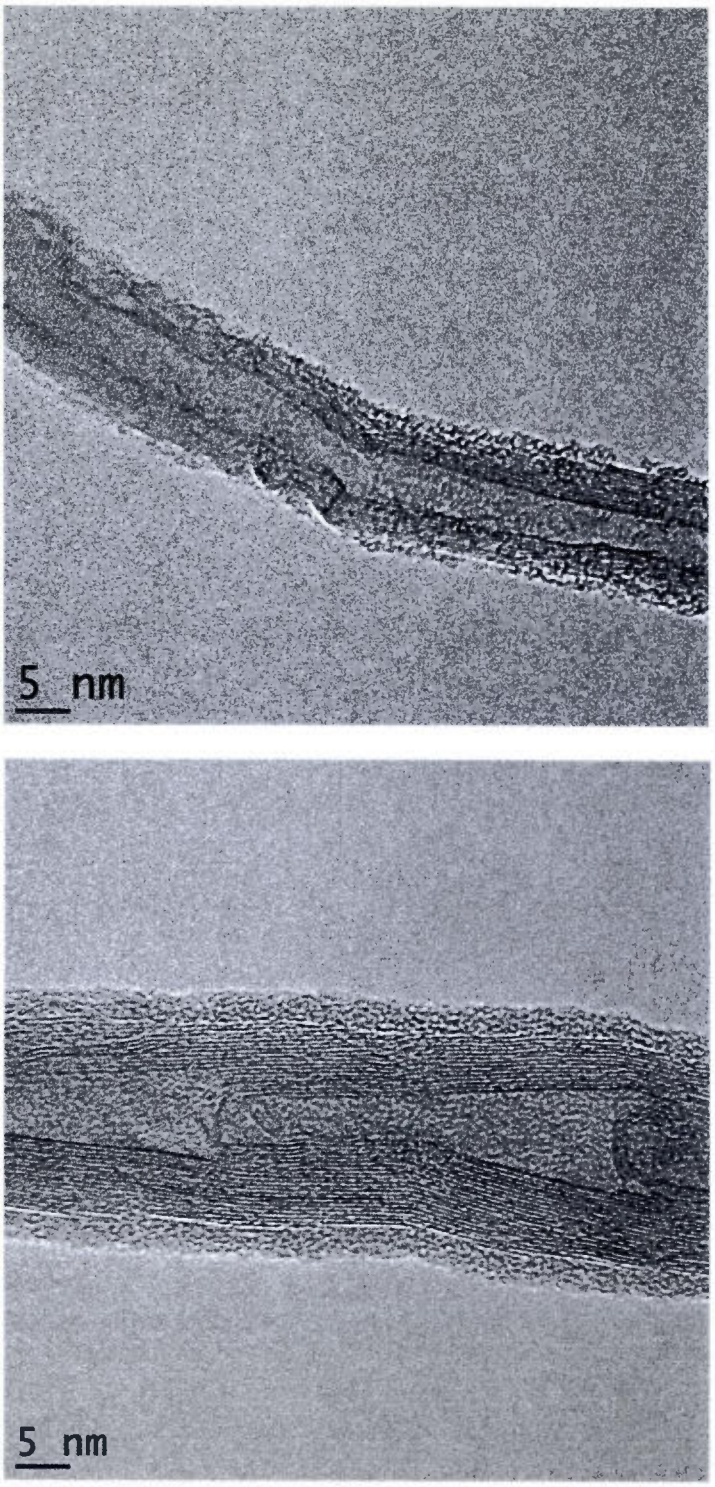

Figure B.34 TEM pictures of MWNT prior encapsulation (PSA)

RAMAN SPECTRA OF THE SWNT DISPERSIONS

1. Intensity (absolute and then relative to the tallest peak) of the D (1342 cm^{-1}), the G1 and G2 (1565 cm^{-1} and 1589 cm^{-1}) Raman bands

sample	D	G1	G2	D2	G1	G3
SWNTdry	901	4383	16095	5,6%	27,2%	100%
SWNT + SDS	911	6464	24692	3,7%	26,2%	100%
SWNT + PAABA	683	10278	40517	1,7%	25,4%	100%
SWNT + PAABA + PS	516	3258	12156	4,2%	26,8%	100%
SWNT + PSAA	762	11788	43186	1,8%	27,3%	100%
SWNT+ PSAA + PS	1820	19483	73160	2,5%	26,6%	100%
SWNT+ PAA	2392	11689	36578	6,5%	32,0%	100%
SWNT + PAA+ PS	1364	8695	29197	4,7%	29,8%	100%

2. Raman spectra

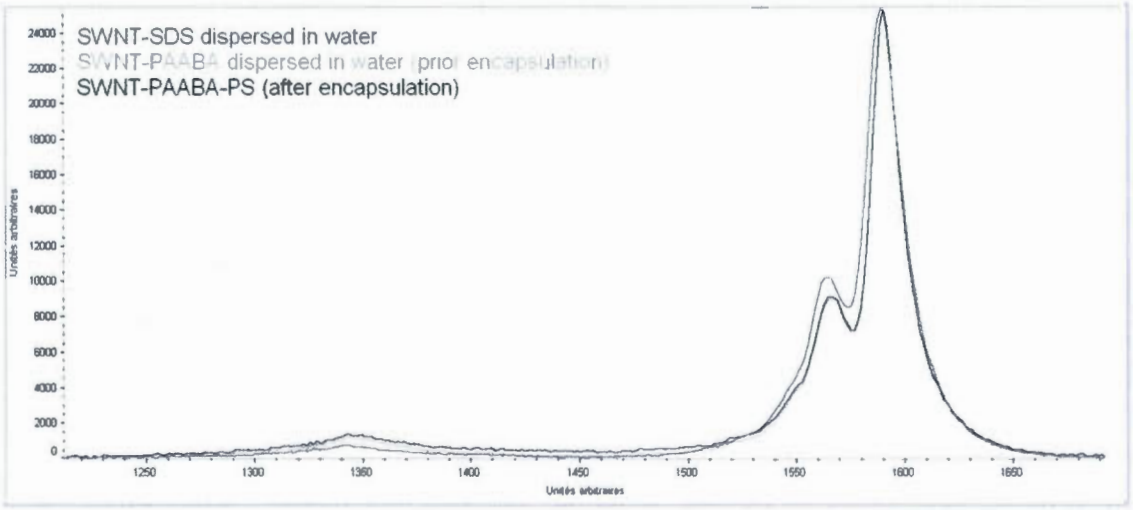

Figure B.35 Raman spectra of SWNT dispersions

3. Deconvoluted spectrum (sample 9)

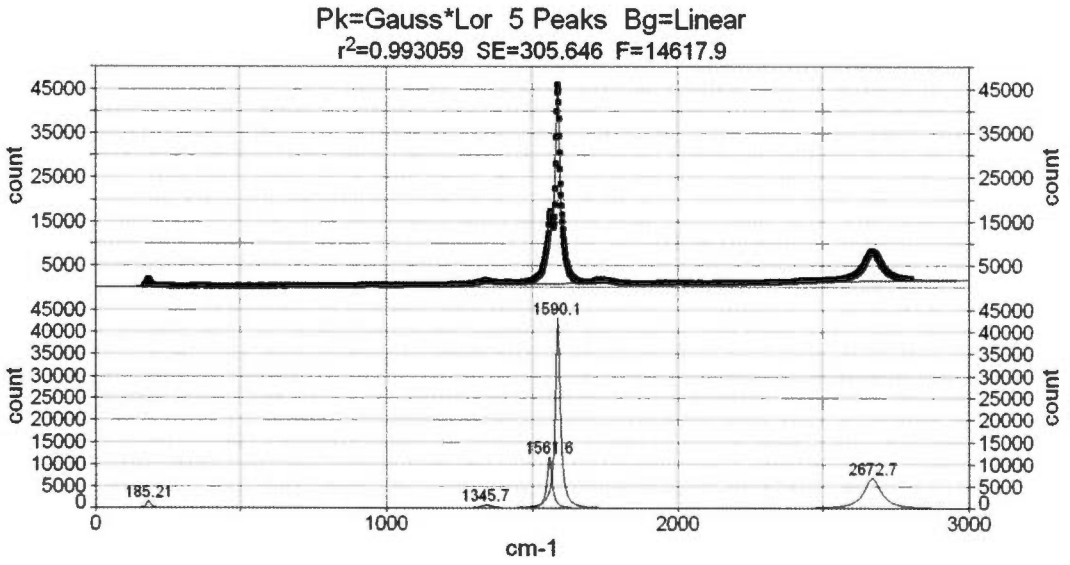

Figure B.36 Deconvoluted spectrum (sample 9)

Representative Gel Permeation Chromatogram

(sample 9)

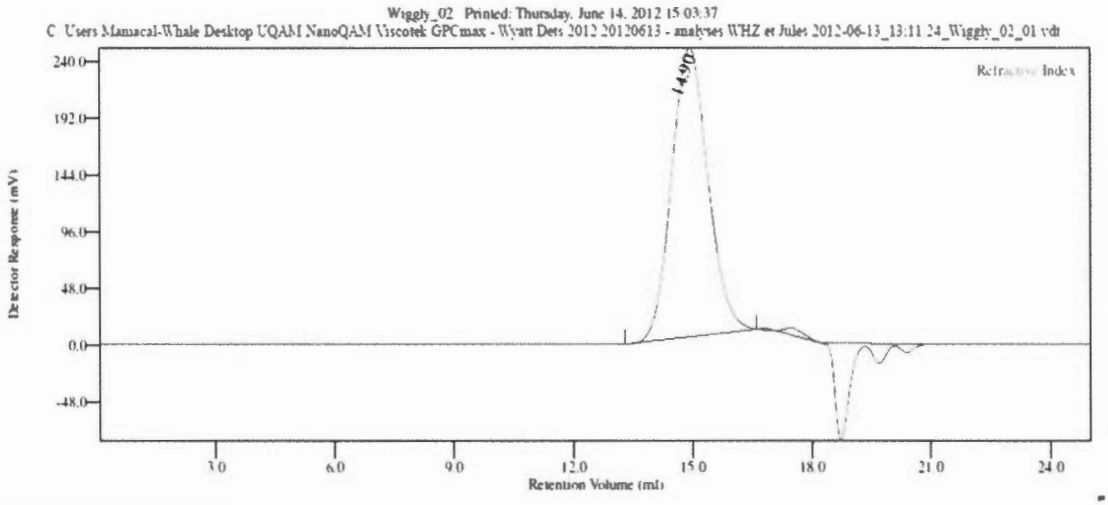

Peak RV - (ml)	14.900
Mn - (Daltons)	9,787
Mw - (Daltons)	13,799
Mz - (Daltons)	17,494
Mp - (Daltons)	13,190
Mw / Mn	1.410
Percent Above Mw: 0	0.000
Percent Below Mw: 0	0.000
Mw 10.0% Low	3,860
Mw 10.0% High	28,231
RI Area - (mvml)	259.35
UV Area - (mvml)	0.00

Figure B.37 Representative Gel Permeation Chromatogram (sample 9)

References

1. Musumeci, A.W.; Waclawik, E.R.; Frost, R.L. *Spectrochim. Acta, Part A.* **2008**, *71*, 140-142
2. Zhong, W.; Claverie, J.P. *Carbon* **2013**, 51, 72-84
3. Nguyen, D. ; Zondanos, H. S.; Farrugia, J. M.; Serelis, A. K.; Such, C. H.; Hawkett, B. S. *Langmuir* **2008**, *24*, 2140-2150
4. *Loiseau, J; Doërr, N.; Suau, J. M.; Egraz, J. B.; Llauro, M. F.; Ladavière, C.; Claverie J. Macromolecules* ***2003****, 36, 3066-3077*
5. *Beattie, D; Wong, K.H.; Williams, C.; Poole-Warren, L.A.; Davis,T.P.; Barner-Kowollik, C.; Stenzel, M.H. Biomacromolecules* ***2006****, 7, 1072-1082.*